Desalination and Water Treatment
www.deswater.com

doi: 10.5004/dwt.2018.22184

110 (2018) 27–64
April

A comprehensive review of air gap membrane distillation process

Habis Al-Zoubi[a,*], Fahad Al-Amri[b], Atia E. Khalifa[c], Ahmad Al-Zoubi[d], Muhammad Abid[b], Ebtehal Younis[b], Tapas Kumar Mallick[e]

[a]*Environmental Engineering Department, College of Engineering, Imam Abdulrahman Bin Faisal University, Dammam 31441, Saudi Arabia, Tel. +(966) 566832600; Fax: +(966)38584331; emails: hsalzoubi@iau.edu.sa, habisa@yahoo.com (H. Al-Zoubi)*
[b]*Mechanical and Energy Engineering Department, College of Engineering, Imam Abdulrahman Bin Faisal University, Dammam 31441, Saudi Arabia, emails: fgalamri@iau.edu.sa (F. Al-Amri), maakhan@iau.edu.sa, abid.528633@gmail.com (M. Abid), eyounis@iau.edu.sa (E. Younis)*
[c]*Mechanical Engineering Department, King Fahd University of Petroleum and Minerals, Dhahran 31261, Saudi Arabia, email: akhalifa@kfupm.edu.sa*
[d]*Computational Engineering Division, FMP Technology GmbH, Am Weichselgarten 34, D-91058 Erlangen, Germany, email: ahmad.alzoubi06@gmail.com*
[e]*Environment and Sustainability Institute, University of Exeter, Penryn Campus, Cornwall TR10 9EZ, UK, email: t.k.mallick@exeter.ac.uk*

Received 1 November 2017; Accepted 21 March 2018

ABSTRACT

Membrane distillation (MD) is a promising thermally driven membrane separation technique. In MD, water vapor is being separated from the hot feed water solution using a microporous hydrophobic membrane, due to the difference in temperature, and hence vapor pressure, across the membrane. Air gap membrane distillation (AGMD) process is one of the common configurations of applying the MD process for water desalination and other applications. In AGMD, a stagnant air gap is introduced between the membrane and a condensation surface within the membrane module to reduce the conduction heat loss through the membrane. In this review article, design characteristics and operating conditions of AGMD and its modified designs to enhance the productivity and reduce the energy consumption are surveyed and discussed. Previous work on pilot AGMD systems and multi-stage or multi-effect systems with energy saving modules is highlighted. Membrane materials and developments used with the AGMD modules are presented with discussion of membrane fouling and scaling problems. In addition, modeling techniques based on the heat and mass transfer equations and simulation approaches of the AGMD process are presented. The merits of operating the AGMD systems with solar and other renewable energies are discussed along with the economic aspects. The future research directions of AGMD are highlighted in this review. This will help researchers to direct their research without repetition of previous known studies.

Keywords: Air gap membrane distillation; Module configurations; Fouling; Heat and mass transfer; Solar energy

1. Introduction

There is a growing demand for access to clean water sources, for both domestic and industrial use. The abundant availability of seawater and brackish water makes technology for desalination processes increasingly desirable [1]. Membrane technology is considered as the most suitable desalination process. Pressures and concentrations are the main driving forces through the isothermal membrane processes such as nanofiltration (NF) membranes [2] and reverse osmosis (RO) processes [3]. In addition, there are other membrane processes that are non-isothermal requiring a thermal

* Corresponding author.

driving force to establish the required trans-membrane partial vapor pressures. Membrane distillation (MD) technology represents one of these processes that is used in the desalination process. The MD process was introduced at the beginning of 1960s [4]. Later, few researchers conducted the research on the process until the middle of 1980 [5–9] for the simple reason that membranes were not available at the suitable characteristics for MD compared with RO [10]. In 1997, Lawson and Lloyd [11] conducted a historical review on development of MD process, and later in 2011, Susanto [12] summarized the historical development in MD process in different phases as shown in Fig. 1. After the development of modified membranes and establishment of membrane companies, an interest in the MD process has grown substantially and was classified as new technology [11,13–16] or as a supplement for desalination processes [17,18]. This growth led MD processes to yield promising results in waste water treatment and many other applications [19–29]. In the period 2011–2017, a hybrid of MD with renewable energy plant was widely studied at pilot plant scale to desalinate salty water and produce hot water and electricity. More details of these plants are discussed later in this study.

MD is a thermally driven membrane separation process, in which only vapor molecules are transported through hydrophobic membranes. The driving force for the process is the trans-membrane vapor pressure difference. MD process has many advantages, namely, low operating temperature and hydraulic pressure, high rejection of solutes, performance independent of high osmotic pressure [11], less-sensitive to feed concentration for seawater desalination, less requirements on membrane mechanical properties and potentially good permeate flux [7,30].

The distillation occurs in an MD process below the normal boiling point of the feed solution, and the process takes place based on equilibrium between the vapor and liquid of the feed liquid mixture [31]. A greater difference in temperature produces greater vapor pressure to drive vapor through the membrane. The appeal of the technology is the fact that a low-temperature differential is needed. Practical field demonstration units have performed with temperature differences between the hot and cold sides of only 10°C, and with feed water temperatures of 67°C–93°C. Pumping energy is still required to move pre- and post-treated water through the system, but typical pump pressures are limited to a few psi. The ratio of thermal energy input to electrical energy input is about 10 to 1 [32]. On the other hand, MD does not require intensive pretreatment and is less susceptible to organic and colloidal fouling in comparison with RO [3]. MD can directly use waste heat and solar thermal as its main source of energy as the operating temperature in the range of 40°C–80°C [33,34]. Compared with thermal desalination process such as multi-stage flash distillation (MSF) and multiple-effect distillation (MED), MD is less demanding regarding vapor space and building material's quality leading to potential lower construction costs and compact design [35].

Therefore, MD can be a promising process for small-to-medium scale and off-grid seawater desalination applications in remote coastal areas. However, MD has some limitations, that need to be addressed, such as high susceptibility to the polarization in the feed channel, membrane pore wetting [11]; high resistance to water vapor flow through membrane due to the presence of trapped air in the pores [36]. Also, the heat lost by conduction through the membrane is relatively large and the low thermal efficiency has resulted in the limited commercialization of MD process [37].

The MD process can be conducted using different configuration designs [8] which differ based on the nature of the cold side of the membrane. These configurations include direct contact membrane distillation (DCMD) [38], air gap membrane distillation (AGMD) [39], sweeping gas membrane distillation (SGMD) [40,41], and vacuum membrane distillation (VMD) [42]. In DCMD, both the feed solution and permeate solution, which is colder than the feed solution, are in direct contact with the membrane; the former at the feed side and the latter at the permeate side of the membrane. The AGMD configuration contains a stagnant air gap between the membrane and a condensation surface where the evaporated volatile molecules cross both the membrane pores and the air gap to condense over a cold surface in the membrane module. As for the SGMD, a flowing stream of gas sweeps the membrane surface at the permeate side which is followed by the condensation of the vapor molecules outside the membrane module. In the VMD, vacuum is applied to the permeate side where the applied pressure is less than the volatile molecules saturation pressure. Typical configurations of these distillation methods are shown in Fig. 2.

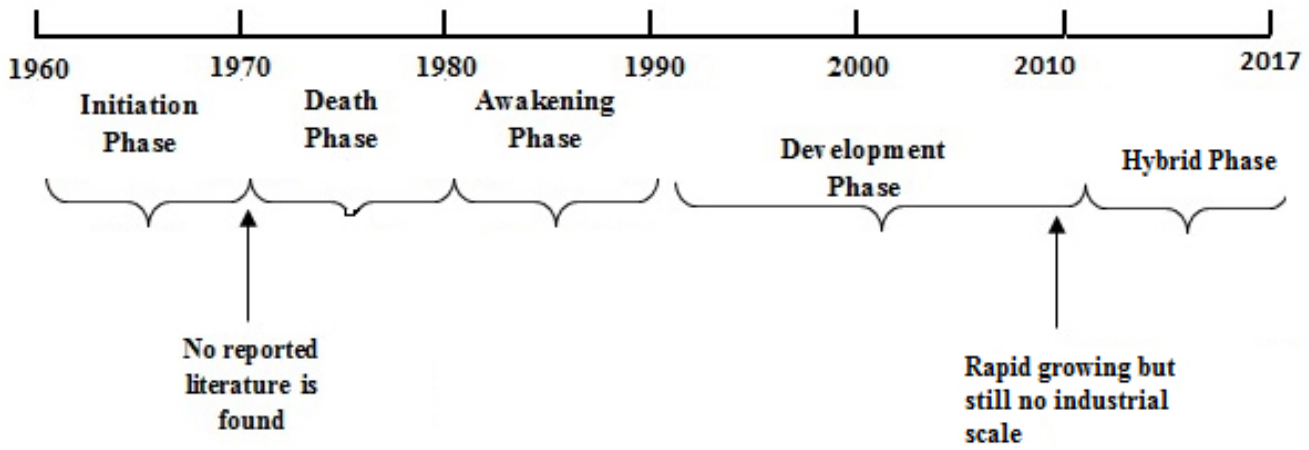

Fig. 1. Historical development of membrane distillation [12].

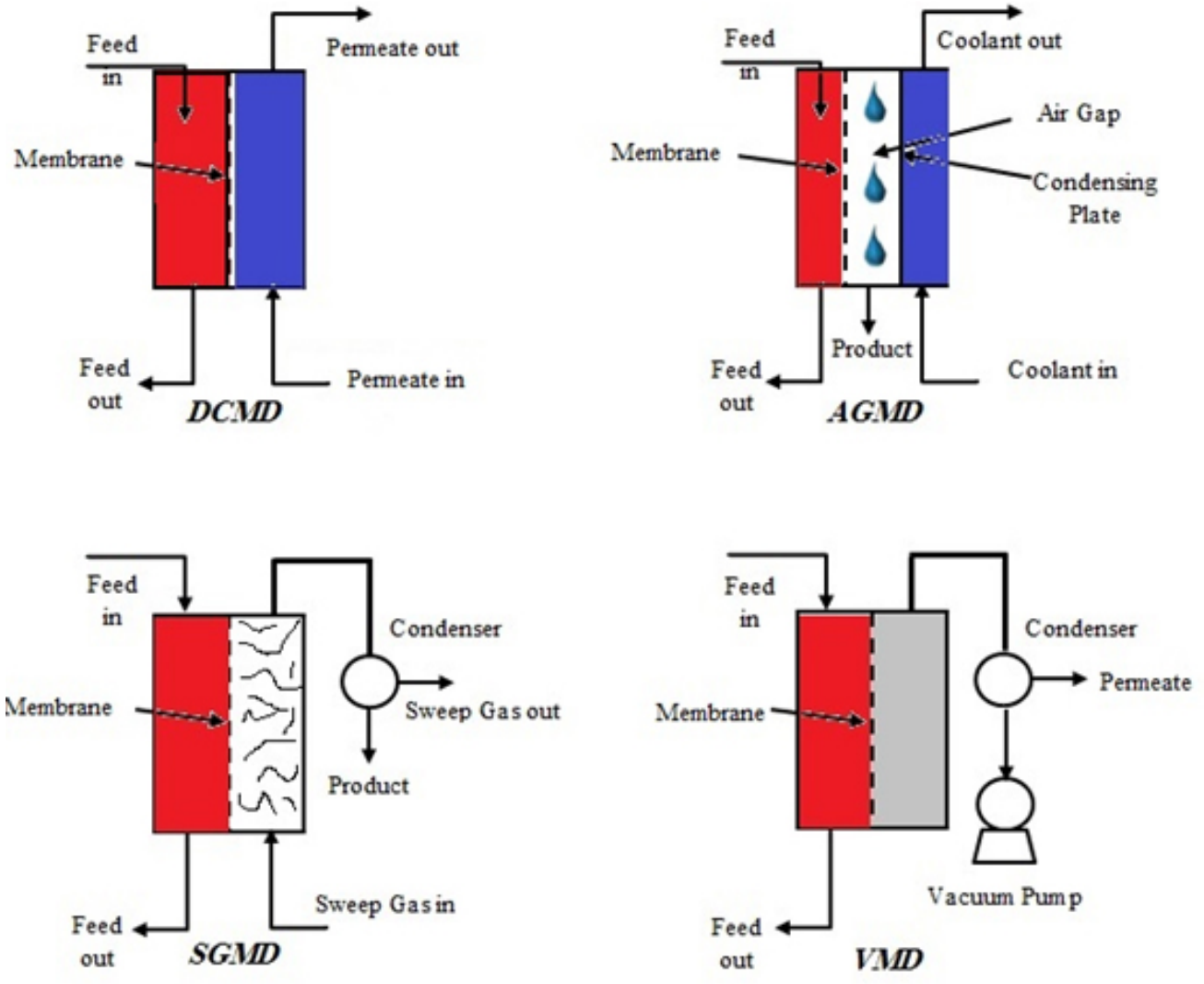

Fig. 2. Four MD configurations.

Modified configurations were developed and designed to improve the flux and the efficiency of MD process. A material gap membrane distillation (MGMD) was developed by Francis et al. [43]. In this configuration, air gap in AGMD was filled with different materials such as sand, deionized (DI) water, sponge (polyurethane) and polypropylene (PP) mesh as shown in Fig. 3(a). Another recent study was conducted using hollow fiber membranes as a filling material [44]. Swaminathan et al. [45] introduced another AGMD configuration called conductive gap membrane distillation where a high conductivity material (such as a metal mesh) is inserted into the gap of AGMD system. Another configuration called permeate (liquid or water) gap membrane distillation (PGMD) was explored by Winter et al. [46,47] and Ruiz-Aguirre et al. [48] as shown in Fig. 3(b). In this configuration, a third channel is introduced as an additional non-permeable foil. Khalifa [49] used only water gap in AGMD design. In these configurations, the gap is additionally allowed to be flooded with water where the distillate is collected from the top of the gap rather than the bottom. The vacuum air gap membrane distillation (V-AGMD) process is another MD configuration as shown in Fig. 3(c). In this design, the AGMD was supplemented by a vacuum pump [50–52]. More details about these configurations are covered later in this study.

Many literature reviews have been conducted on the MD subject. An old historical review was made in 1997 by Lawson and Lloyd [11]. Later, different reviews were performed on the principle and modification and developments of MD process by many authors [3,37,53–55]. The applications of MD process in desalination and water and waste water treatment were covered by Hassan and Fath [56], Camacho et al. [31], Susanto [12], Shirazi and Kargari [57], and Pangarkar et al. [58]. In addition, modified membranes in MD process for higher permeate flux were reviewed [59–61], while the fouling and scaling over MD membrane were covered in other works [62–64].

The energy consumption aspects of MD including the use of solar energy, heat recycling, and other alternative forms of energy have also been reviewed elsewhere [65–68]. Khayet [69] and Hitsov et al. [70] reviewed the theoretical modeling of MD process. Optimization of the membrane properties for MD process has also been investigated [71]. Recently, comprehensive reviews on principles and applications of VMD

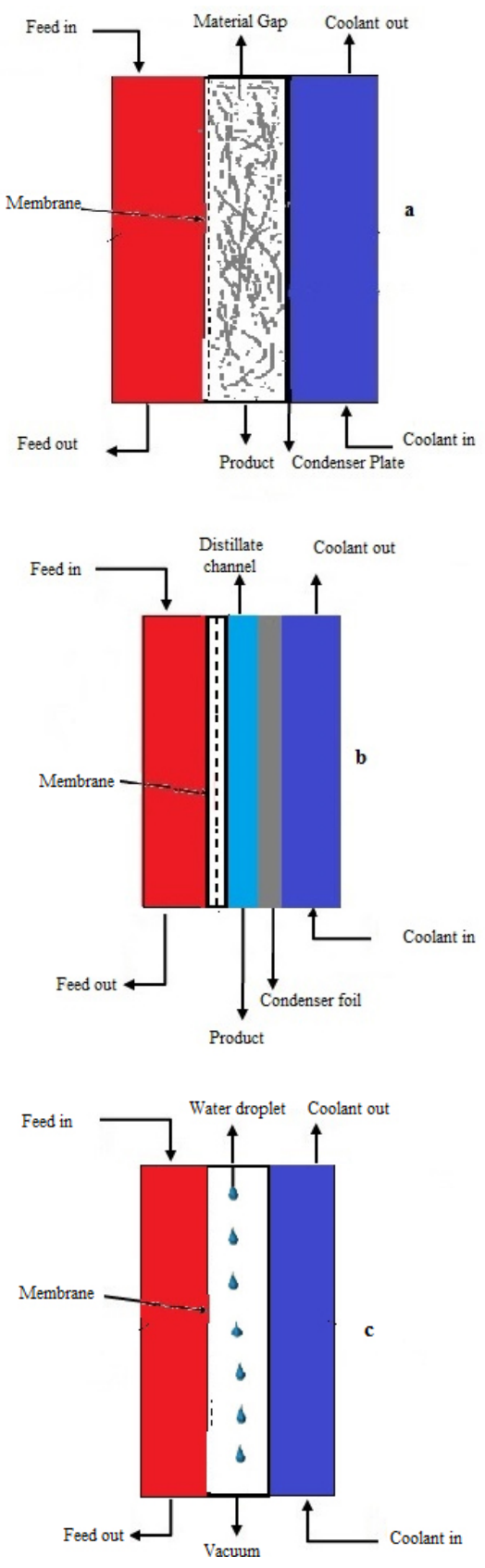

Fig. 3. Schematic diagram of (a) MGMD, (b) PGMD, and (c) V-AGMD configurations.

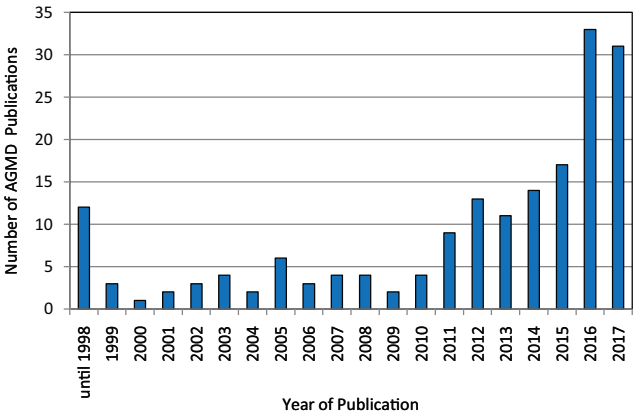

Fig. 4. History of published AGMD papers over the past few decades.

[72] and DCMD [73] were conducted. On the other hand, many patents have been recently published about the modifications and developments of MD process [3]. These patents mainly cover the membrane casting methods, integrated MD with the other processes to achieve complex separations, module designing, and configuration modifications to improve the MD process.

Based on the available literature and to the best of our knowledge background, no systematic review covered the AGMD configuration. Therefore, the main objective of this work is to conduct a comprehensive review of the AGMD configuration. The topics covered in this review include the AGMD technique and its modifications, operating variables affecting AGMD, AGMD modules, membrane development in AGMD, scaling and fouling in AGMD, integration of solar energy with AGMD, theoretical modeling of AGMD, and AGMD in desalination process. Fig. 4 shows a history of all AGMD published papers over the past few decades as found in the literature. It clearly indicates that interest in the AGMD research has soared in the last 5 years.

2. AGMD process

In AGMD configuration, a thin air gap is interposed between the membrane cold surface and a condensation surface. The evaporated volatile molecules pass through both the membrane and the air gap, and then condense on the cold surface [39]. The temperature difference between the feed solution and the cold condensation surface is the driving force for permeation of water vapor and volatile compounds at the hot liquid/vapor interfaces formed at the feed membrane surface. The mass transfer in the AGMD process includes the movement of the water molecules from the bulk liquid toward the membrane. The molecules are evaporated at the membrane surface. Then, the vapor is transported through the membrane pores and diffusion through the stagnant air gap by natural convection. Finally, the condensation takes place over the cold surface [74].

The main benefit of the air gap is to solve the problem of heat loss by conduction through the membrane as compared with DCMD, which leads to relatively low efficiency of the MD process. However, as the vapor has to move through stagnant air, its flux is reduced depending on the thickness

of the air gap and therefore its flux is lower than DCMD or VMD configurations [75]. Compared with a DCMD process, an AGMD process provides the freedom of using any coolant, as the coolant does not mix with the condensate as in the case of DCMD. Moreover, DCMD is relatively less efficient in heat utilization. On the other hand, AGMD has a high thermal efficiency due to air insulation between the heated feed stream and the coolant stream [76]. AGMD can deal easily with membrane leakage and as well as membrane damage, in which the MD process can be stopped for a while and the distillate does not have the chance to get contaminated as that in DCMD [76]. However, this configuration still suffers from producing low flux compared with DCMD [77,78]. Therefore, many studies were interested to overcome this problem by modifying the AGMD configuration, which will be discussed in the following section.

3. Modified AGMD configuration

Tian et al. [79] presented an innovative design of AGMD configuration which improved the permeate flux. The modern design includes a tangent directional and rotational inlet turbulent manipulated flow of hot feed and a partial contact between the membrane and the cooling plate in a small air gap thickness. The turbulent flow accelerates the diffusive process of mass and heat, reduces the boundary layer thickness of temperature and concentration and at the same time washes the membrane surface. This improves the temperature and concentration polarization on the membrane surface and raises the efficiencies of mass and heat transfer. The results of the new design showed that a 2.5-fold improvement of flux was achieved using tap water as a feed over the traditional AGMD technique at almost the same conditions. The same improvement was obtained by Chernyshov et al. [80] who introduced spacers inside the feed chamber of an AGMD module. Five spacers of the same thickness with different geometries were investigated in this work and include: two spacers of twisted tapes and three others made of round rods. They differ from each other in the type of filaments and angles, at which the filaments are placed with respect to the main flow direction. Filament orientation is described using two angles: angle between filaments and flow angle of attack as shown in Fig. 5. The results showed that the maximum flux with spacers was about 2.5 times higher compared with an empty channel.

In another study, a channeled coolant plate was designed instead of a flat plate for distillation of saline water using AGMD [81] as shown in Fig. 6. The channels consisted of different types of fins over the plate. Fig. 6 shows cylindrical fins over coolant plate used in the study. For the same equivalent air gap, the flux enhanced maximum up to 50% compared with a flat coolant plate for a coolant temperature of 25°C. On the other hand, an integrated vacuum system with AGMD was investigated by Alsaadi et al. [50] and recently by Liu et al. [52] to improve the permeate flux. The new configuration shown in Fig. 7 removes all non-condensable gases from air gap. It was concluded that the new system increased the flux by more than three times when the gap pressure is maintained at the saturation pressure of the feed temperature. However, the author noted that this system will increase the operating cost of the process.

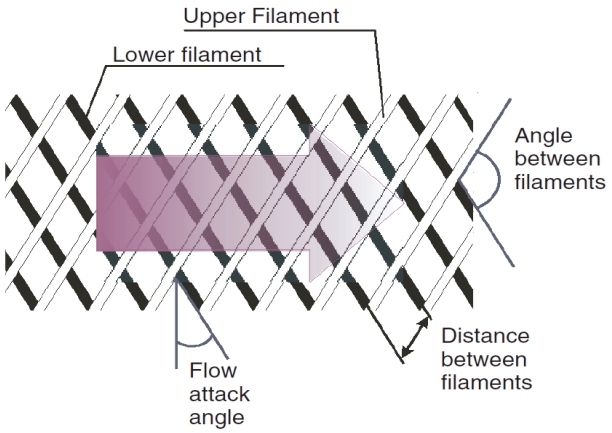

Fig. 5. Convention used for description of the spacers [80].

Fig. 6. Channeled coolant plate used for condensation in AGMD [81].

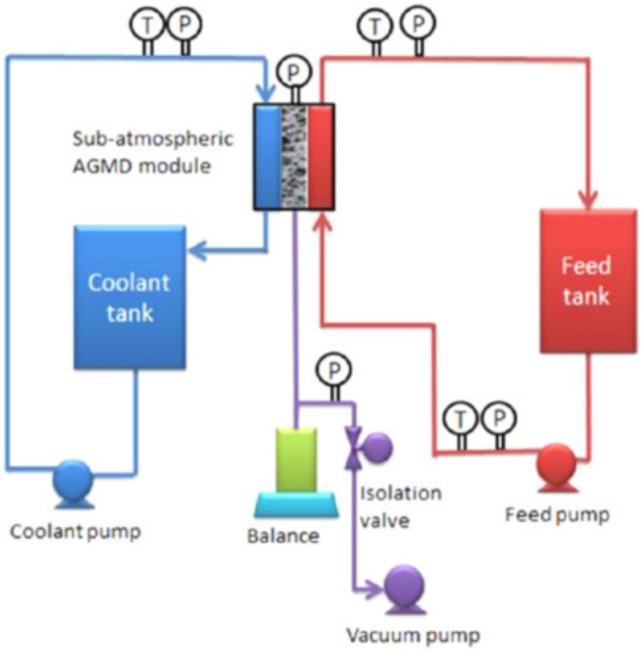

Fig. 7. V-AGMD configuration modified by Alsaadi et al. [50].

Recently, Abu-Zeid et al. [51] modified a similar configuration to improve the performance of the AGMD process as depicted in Fig. 7. It was found that the integration of vacuum pump with AGMD could improve the flux, gained output ratio (GOR), thermal efficiency and performance ratio. The GOR is defined as the ratio of the latent heat of evaporation of the water produced to the input thermal energy. Most of the pilot plants use AGMD configuration with or without enhancement of vacuum system. On the other hand, MGMD was studied to fill the gap between the membrane and the condensation plate with different materials in AGMD module [43]. The proposed materials were DI water, sand, PP, and sponge (polyurethane).

A very high flux was obtained in the range of 200%–800% by filling the gap with sand and DI water at different feed water temperatures. The study also found that PP and polyurethane had no effect on the permeate flux. Other investigators studied a water gap membrane distillation instead of AGMD where the air was replaced by the water [49,82]. The study showed that the water gap system enhances the permeate flux significantly. In another study, a new AGMD configuration referred to as bulky modules was designed as a result to incorporate the air gap, condensing plate, and cooling channel [83]. The authors introduced porous and non-porous hollow fibers to compact the module volume. The vapors passing through the porous fibers are condensed at the outer wall of non-porous fiber which is cooled by the circulation of a cold fluid inside the fiber. As mentioned earlier, PGMD was modified using a foil as a coolant plate [46]. In this configuration, the sensible and latent heat is transferred through the condenser foil to preheat the feed water in the condenser channel by internal heat recovery. This reduces the specific energy demand due to an additional heat transfer resistance in the PGMD system. Another improvement of AGMD configuration by coating the condensing surface with a nano-structured copper oxide was conducted by Warsinger et al. [84]. It was found that there were improvements in flux in excess of 60% over original AGMD configuration. On the other hand, Criscuoli [85] investigated the integration of AGMD with DCMD modules at lab scale. In this integration, the feed exiting from the DCMD module is sent as coolant stream in the AGMD module – where it is heated by the permeating vapor, before being recycled back to the DCMD unit. The results showed that the integration system gave a lower specific thermal energy consumption and higher permeate flux than that single DCMD unit. Additionally, the suggested system gives chance to simultaneously treat two different feeds at different operating temperatures.

Recently, AGMD system with double-sided cooling channel was investigated [86]. In the same direction, the integration of hollow fiber AGMD configuration with multiple cooling channels made of stainless steel was developed [44]. In this work, the hollow fiber membranes were packed in the air gap area between the outer and inner cooling channels. The investigators claim that the flux and heat efficiency of this configuration were higher than those observed in the original AGMD models. Another novel configuration called double-pipe AGMD module (DP-AGMD-M) was presented by Liu et al. [87]. This configuration consisted of polyvinylidene fluoride (PVDF) hollow fiber membrane and heat exchange capillary copper tubes as depicted in Fig. 8. The feed was

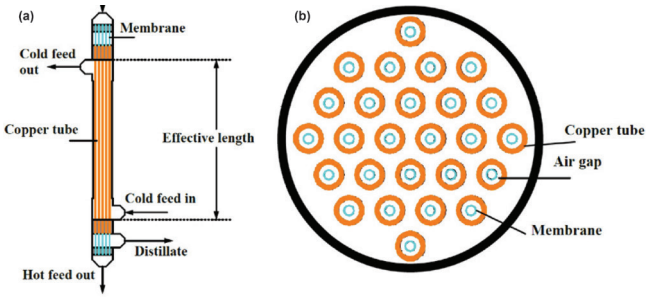

Fig. 8. (a) Configuration and (b) cross-section of DP-AGMD-M [87].

wrapped with thermal insulation cotton to reduce heat loss to surrounding. The results showed an improvement in the performance of AGMD process. On the other hand, a multi-stage AGMD process using hollow fiber membranes for further concentrating RO brine and obtaining a high flux was investigated [88]. The results showed that a multi-stage AGMD improved the flux in comparison with a single-stage AGMD process. In the same direction, multi-effect air gap membrane distillation process was also developed [89]. Many parameters such as feed temperature, feed flow rate, coolant temperature, coolant flow rate, and air gap thickness were studied. A high flux up to 166.4 kg/m^2 h at the feed temperature of 80°C, coolant temperature of 20°C, coolant flow rate in each cooling channel of 0.75 L/min, and air gap thickness of 5 mm using flat sheet polytetrafluoroethylene (PTFE) membrane under four AGMD stages with total membrane area of 224 cm^2.

In a very recent study, Khalifa et al. [90] experimentally investigated multi-stage air AGMD (MS-AGMD) with parallel and series flow stage connections for the feed stream and coolant stream. In terms of permeate flux and energy consumption, the results showed that the parallel stage connection gave better performance than series connections. In addition, the flux of MS-AGMD module is found to be 2.6–3.0 times the flux of single-stage AGMD module, for series and parallel stage connections, respectively.

In another study, a pilot plant employing a spiral-wound AGMD membrane was utilized for seawater desalination [91]. The results showed that there is a notable influence of evaporator inlet temperature and water circulation rate on process performance. There was a trade-off between the flux and energy efficiency when the water circulation rate varied. The energy efficiency is defined as the ratio between the amount of heat brought into the membrane and the total heat actually used for evaporation of the feed to produce fresh water: Increasing the water circulation rate resulted in not only an improvement in the flux but also an increase in both specific thermal and electrical energy consumption. The optimum operating conditions were obtained at specific thermal and electrical energy consumption of 90 and 0.13 kW h/m^3, respectively.

The flat sheet module is the most common type of AGMD used in MD research [49,92–96] for its simplicity. The hollow fiber module of AGMD has been investigated by other researchers [83,97–104] and has been found to be better than the flat sheet module as it has higher specific surface area and packing density. Moreover, hollow fiber membrane has

other advantages such as it does not require any additional support, and has relatively low mass and heat transfer resistance in the boundary layer [66,105]. A spiral-wound module is rarely used in MD configuration which was mentioned in literature [46,106].

Guijt et al. [107] conducted an AGMD experiment using a single hollow fiber membrane. In this study, one piece of hollow fiber membrane was simply stretched inside a small tubular module and tightly sealed at the top and bottom parts of the module. The results revealed that the thermal efficiency of the AGMD process was in the range of 85%–90%. The advantages of hollow fiber membrane have encouraged researchers to design several tubular AGMD modules by using parallel PP hollow fiber membranes and PP hollow fiber heat exchange tubes [88,98]. Additionally, porous and non-porous hollow fibers were used as channels for hot salt and cold water, respectively. The experimental results proved that these modules exhibited excellent heat recovery characteristics.

A similar study was conducted by Yao et al. [98] in which a maximum flux of 9.2 kg/m^2 h was obtained. Later, Geng et al. [99] introduced a net to maintain the air gap width among porous and non-porous hollow fiber membranes. Their module had relatively large area of 0.204 m^2 and gave a flux of 2.5 kg/m^2 h. Recently, a hollow fiber module with multiple cooling channels for the AGMD process was developed by Aryapratama et al. [44]. A 12.5 kg/m^2 h of a flux was obtained in this model, which is higher than most of the previous studies that used polymeric fibers as coolant channels. In a very recent study [108], unexpected finding was obtained for the desalination of NaCl (18 wt%) using both configuration AGMD and DCMD at pilot scale with feed and coolant temperatures of 70°C and 20°C, respectively. The results showed that the flux for AGMD was 1.2 times higher compared with the flux for DCMD. Another recent study [109] proved that AGMD gave higher GOR than DCMD and PGMD configurations in large area modules.

4. Operating variables affecting AGMD process

Different operating variables affect the AGMD performance. This includes feed temperature, feed flow rate, feed inlet concentration, coolant temperature, coolant flow rate, and gap width. These variables are highlighted in the following sections.

4.1. Effect of feed temperature

The feed temperature in AGMD is usually varied in the range of 40°C–80°C. Many researchers have studied this variable and showed its effect on performance of AGMD process [93,110–122]. All the results of these studies showed that the permeate flux increases with the increase in the feed temperature. In more details, Khalifa and Lawal [93] found that 80°C is an optimum feed temperature of AGMD desalination system. Another similar study was conducted on AGMD for desalination of seawater (30,000 ppm) and ground water (4,000 ppm) at 40°C [111]. The results showed that the permeate flux increased with increasing feed temperature from 40°C to 46°C and maximum flux was found to be 22.98 and 12.48 kg/m^2 h of ground water and seawater, respectively, at the operating conditions are: feed temperature of 60°C; feed flow rate of 55 L/h; coolant temperature of 15°C; and air gap thickness of 1.2 mm. Another study proved experimentally that the flux was increased in the range of 550%–750% when the feed temperature is increased from 40°C to 80°C, depending on the other operating variables [113]. Based on that, Abu-Zeid et al. [72] concluded that there is an exponential increase of the permeate flux with the increase of the feed temperature for all MD configuration. This is due to the exponential increase of the vapor pressure of the feed solution with temperature (e.g., Antoine equation), which increases the trans-membrane vapor pressure. In addition, increasing feed temperature will decrease the temperature polarization [20]. Recently, it was found that the permeate flux increased by about 3.8-fold with the increase of feed temperature from 45°C to 65°C for 35 g/L NaCl solution using AGMD system [123].

4.2. Effect of feed flow rate

The effect of feed flow rate in the hot feed channel on the permeate flux has been investigated by many authors [93,111,112,116]. The increase of the flow rate leads to a reduction in the negative effect for temperature and concentration polarizations and enhances the evaporation process at the liquid–vapor interface on the hot membrane side [37]. It also enhances the mixing level in the boundary layer that improves the heat and mass transfer coefficients. Therefore, a turbulent flow regime is preferable to obtain a relatively high permeate flux. However, the increase of the flow rate is limited since the feed channel should not exceed its liquid water entry pressure (LEP_w) value. Khalifa and Lawal [93] concluded that if the feed flow rate is increased from 1 to 5 L/min, this will result in 30% increase in the permeate flux. However, for feed flow rates above 3 L/min, the incremental increase in permeate flux becomes less significant. Similar results were obtained for desalination of seawater using AGMD [111]. Another study showed that feed flow had a slight effect on the permeate flux when AGMD was carried out for desalination of 75 ppm NaCl at the operating conditions of coolant temperature of 20°C, coolant flow rate of 3 L/min, and air gap thickness of 3 mm [113]. A similar conclusion was drawn by another investigator [124]. The permeate flux using TF1000 membrane in AGMD increases from around 0.132 to 0.174 L/m^2 min when the feed flow rate increases from 0.5 to 1.89 L/min [20]. The same authors obtained the same trend for desalination using different salty solutions [125].

4.3. Effect of feed salt concentration

The effect of the concentration of feed water on the permeate flux was studied by Khalifa et al. [113]. The tested feed solutions were fresh water (TDS of 0.075 g/L); NaCl solutions with concentrations ranging from 4 to 50 g/L, and raw seawater (TDS of 60 g/L). The results showed that the permeate flux decreased gradually with increasing feed salt concentration. The maximum and minimum percentage reduction in permeate flux when the feed concentration was increased from 0.075 to 60 g/L is about 17% and 5% corresponding to feed temperatures of 40°C and 80°C, respectively. The reason for that is increase of feed salinity increases the effect of

concentration polarization, which reduces water vapor pressure difference across the membrane. A decrease in flux of around 27% was reported in another work at feed temperature of 80°C when the concentration of salt solution increased from 0.145 to 60 g/L [49]. The change in the reduction is due to the change of the type of used membranes in both works. Martinez [126] attributed this reduction to the decrease in water activity. Yun et al. [127] claimed that the boundary layer solution at high concentration reaches the saturation state where its properties are changed. Its density, boiling point, surface tension, and viscosity are increased, while the vapor pressure is decreased.

Alkhudhiri et al. [128] studied the effect of concentration of four different salts (NaCl, $MgCl_2$, Na_2CO_3, and Na_2SO_4) on flux using AGMD cell. It was found that for all investigated salts, the permeate flux declined when their salt solution increased due to the reduction of vapor pressure of feed solution. Other works concluded similar findings in which the flux tends to decrease slightly with increasing in the feed saline concentration [86,116,128–130].

4.4. Effect of coolant temperature

In one study [113], a maximum of 11% reduction in permeate flux has been observed when coolant temperature was increased from 15°C to 30°C at 1 L/min coolant flow rate and at a feed temperature of 70°C. In another study [20], a range of coolant temperature of 5°C–25°C was studied at constant hot feed temperature and flow rate. The result showed that the permeate flux of TF200 dropped off from 2.4 g/m^2 s at a coolant temperature of 5°C to 1.4 g/m^2 s at a coolant temperature of 25°C. This result can be attributed to the fact that decreasing the coolant temperature at constant feed temperature leads to an increase in the vapor pressure difference across the membrane, which in turns leads to enhanced flux. Therefore, it is recommended to use cooling water at atmospheric condition if the feed temperature is high enough. This will lower the cost of energy input for keeping the cooling water below the room temperature.

4.5. Effect of coolant flow rate

It has been observed in numerous studies that the coolant flow rate has little effect on the permeate flux as long as it is able to keep the condensation surface at an acceptable low temperature for vapor condensation. The fact has been attributed to the presence of the air gap [93,110]. For example, increasing the coolant flow rate from 2 to 4 L/min was found to result in about 5% increase in flux [49]. In another work, around 13% increase in the flux was observed when the coolant flow rate was increased from 1 to 3.5 L/min [92]. However, the importance of higher coolant flow rate is to reduce the air condensate interfacial temperature [74]. In another work, it was found that the effect of coolant flow rate depends on the gap width and feed temperature [93].

4.6. Effect of gap width

Khalifa [49] studied the effect of the gap width on the permeate flux. The gap width was changed from 4 to 8 mm using a thicker gasket between the membrane support plate and the condensation plate. The results confirmed that the increase of the gap width reduces the flux, particularly at higher temperature. For example, at 90°C the flux decreased by 22% when increasing the gap from 4 to 8 mm in the AGMD. Another work showed that reducing air gap width from 7 to 3 mm resulted in considerable rise in permeate flux [86]. The authors attribute the rise in flux to the increment in temperature gradient within the vapor compartment as a result of decline in resistance to mass transfer. Banat and Simandl [131], and Chouikh et al. [132] studied the effect of the air gap width of flux experimentally and theoretically and found that reducing the air gap width increased the temperature gradient within the vapor compartment and increased the flux.

In another study by Khalifa and Lawal [93], the flux was observed to increase by 100% when the air gap width was reduced from 7 to 3 mm, at a given feed temperature. Jonsson et al. [103] found theoretically that the air gap width becomes more significant for air gaps thinner than 1 mm. However, the practicality of conducting experiments limits the ability to use smaller gaps. Similar findings regarding the relation of the flux with the air gap width have been observed in other works [23,54,116,122,131,132]. Recently, Swaminathan et al. [109] concluded that air gap has an advantage in AGMD performance in desalination of high feed salinity levels. The results showed that AGMD achieved a higher GOR than PGMD and DCMD systems as the air gap effectively makes the AGMD system behaves as though it has a thick membrane.

5. Membrane development in AGMD

5.1. Membrane properties

The lack of available commercial MD membranes with high performance, minimized fouling/scaling tendency, and excellent wetting resistance is one of the major difficulties in MD process. It has been established that the performance of a process is a direct consequence of the utilized membrane parameters (thickness, porosity, mean pore size, pore distribution, contact angle, surface tension, and geometry) [58]. The reduction of the membrane production costs and improvement of the membrane performance in terms of energy efficiency and flux by optimizing the membrane properties are important technical challenges which have gained the interest of many researchers [39,99,133–135]. Ali et al. [133] examined the effect of the five MD membranes characteristics (porosity, tortuosity, thermal conductivity, pore diameter, and thickness) on production cost using factorial design (FD) and numerical model of two MD configurations: DCMD and AGMD in a small-scale and single-stage process setup. They found that the five MD membrane characteristics affect water production cost to varying degrees (Figs. 9 and 10). They observed that the pore size has a minor effect on water cost for AGMD in comparison with DCMD as shown in Fig. 9. They attributed this to the high diffusion resistance across the air gap in AGMD which dominates its mass transfer processes. Therefore, it is recommended to reduce the diffusion resistance by increasing porosity or decreasing membrane thickness or tortuosity in order to yield high flux (low cost) of the water as shown in Fig. 10.

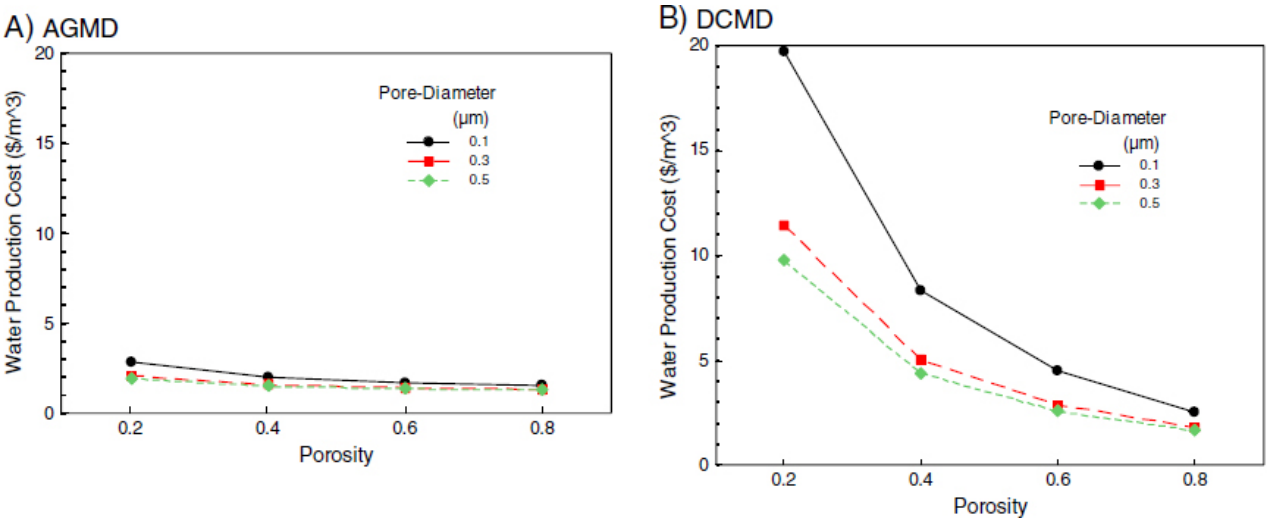

Fig. 9. Effects of membrane average pore size and porosity on water production cost at average thickness and tortuosity values for (a) AGMD and (b) DCMD [133].

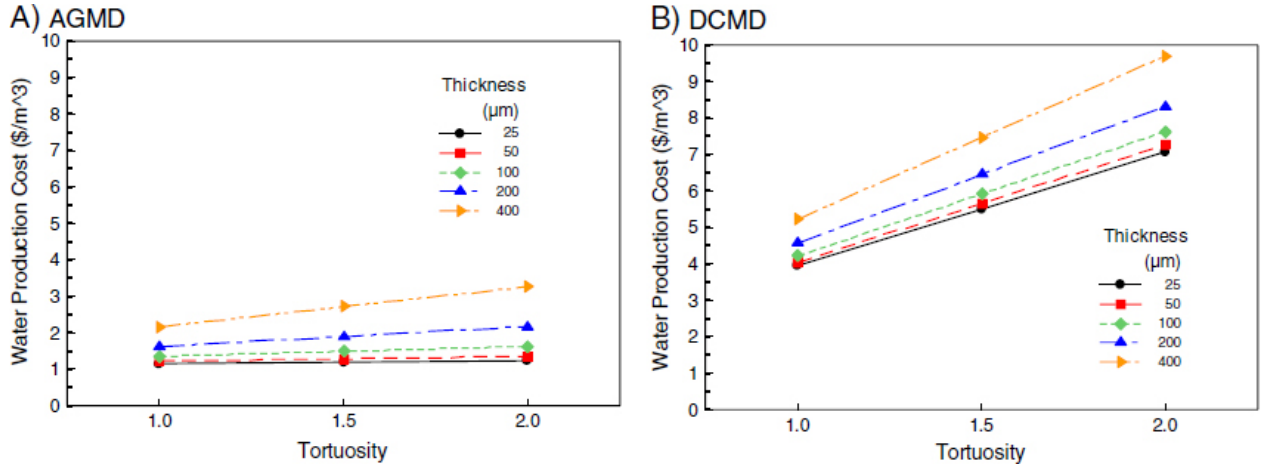

Fig. 10. Effects of membrane tortuosity and thickness on water production cost at average porosity and pore size values for (a) AGMD and (b) DCMD [133].

For improvement of the membrane performance in terms of energy efficiency and flux, Eykens et al. [71] demonstrated in their review paper that the membrane porosity and the optimized membrane thickness are the most important parameters in designing the membranes for MD process, while the tortuosity is preferably as low as possible. In another study by Asghari et al. [115], an increase in membrane porosity and pore size distribution increases the permeate flux. In contrast, the permeate flux decreased with thickness and tortuosity of the membrane. However, both Cho et al. [136] and Woods et al. [134] proved that the nominal pore size of the membrane is not a critical factor to determine water flux for AGMD configuration and it can be neglected. Alklaibi and Lior [137] showed that the thermal conductivity of the membrane material has higher effect on the mass transfer of AGMD than on that of DGMD.

In one study by Xu et al. [138], 10 different commercially available PTFE, PP, and PVDF membranes were tested in desalination of highly saline water reaching 120 g/L by AGMD. Process performance was investigated with different membrane characteristics, such as membrane material, thickness, pore size and support layer, using a locally designed and fabricated AGMD module and spacer. Based on results, the PP membrane showed a better performance than the PVDF and PTFE membranes especially the membranes which have pore sizes of 0.2 and 0.45 mm. In general, smaller pore size led to lower flux and larger pore size led to pore wetting due to lower LEP_w values. Recently, discarded PTFE membranes used in AGMD were reused as microfiltration (MF) cell to filtrate humic acid aqueous solutions (15 mg/L) to prevent membrane disposal issues and save costs [139]. The virgin PTFE membranes were used for the treatment of NaCl (65 g/L) and RO brines (50 g/L) until the membrane pores were blocked or wetted. The results observed that the reused AGMD membranes gave better results than that new MF membrane.

5.2. Membrane materials and fabrication

The structure and chemistry of membranes are highly important, and the requirements vary depending on

application and the type of used MD configuration. In general, hydrophobicity is the main requirement for MD membranes in most applications. The membranes must be made from intrinsic or modified hydrophobic polymers [60].

5.2.1. Polymeric membranes

The most popular polymers used in MD membranes are PTFE, PP, and PVDF [39,60,83,140,141]. PTFE is a highly crystalline polymer with excellent chemical resistance and thermal stability. It has the lowest surface energy among the polymers considered. PTFE are often used in commercial MD systems due to the good wetting resistance, accepted water flux, and very good stability in various operation conditions [142–145]. The main disadvantage of PTFE lies in its difficult processability. On the other hand, PP also has a highly crystalline structure but higher surface energy than PTFE [141]. However, the membrane performance is generally lower due to the symmetric structure and the moderate thermal stability at elevated temperatures. PVDF is a semi-crystalline polymer with a similar surface energy of PP. Unlike PTFE and PP, PVDF can be easily dissolved in common solvents such as n-methyl-2-pyrrolidone, dimethylacetamide, and dimethylformamide (DMF). More importantly, PVDF is the cheapest membrane among these three membranes [54].

Several comparative studies to evaluate the performance of PVDF, PP, and PTFE membranes are found in literature. One of these studies by Moradi et al. [144] compared the performance of PVDF membrane which was prepared using the optimized needleless electrospinning technique with the commercial PTFE. The comparison was based on the results of the wettability tests, water flux, scanning electron microscopy (SEM), mechanical strength, and LEP_w measurements. In addition, the salt rejection performance and the durability of membranes were investigated using AGMD experiment. The results showed that the AGMD permeate flux declined more slowly for PVDF membrane compared with that of PTFE membrane. Furthermore, AGMD experiments fed with real seawater proved that PVDF membrane was more resistive to fouling effects. Another study by He et al. [124] compared the performance of nine types of flat sheet porous membranes made of PVDF, PTFE, and PP materials with different pore sizes. The comparison was based on the results of LEP_w test, gas permeability test, measurement of contact angle test, water flux, and salt rejection [124]. The results showed that PTFE membrane with pore size of 0.22 μm is more suitable for MD process due to high porosity and high hydrophobicity. The PTFE gave higher permeate flux than PVDF and PP membranes. A porous composite hydrophobic/hydrophilic membrane was tested in AGMD and liquid gap MD (LGMD) cells [146]. It was concluded that the LGMD was more attractive than AGMD for desalination process using this composite.

5.2.2. Modification of membrane fabrication methods

Woo et al. [140,141] fabricated enhanced PVDF and PVDF-HFP (PH) nanofiber membranes by using different concentrations of graphene utilizing different fabrication methods. The use of graphene significantly enhanced the membrane properties and robustness as depicted in Fig. 11. Phase inversion

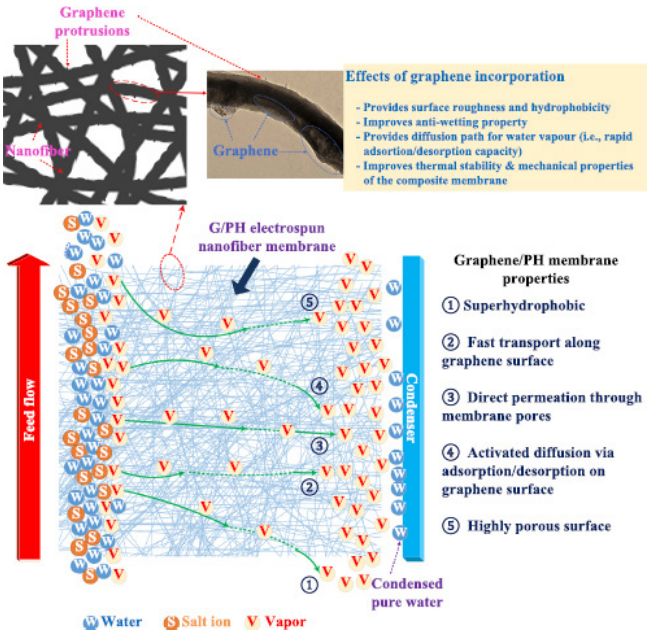

Fig. 11. Schematic of the effect of graphene on the membrane for AGMD process [141].

method was used in fabricating the (G/PVDF) membrane [140], and fluorinated surface-modifying macromolecules (SMM) mixed with polyetherimide [147]. During casting procedure, SMM migrated to the membrane surface rendering it more hydrophobic with small pore size and low roughness parameters compared with the bottom membrane surface. The modified membrane was tested in AGMD configuration. Recently, Woo et al. [148] studied the development of an omniphobic PVDF by electrospinning and CF_4 plasma surface modification for AGMD applications using real RO brine produced from coal seam gas (CSG) water as a feed solution. The modification process improved the wetting properties of the modified membrane, as the plasma treatment lowered its surface energy and gave omniphobic property to the membrane. Moreover, the obtained flux was 15.28 kg/m^2 h and salt rejection of 100% for feed concentration of 15,354 ppm at feed temperature of 60°C, at 20°C of coolant water, and 3 mm air gap thickness. In another work, a one-step electrospinning technique in fabricating the PVDF-HFP (G/PH) electrospun membrane was used [141].

The use of different graphene concentration led into different membranes with different characteristics. The results showed that when graphene concentration was increased over (0.7 wt%) for (G/PVDF) membranes, the fabricated membranes tended to have higher thickness, lower porosity, smaller pore size, and higher contact angle than that of (G/PVDF-0.5) membrane. While for the (G/PH) electrospun membrane, 5 wt% was used as the optimal graphene concentration in these experiments and the results revealed the membrane contact angle of (>162°), membrane porosity of (>88%), and LEP_w of (>186 kPa). At graphene concentration of (0.5 wt%), the obtained flux of the (G/PVDF-0.5) membrane was the highest for 24 h of AGMD test, while (G/PH) electrospun membrane showed stable AGMD flux (22.9 kg/m^2 h) for 60 h of operation as shown in Fig. 12.

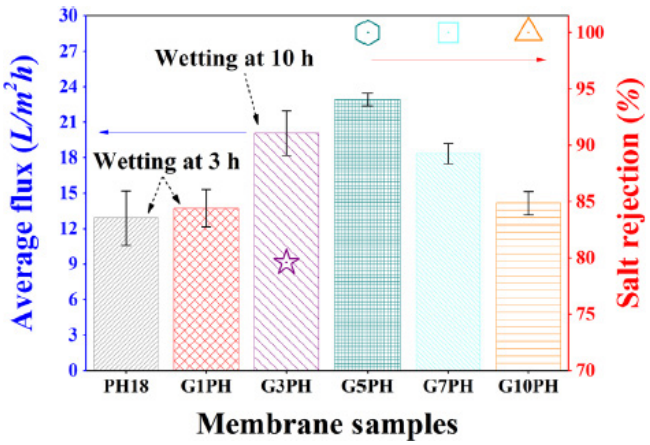

Fig. 12. Flux and salt rejection performances of the G/PH and neat PH membranes for 20 h operation (at feed temperature of 60°C; and coolant temperature of 20°C) [141].

Argon plasma sputtering of PTFE was used to produce porous hydrophobic coatings on a polyethersulfone (PES) membrane via RF magnetron plasma reactor [149]. By changing the deposition conditions (applied RF power, working gas pressure, and distance between the target and the substrate), different polymeric films with different morphologies and/or chemical compositions were obtained. By studying the morphologies of the films, the deposition conditions at which the sputtered film had a chemical structure and surface composition close to those of the PTFE film are high pressure, moderate RF power and longer target–substrate distance as depicted in Fig. 13. The presented PES membrane was tested in AGMD process for removal of benzene from water. The results showed that the treated PES membrane is comparable to the commercial PTFE membrane with similar separation factor and permeate flux after 20 h operation AGMD process. In another work, Gancarz et al. [150] investigated a vacuum plasma coating using perfluorohexane and hexafluorobenzene on a track-etched polyethylene terephthalate (PET) membrane for AGMD applications. The modified membranes gave lower fluxes in comparison with commercial members (PTFE). This is due to the narrowing and plugging of pores appearing over the surface of the modified membranes.

The role of membrane thickness is not straightforward. For example, low thickness membranes offer less resistance to the mass transfer. However, they suffer from more energy losses [151]. To overcome this issue, dual and triple layer membranes have been introduced. A triple layer configuration, consisting of a thin hydrophobic nanofiber layer over the conventional casted microporous layer in addition to the support layer was prepared by Prince et al. [152], (Fig. 14) where the layers were bound to each other by heat pressing and solvent binding. For the prepared membrane, LEP_w was found to be 1.6 times higher than the conventional dual layer membrane and more than 8.7 times higher than that of the nanofiber membrane. Regarding salt penetration, the triple layer membrane had the lowest salt penetration (<0.02%) at different feed temperatures, while the dual layers exhibited salt penetration higher than (<0.07%) which increase as the feed temperature increases. The results showed a high robustness during the long-term AGMD operation of 40 h. In another work, an ultrasonic irradiation technique was applied to AGMD system to enhance the permeate flux [153]. An ultrasonic stimulation of resonance frequency of 20 kHz and irradiation power up to 90 W was applied to a flat-plate AGMD system of PTFE membrane with a temperature difference up to 55°C. The results showed that the flux was increased up to 25%.

A two hollow fiber set based compact membrane device was developed by Singh and Sirkar [83], the first set consists of porous hydrophobic hollow fibers of either PP or PVDF. The second set consists of solid PP through the bore of each fiber. Different modules with different packing densities of hollow fibers were investigated for desalination of brine containing 1% NaCl as shown in Table 1. Experimental results showed that the flux values using modules with porous PP hollow fibers are significantly higher than those in the module with PVDF. In general, 25 kg/m^2 h water vapor flux were produced. In addition to the most popular polymers such as PP, PVDF, and PTFE, MD membranes can be made from their copolymers with enhanced hydrophobicity and durability. Table 2 shows the types of the modified AGMD membranes with their characteristics and the used feed solutions found in the literature.

In another study by Wang et al. [155], hollow fiber membranes with three different thickness isotactic polypropylene (iPP) were prepared through thermally induced phase separation (TIPS) with cosolvent di-n-butyl phthalate and dioctyl phthalate. The ratio of membrane thickness to membrane inner diameter was held constant at 0.2. The maximum value of water flux and GOR reached 6.62 kg/m^2 h and 6.95, respectively, for a membrane thickness of 67.2 μm, while the maximum thermal efficiency of 89.42% was achieved for a membrane thickness of 100.3 μm. The authors claim that the prepared iPP hollow fiber membrane by TIPS method has great potential to be considered in AGMD process in future.

Electrospun fibers can be assembled into a nonwoven like structure. By changing the spinning conditions, the porosity, pore size, and thickness can be tuned [158]. The first attempt to use electrospun nanofiber membrane in MD was produced by Feng et al. [39]. Electrospun PVDF membranes were prepared using a typical electrospinning setup, where 18 wt% solution of PVDF Kynar761, Elf-Chem USA, in DMF was used as the polymer dope. The polymer solution was electrospun at a rate of 2 mL/h. Using AGMD configuration, the observed membrane flux was comparable to those obtained by the commercial membranes (5–28 kg/m^2 h) at temperature differences ranging from 25°C to 83°C. In addition, the membrane performance was stable after almost 2 months of operational period.

Recently, Woo et al. [156] conducted the electrospinning technique to prepare the dual-layer hydrophobic/hydrophilic nonwoven membrane for distillation. The top layer for the neat single and dual-layer nanofiber membranes composed of a hydrophobic polyvinylidene fluoride-*co*-hexafluoropropylene (PH) while the bottom support layer was made of either PAN, nylon-6 (N6), or polyvinyl alcohol (PVA) nanofibers which were fabricated with and without heat-press post-treatment. The active layer of all electrospun nanofiber membranes which faces the feed side exhibited a highly porous (porosity > 80%), rough, and hydrophobic surface,

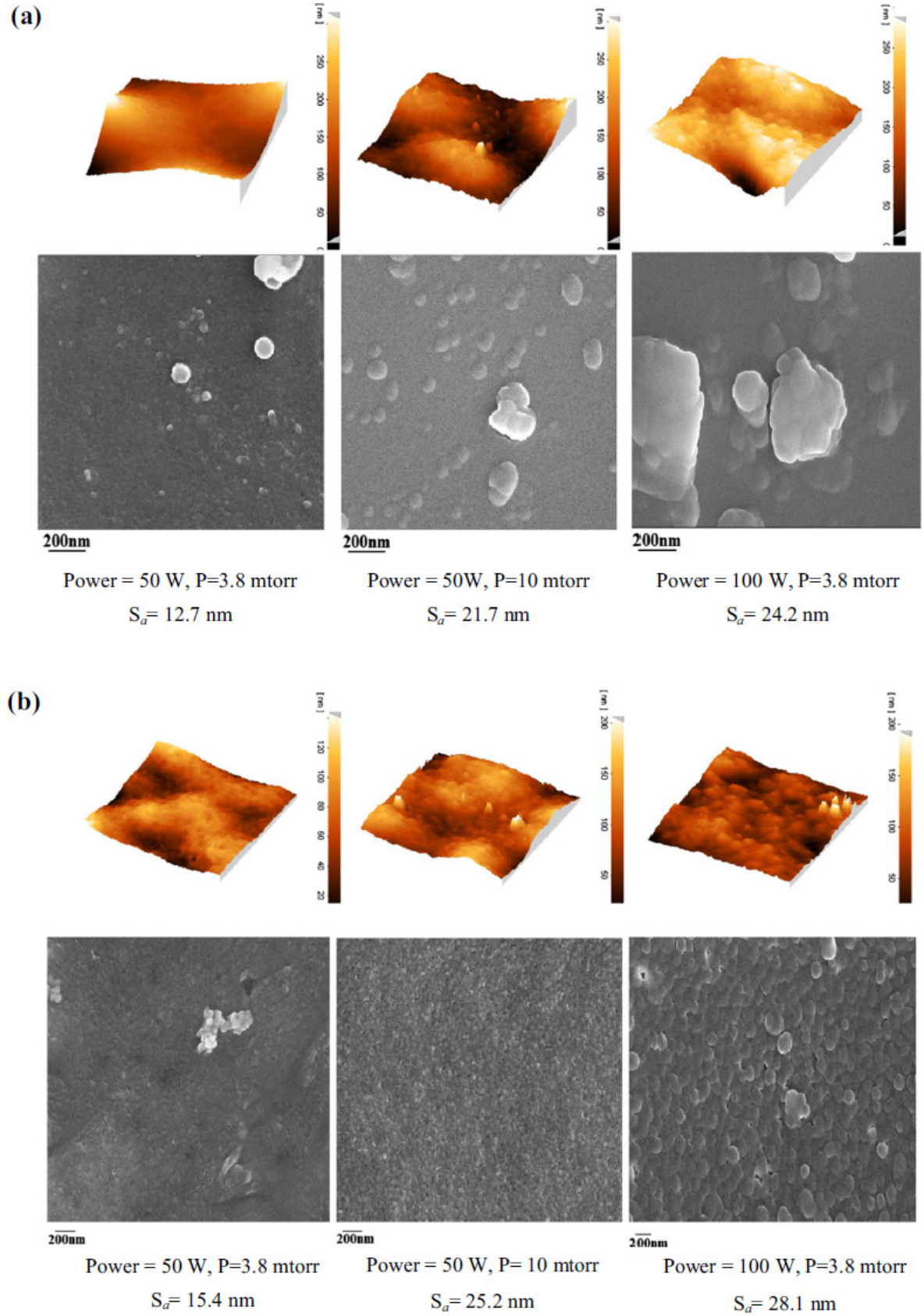

Fig. 13. Atomic force microscopy (top) and SEM (bottom) scans of fluorocarbon plasma polymer films deposited at different pressures and powers at sputtered target–substrate distances of (a) 5 and (b) 10 cm [149].

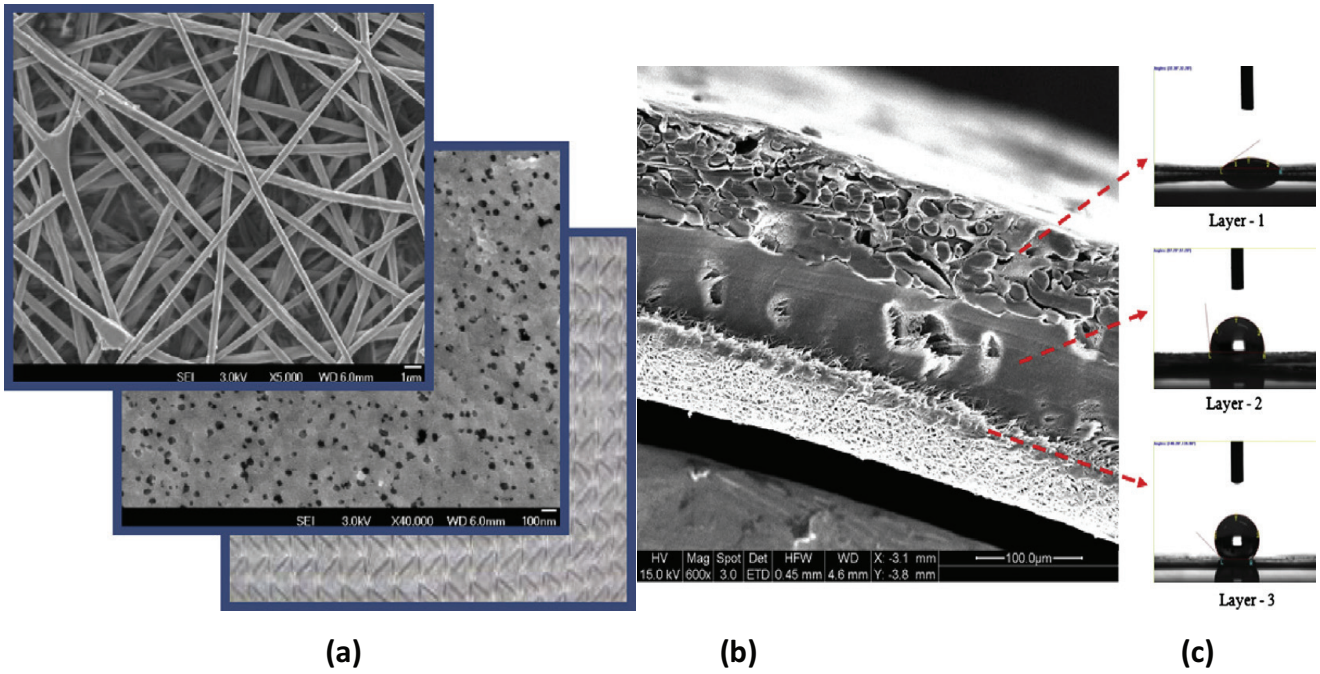

Fig. 14. SEM image of the various layers of the triple layer membrane. Layer 3 faces the hot feed water side and layer 1 faces the side with the air gap. (a) Top surface of the triple layer membrane in order of layer numbers from top to bottom. (b) Cross-section view of the triple layer membrane, and (c) contact angle of the respective layers [152].

Table 1
Details of the modules used for AGMD experiments [83]

Membrane	No. of porous hollow fibers	No. of solid fibers	Length (cm)	I.D of porous hollow fiber (μm)	Effective surface area of porous hollow fibers (based on I.D) (cm^2)	Outside surface area of porous hollow fibers/ volume of shell (cm^{-1})	Packing fraction
Module #1	10	10	15.5	330	16	2.51	0.072
Module #2	14	14	14.4	330	20.9	3.675	0.101
Module #3	21	21	14	330	30.35	5.269	0.151
Module #4	29	29	14.2	330	42.7	7.31	0.210
PVDF E	7	35	15.5	691.7	23.58	2.59	0.176
PVDF H	3	35	14.0	900	11.87	2.24	0.196

while the other side was hydrophilic with varying porosity. The prepared membrane produced a permeate flux of about (10.9–15.5 kg/m^2 h), which was much higher than that of a commercial PVDF membrane. In another work, fabricated carbon nanotubes composite electrospun membrane was studied and has showed a higher permeate flux compared with poly(vinylidene fluoride-*co*-hexafluoropropylene) electrospun membrane in DCMD configuration [167]. However, there is no study of AGMD process that uses modified membranes with nanotubes found in literature. Therefore, the authors suggest that this area should be focus of investigation in future.

5.2.3. Ceramic membranes

Metal oxides of titania, silica, zirconia, alumina, or iron are commonly used for the fabrication of ceramic membranes. Some researchers preferred the ceramic membrane over polymeric membrane due to its fundamental properties, such as high mechanical strength and long life. Similar to the hydrophilic polymers used in MD processes, ceramic membranes (i.e., zirconia, alumina, and titanium) need to be modified to improve their hydrophobicity. The first example of using ceramic membrane in membrane desalination was presented in 2004 by Larbot et al. [159] where zirconia and alumina membranes were grafted with fluoroalkylsilanes (C8, C1, and C6). The whole process was controlled by thermogravimetric analysis (TGA) apparatus. Three tubular membranes were tested, one from alumina and two from zirconia. A ZrO_2 membrane with 200 nm pore diameters (denoted as Z2), was prepared in the laboratory, while a ZrO_2 membrane, 50 nm (denoted as Z1) in pore diameters, and an Al_2O_3 membrane with 200 nm pore diameters (denoted as A1), were produced by Pall Exekia. Results showed that surfaces had a hydrophobic behavior with high values of contact angles and that the contact angle values were independent of pore diameter. Using NaCl solution with different NaCl molarity as feed solution, the observed flux was highest for the Z2 membrane

Table 2
Modified AGMD membranes found in the literature

Reference	Modified membrane type	Thickness (μm)	Pore size (μm)	Feed solution with its observations	Flux (kg/m^2 h)
[154]	PVDF/LiCl/DMA 8/3/89	Not available	0.35	1%–2% aqueous NaCl solution, T_f = 59.85°C, T_p = 19.85°C	23.4
[141]	G/PVDF-HFP	100	0.86	3.5 wt% NaCl, T_f = 60°C, T_p = 20°C, salt rejection 99.99%	22.9
[140]	G/PVDF-0.5	88	0.11	RO brine from CSG produced water, salt rejection 99.99%, T_f = 60°C ± 1.5°C, T_p = 20°C ± 1.5°C	20.5
[155]	iPP (M-1)	67.2	0.25	6 wt% NaCl	6.6
[156]	Dual-layer nonwoven nanofiber membranes PH/PAN, N6, or PVA	92.7	0.18	3.5 wt% NaCl, T_f = 60°C, T_p = 20°C	15.5
[157]	Clay–alumina	–	1.43	Solution, salt rejection 99.96%, temperature difference 60°C	4.1
[158]	FAS grafted ceramic membranes	–	0.05 and 0.2	NaCl, T_f = 90°C, T_p = 5°C, salt rejection close to 100%	6.7
[39]	Electrospun PVDF membranes	–	0.2	1 wt% NaCl, temperature difference 60°C	12.0
[136]	Polyvinylidene fluoride	–	0.1	1 g/L NaCl, T_f = 60°C	13.0
[152]	Triple layer membrane:	175	0.1	3.5 wt% NaCl, T_f = 80°C	15.2
	Layer 1: PET support				
	Layer 2: PVDF casted				
	Layer 3: PVDF nanofiber				
[159]	Grafted ceramic membranes:	–		NaCl molarity is 0.1 M, T_p = 5°C, T_f(Z2	
	Z1		0.05	and A1) =95°C , T_f(Z1) = 90°C	3.97
	Z2		0.2		8.43
	A1		0.2		6.8
[160]	Grafted Al hollow fiber ceramic membrane by the phase inversion	181	0.185	6.5 wt% NaCl, T_f = 80°C, T_c = 20°C	30.6
[161]	Grafted ceramic membranes using Tunisian clay	–	0.18	NaCl molarity is 1 M, T_f = 95°C, T_p = 5°C, flow velocity = 2.6 m/s	6.5
[162]	Grafted ceramic membranes using Tunisian olive oil molecules.	9	0.011	99% salt rejection	7.0
[163]	Modified ceramic membranes using Zr, Al and AlSi	–	0.05	1 mol/L NaCl, ΔT = 70°C	4.6
[164]	Modified ceramic membranes using:	–		0.5 M NaCl solution, T_f = 95°C	
	Zr50		0.05		4.7
	Ti5		0.005		0.83
[165]	Ceramic titania membranes and metal oxide			3 wt% NaCl, *Tf* = 90°C, *Tc* = 5°C	3.7
[166]	Modified nanospiked glass membrane	500	4	5 wt% NaCl, T_f = 95°C	11.1
[150]	Plasma coating using perflourohexane (PFB) and hexafluorobenzene (HFB) on PET	–	<0.3	Juice	4.0
[147]	Surface-modifying macromolecules on polyetherimide (PEI)	64.7	0.027	30 g/L NaCl, T_f = 60°C, *Tp* = 20°C, salt rejection 99.94%	5.4
[148]	Modified PVDF by electrospinning and CF_4 plasma	150	0.81	RO brine, salt rejection 100%, T_f = 60°C ± 1.5°C, T_p = 20°C ± 1.5°C	15.3

when temperature difference was kept at 90°C and the molarity at 0.1 M (Table 3).

Das et al. [157] fabricated a clay alumina (0%, 20%, 40%, and 55% clay by weight and rest alumina) that were maintained in porous support preparation by extrusion followed by sintering at 1,300°C for 2.5 h to obtain 3 mm/2 mm (outer diameter/inner diameter) capillary. 1H, 1H, 2H, 2H-perfluorodecyltriethoxysilane (97%) (C8) was used as grafts to modify the surface hydrophobicity. Capillary with 45 wt% ceramic produced a pore size of 1.43 micron and was considered as a perfect candidate for grafting with C8 polymer. The maximum theoretical permeate flux obtained was 4.11 kg/m^2 h, while the experimental flux value was within ±5% of the theoretical values. Another type of ceramic membrane (Fluorosilanes [FAS] grafted ceramic membranes) was prepared and characterized in AGMD by Krajewski et al. [158]. The hydrophobic active layer was created by grafting 1H, 1H, 2H, 2H-perfluorodecyltriethoxysilane (C8 compound) on commercial ceramic membranes. The membrane morphology of the asymmetric zirconia membrane is presented in Fig. 15. The efficiency of grafting process was characterized by TGA, contact angle, and LEP_w measurements. The results showed that the rejection of NaCl was found to be close to 100%, indicating good hydrophobic behavior of the FAS grafted ceramic membranes. The permeate fluxes were in the range of 1.0–7.0 kg/h m^2, depending on NaCl concentration and temperature difference, which are comparable to those observed for the polymeric hydrophobic membranes. A similar study by Gazagnes et al. [163] was conducted in which hydrophobic ceramic membranes of different nature; zirconia, alumina, and aluminosilicate, with pore diameters of 50, 200, 400, and 800 nm, were chemically modified with 1H, 1H, 2H, 2H-perfluorodecyltriethoxysilane and tested in desalination of seawater and NaCl solutions of various concentrations (0.5–2 mol/L) using AGMD. High rejection rates of 95%–100% were obtained. The same modification was grafted elsewhere on the Tunisian clay ceramic membranes with pore diameters of 0.18 μm (MF) and 15 nm (UF) [161]. Both seawater and sodium chloride were used as a feed solution using the modified membrane in AGMD cell. An appropriate flux (6.5 kg/m^2 h) with high rejection (99.2%) was obtained for desalination of 1 mol/L NaCl at feed and permeate temperatures of 95°C and 5°C, respectively. Again, the same modification was grafted recently on alumina hollow fiber ceramic membranes prepared by the phase inversion technique [160]. A very high flux (30.6 kg/m^2 h) was obtained using the modified membrane through AGMD system.

Recently, a UF ceramic membrane was modified by grafting Tunisian olive oil molecules [162]. Although the modified UF membrane gave a high rejection of seawater, the water permeability showed a high decrease from 90 to 7 kg/m^2 h bar, before and after grafting, respectively. In another work, membrane was prepared using the grafting parameters applied for the grafting of C8 on zirconia powder [168].

A comparison of various MD methods for desalination (AGMD, DCMD, and VMD) using modified zirconia and titania ceramic membranes with pore diameters of 50 nm (Zr50) and 5 nm (Ti5) by grafting perfluoroalkylsilane molecule (C8) were presented by Cerneaux et al. [164]. Using NaCl solution as a feed solution, Zr50 showed rejection rates higher than 99% obtained in DCMD and AGMD configurations. Whereas in VMD configuration, lower rejection rates were obtained. The highest value of flux (4.7 kg/m^2 h)

Table 3
Daily flux and rejection rate for different NaC1 solutions and temperature differences for the three membranes [159]

NaCl molarity	Feed/permeate temperature, °C	Average daily flux, kg/d m^2	Rejection rate, %
A1 membrane			
0.001	63/5	21.4	90
	95/5	140.5	96
0.01	63/5	19.8	95
	95/5	156.1	99.5
0.1	63/5	20.9	100
	95/5	163.2	100
1	63/5	18.2	100
	95/5	129.5	100
Z1 membrane			
0.1	60/5	16.8	100A
	90/5	95.3	100
1	60/5	15.7	100
	90/5	82.7	100
2.9	60/5	12.1	100
	90/5	68.8	100
Z2 membrane			
0.1	60/5	28.2	99.0
	95/5	202.3	99.5
1	60/5	25.6	99.1
	95/5	165.7	98.5

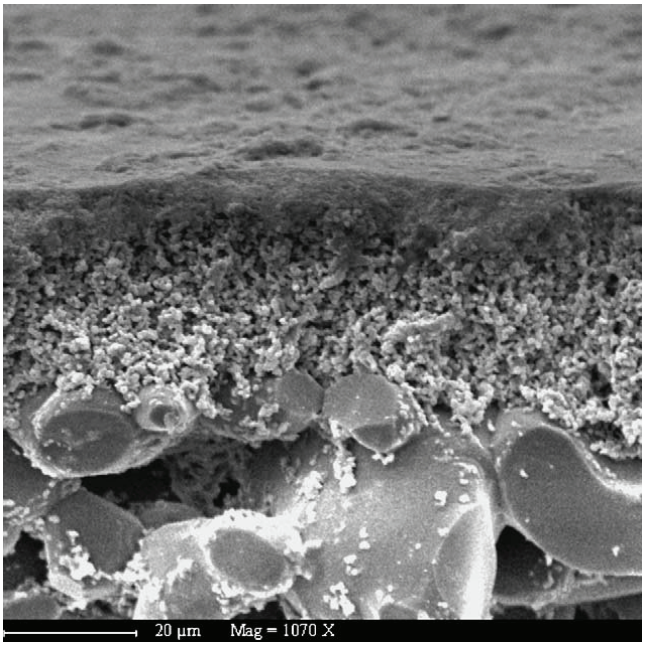

Fig. 15. SEM picture of the morphology of the asymmetric zirconia supported alumina membrane [158].

was obtained while performing AGMD at a feed temperature of 95°C. Concerning Ti5, similar high rejection rates were obtained in VMD and DCMD. But poor flux of only 0.83 kg/m^2 h was measured while performing DCMD compared with 6.1 kg/m^2 h while performing VMD. In another study, ceramic titania membranes and metal oxide powders (Al_2O_3, TiO_2, and ZrO_2) were modified by various perfluoroalkylsilanes molecules [165]. A 3.7 kg/m^2 h of flux was obtained for desalination of NaCl solution (3 wt%) using AGMD configuration.

5.2.4. Glass membranes

Glass membranes are another type of membranes which can be used in AGMD process for water desalination. Superhydrophobic glass membranes that have ordered arrays of nanospiked microchannels were fabricated by Ma et al. [166] using a process that involves fiber drawing, template removal, differential etching, and surface modification. The presented membranes have shown higher flux and better antifouling ability than those of existing polymer membranes, especially at high salt concentration. This is because of its large pore diameter, narrow pore size distribution, straight pore shape, water-repelling ability and high chemical and thermal stabilities.

6. Fouling and scaling in AGMD

Fouling has two main types: (i) biological fouling is growth of microorganisms, such as bacteria and viruses, and aquatic organisms, such as fungi and algae, on the membrane surface, (ii) organic fouling occurs through adsorption of natural organic matter compounds on membrane, causing gel formation of macromolecular substances. On the other hand, scaling occurs due to precipitation deposits resulting in high concentration of bulk solution on the membrane surface [169–172]. In MD configuration, both fouling and scaling have lower effect than the conventional pressure-driven membrane separation (e.g., RO) as the operating pressure is relatively low. However, Shirazi et al. [170] concluded that membrane fouling in MD depends on the membrane properties, module geometry, feed solution characteristic, and operating conditions. Moreover, fouling process accelerates wetting of MD membranes. The indicted parameters for this phenomenon are flux decline, membrane hydrophobicity reduction, and permeate quality [173,174]. Other works concluded that the membrane fouling mitigation techniques in AGMD are different than that in other configurations such as DCMD [75,175]. Therefore, this section will review and highlight the fouling occurred in AGMD and its mitigation techniques.

A pilot treatment of CSG produced water by a combination of UF/RO and AGMD was conducted by Duong et al. [175]. The authors reported that the possible precipitation of silica and calcium may pose a scaling risk in long-term operation. As a result, a commercial anti-scalant was added to the CSG water just before the RO treatment at a dosage of 5 mg/L. The results showed that operating the pilot MD system at a low permeate flux (1.4 kg/m^2 h) together with anti-scalant could be an effective measure to control membrane fouling. Another long-term field operation on a AGMD pilot plant [176] observed that mineral acids such as HCl and H_2SO_4 could effectively clean and remove a significant amount of fouling and reduce the wetting of the membranes. In other works, a diluted HCl (2%–5%) has been used to wash and remove inorganic scale deposited on the membrane surface after treatment of tape water using AGMD system [177,178]. Moreover, it was found that the fouling layer consisted of uneven accumulation of granular pollutants and cuboid crystals. After the washing process, the flux recovered to its initial value.

Given their corrosive nature, mineral acids are unsafe for use and storage in a household, which is the key target of small-scale seawater AGMD systems. Therefore, Duong et al. [179] used vinegar, mainly consisting of acetic acid (i.e., 5–8 vol%) as the cleaning agent and found it to be much more efficient than fresh water. In one study, precipitation of silica compounds formed on the membrane after filtration of demineralized water using NF/MD system [180]. The silica clogged capillary membrane inlets, causing a gradual decline of the module efficiency. The silica layer was significantly limited with acidification of NF permeate to pH 4. In another work, AGMD system was employed to treat pond water. A decline in flux was reported after 800 h as a result of biofouling [18]. In this work, the original flux was restored by reversing the direction of the flow.

Recently, a very high salty concentration (65 g/L of NaCl), above the saturation concentration of NaCl at different feed inlet temperatures up to 82°C, was tested using the AGMD configuration [181]. The authors claimed that, at saturated phase, crystallization fouling occurs by blocking or wetting the membrane pores due to the continued deposition and growth of salt crystals on the membrane surface and inside the membrane pores. Moreover, they suggested a simple mitigation technique to overcome the fouling by washing the membranes with water which is enough to partially recover the initial properties of the membrane. More details about fouling, scaling, and cleaning are found elsewhere [62,63].

7. Integration of AGMD with solar energy and other renewables

Utilization of solar thermal energy for solar membrane distillation desalination system (SMDDS) is a green technology for the solution of the water resource problem and high energy cost [182–185]. The components of a SMDDS system are a solar collector, heat storage tank, heat exchanger, and MD module as shown, for example, the solar DCMD in Fig. 16 [186]. The energy generated by the solar collectors and photovoltaic (PV) panels can either provide the thermal energy supply for the low operating temperatures required by MD or produce electricity required to run the low-pressure pumps in MD process. The feed stream is heated using energy from a solar collector through heat exchanger, while the temperature of the permeate stream is reduced by heat exchange with cooling water in another heat exchanger. The cooling water also acts as the feed make-up, and so this energy is also substantially recovered. In addition, the latent heat required to evaporate the hot water is recovered when the condensation occurs in the cold stream line.

A hybrid VMD with solar energy has been investigated by few researchers [187,188] where extra energy is required

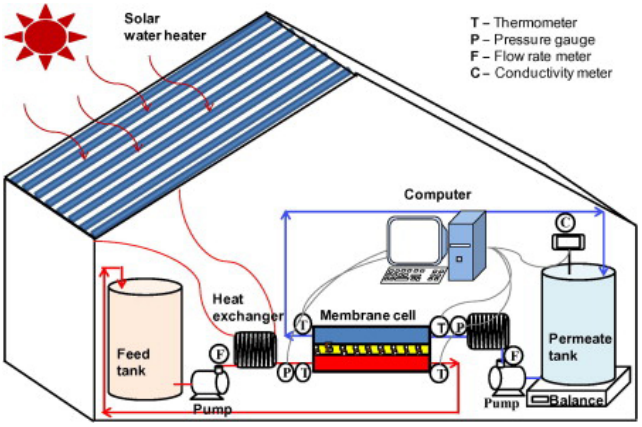

Fig. 16. Schematic diagram of SMDDS system using DCMD [186].

from solar collectors to apply the low pressure (vacuum) on the membrane permeate side. AGMD utilizing solar energy is widely used for its technical simplicity, long maintenance-free operation periods, and production of high quality water.

Banat et al. [189,190] developed a small scale stand-alone solar desalination system in Irbid (Jordan) based on a spiral wound AGMD to provide potable water in remote areas having abundant solar energy. The required energy was supplied entirely by flat plate solar thermal collectors with 5.73 m^2 area and an auxiliary electrical energy supply by a PV panel. A brackish feed water is directly heated in the absorber of the collector. The system produced a flux of 120 L/d with an approximate distillate conductivity of 5 μS/cm with 10 m^2 membrane area. The thermal energy required by the process was in the range of 200–300 kW h/m^3 and the GOR was found to be in the range of 0.3–0.9. Later, a similar pilot plant was installed in Alexandria (Alexandria University, Egypt) [183] and it gave a high salt rejection of 99.5%. In another study by Banat et al. [190], a similar pilot plant with larger flat plate solar thermal collectors (72 m^2) in Aqaba port in south of Jordan was installed to desalinate seawater (55 mS/cm) for a 90 d operation. The results showed that flux varied from 5 to 27 kg/m^2 h with an electrical conductivity varying between 20 and 250 μS/cm. Later, a similar pilot plant was installed in Spain but in this system five membrane modules were used with a maximum design capacity of 1,600 L/d with a solar collector area of 90 m^2 [33]. The maximum permeate flux was about 75 L/d.

In another work, Cipollina et al. [185] designed, developed, and tested a laboratory scale MD unit coupling with solar energy. Multi-stage arrangement, compactness of the unit, internal heat recovery and integration with a heat exchanger for the utilization of waste heat or solar energy for the final brine heating, were the unique characteristics of the unit. Different types of MD such as free air gap, permeate gap, and partial vacuum air gap were tested during the investigation and the effect of the air gap configuration was observed. In their model, a flux of 12 kg/m^2 h was obtained at feed temperature of 80°C and flow rate of 1.2 L/min. In another work, AGMD with solar absorption function (SAF–AGMD) was investigated experimentally [191]. The solar system power consists of eight lamps with adjustable irradiance by a transformer. The results showed an increase of 2%–8% in flux by the solar absorption function was seen.

Duong et al. [91] performed the optimization of the AGMD system in terms of distillate production, solar thermal, and electrical energy consumption. The results showed that a AGMD for seawater desalination can be achieved with 90 kW h/m^3 thermal and 0.13 kW h/m^3 electrical energy consumption. These values suggest that a small scale and off-grid seawater desalination is commercially feasible at locations where the solar thermal or low-grade heat source is available. Chang et al. [192] experimentally tested SMDDS utilizing AGMD configuration. A laboratory-based system with automatic control function using the proportional-integral control algorithm was developed in this work. The control structure adopted proportional integral temperature control for the MD and solar thermal subsystems. The optimization process showed the operating strategies for maximum water production. The proposed proportional integral control scheme could give an output performance up to 80% of water production for a sunny day operation. Later, the same authors optimized the same system using a dynamic modeling on the Aspen custom modeler (ACM) platform [193]. In this model, the effect of solar radiation intensity, thermal energy storage tank configurations, and flow rates effect on the performance of the system were studied. It was concluded that simple thermal storage tank and lower flow rate of the module are beneficial for the amount of water produced. The same authors investigated another SMDDS system at a small scale to produce fresh water for small communities in remote arid areas [194]. They used a flat sheet membrane module in their work.

A model of a solar-driven AGMD system was considered by Chen et al. [195]. The system consisted of solar thermal collector, storage devices, heat exchanger, and MD unit. The system was operated with indirect solar energy due to the intermittent nature of the sunlight. The ACM software was utilized for modeling and simulation of each individual unit. With a given amount of water production rate, 10 design parameters were analyzed to get the minimum total annual cost (TAC) using design degree of freedom analysis. The minimum TAC per cubic meter of pure water production was found at 500 W/m^2. From the simulation results, it was concluded that the pure water production can be kept at constant level irrespective of the weather conditions.

Galvez et al. [196] conducted a project called seawater desalination by innovative solar-powered membrane distillation system (MEDESOL) supported by the European Commission under the Horizontal Program "Global Change and Ecosystems" (Global 4). The main objective of this project was the development and experimental assessment of the solar multi-stage MD concept in order to develop a high-efficiency and cost-effective system for seawater desalination in EU and developing countries. The system involved the integration of several MD modules into a multi-stage MD system in order to minimize the specific energy consumption. Another theoretical model tested the energy efficiency of single-stage MD-based desalination cycles in each of the MD configurations including AGMD, DCMD, and VMD [197] at a bench scale. Both AGMD and DCMD have potential for high GOR. The same authors conducted the same model experimentally with AGMD configuration

using a composite solar-absorbing hydrophilic membrane [198,199]. The top layer of the composite membrane can absorb the solar energy while the underneath hydrophobic surface ensures the required non-wettability. Moreover, they fabricated serpentine flow channel for the coolant and condensate channels as shown in Fig. 17. The importance of reducing the pressure in air gap has also been highlighted in this work. This gave a significant improvement, with performance increasing over 1.5 times as the gap pressure is reduced from 1 to 0.4 atm.

In another study, an integration of evacuated tube and concentrated photovoltaic/thermal (CPV/T) solar collectors

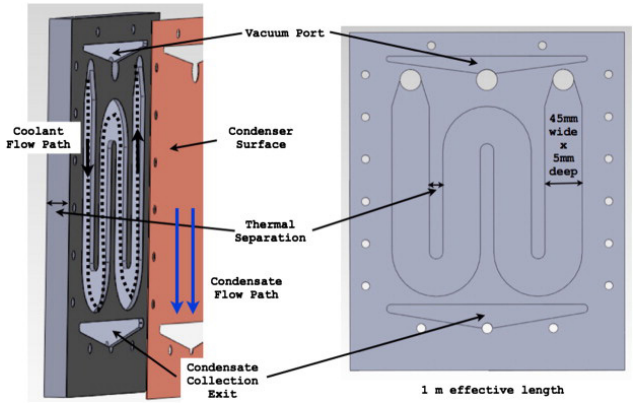

Fig. 17. Serpentine flow channel in a square area showing the coolant channel and condenser surface [198].

with AGMD unit at a bench scale for seawater desalination was conducted by Hughes et al. [200]. The collector used high concentrating optics, allowing for a smaller area of receiver to be used as predicted in Fig. 18. The receiver incorporates a hybrid design, where a thermal collector is placed directly beneath the PV cells. The waste heat generated by the cells is cooled using a salt solution which is pumped into AGMD cell. The cooling process is very important to prevent decrease in the cells efficiency. Therefore, this integration process provided two types of energy; (1) a thermal energy which is required to drive the AGMD unit, and (2) an electrical energy which is required to power the pump and tracking devices. The AGMD module was tested for a fluctuating inlet feed temperature due to the variable energy produced by the solar energy source during the day. The integration process gave a maximum flux of 3.4 kg/m^2 h and a conductivity of 35 μS/cm.

Another solar-powered AGMD system was studied by Kullab et al. [201] at lab scale. The system consisted of AGMD unit integrated with non-concentrating solar thermal collectors and was used to desalinate salty water. A theoretical model was used to analyze the experimental data. Scale-up of the MD unit through the model was accomplished through experimental data obtained from an AGMD test alone and trials were conducted with various feedstock TDS levels, temperatures, and flow rates. The model was successfully applied to the solar data obtained from a case study in Gaza, Palestine. The results showed that the flow rate of permeate was 8.5 m^3/h with high quality water (<10 ppm TDS)

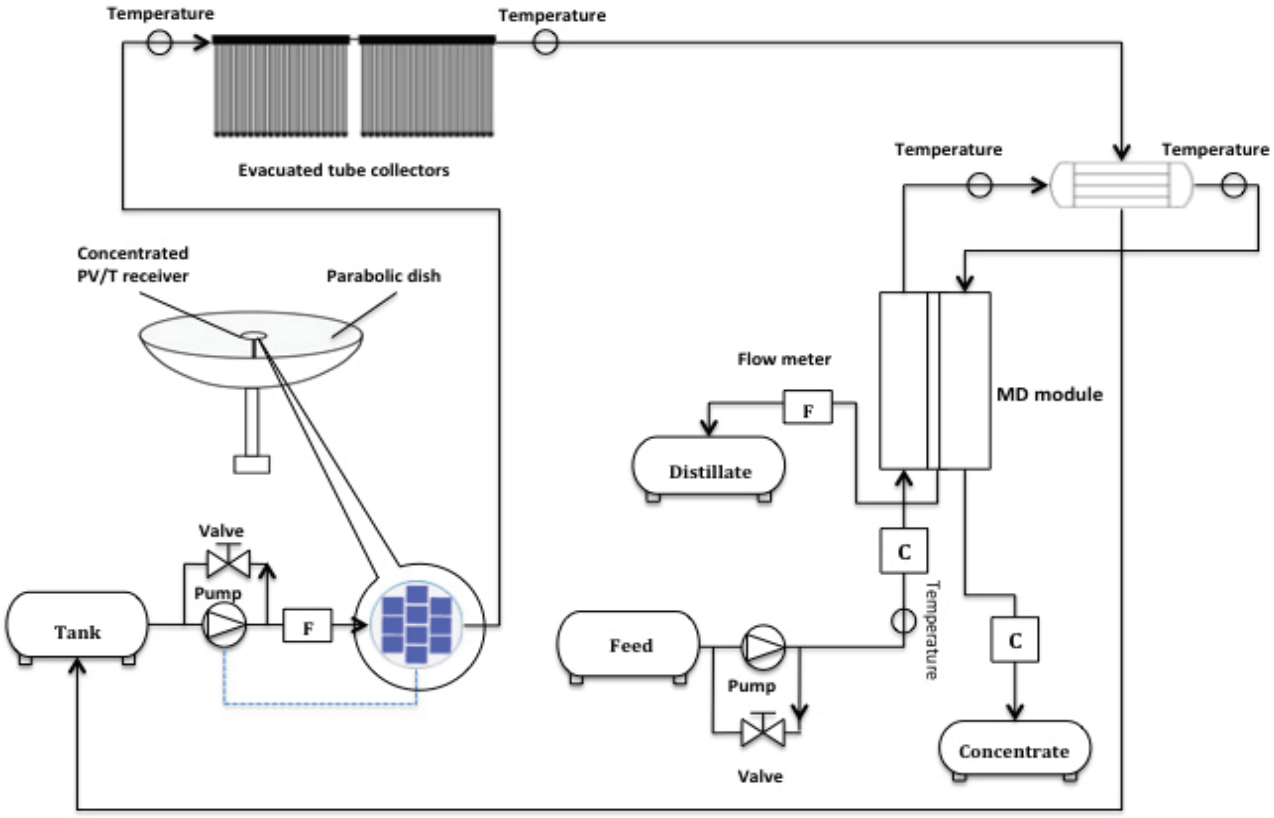

Fig. 18. Schematic diagram of CPV/T solar desalination system [200].

and the power consumption was 150 kW h/m^3. In another work, Khan et al. [202], Khan and Martin [203], and Mohan et al. [204] designed an integrated biomass-based polygeneration system with AGMD providing fresh water to meet the needs of 30 households in a rural village in Bangladesh. This system was successfully implemented to treat ground water with high concentration of arsenic 1,600 μg/L as the product water arsenic levels were lower than detection limits (0.4 μg/L) [205].

Another small unit based on integration of solar domestic hot water and MD (SDHW-MD) was studied and installed in UAE [206,207]. The unit was designed to achieve the demand of 15–25 L/d of pure drinking water and 250 L/d of DHW for a single-family villa. Experimental analyses were performed during summer on flat plate solar collectors having different aperture areas. The average hot-side temperature ranged from 50°C to 70°C awhile the average cold-side temperature was observed to be 35°C. Experimental results were compared with empirical relation–based model developed using laboratory experimental data along with PolySun simulations. Monthly energy consumption and water production profiles were obtained which formed a basis for detailed dynamic simulation and optimization of system performance. Recently, solar membrane distillation (SMD) using AGMD configuration was investigated at small scale [208]. In this work, a hierarchical control system composed by two layers is used for optimizing the operation of a SMD pilot plant, in terms of thermal efficiency, permeate flux, and cost savings.

8. Modeling of AGMD

8.1. Techniques of AGMD modeling

Some of the research presented in the previous sections include modeling and simulation to predict the effect of the different operating conditions and geometrical parameters on the performance of the MD process. The research work in this field can be divided into different categories based on the focus of study and the model details. Some available models in the literature focus on predicting two-dimensional (2D) or three-dimensional (3D) flow field distributions in the feed channel to reduce the temperature and concentration polarization. Other models focused on the membrane structure in order to enhance the understanding of the mass transfer of the water vapor using either generic geometries, which consist of interconnected cylinders, or based on empirical relations. The complete MD module has been studied with simplified analytical and empirical model while the model parameters were obtained from the experimental work [209].

Alsaadi et al. [94] has developed a one-dimensional (1D) model for flat sheet type modules. The model was based on mathematical equations that describe the heat and mass transfer mechanisms of a single-stage process to simulate AGMD modules in both co-current and counter-current flow regimes. They validated the model with experimental data obtained under different operating conditions and parameters. The predicted values of water vapor flux were compared with the experimentally observed values and good agreement was achieved (with ±10%). Khalifa et al. [210] used an analytical model for heat and mass transfer to predict the permeate mass flux and they found that the model delivered good results in comparison with experiments. In another study, Alklaibi and Lior [114] carried out a modeling and sensitivity analysis for AGMD module. They modeled the AGMD module as a 2D conjugate problem in which a simultaneous numerical solution of the momentum, energy, and diffusion equations of the feed and cold solutions have been carried out. They validated the numerical results with that available from experiments. Warsinger et al. [211] set a model based on 1D transport of mass and energy across a unit cell, with 400 unit cells used to describe the experimental system. The model takes input parameters including Reynolds number, bulk temperature and mass flow rate of the hot side feed, and condenser temperature and calculates a variety of parameters including Nusselt numbers, Sherwood number, Schmidt number, effective conductivities, condensation film thickness, diffusion, thermal resistances, and MD membrane flux. The modeling includes concentration and temperature polarization effects in the feed channel near the membrane surface.

8.2. Computational fluid dynamics and optimization

In order to understand the performance of the AGMD module, the complete MD unit has been investigated. Different authors (e.g., Chang et al. [212] and Cheng et al. [213]) built the models for DCMD and AGMD modules on Aspen Plus platform. They have used the model to analyze and optimize large-scale systems. Khayet and Cojocaru [214] constructed an experimental based artificial neural network (ANN) model to describe the performance of AGMD process for different operating conditions. These conditions, which represent the input variables of this process, include the air gap thickness, the condensation temperature, the feed inlet temperature, and the feed flow rate of salt aqueous solutions. The response was set to the performance index, which takes into consideration both the permeate flux and the salt rejection. A neural network–based optimizing control system for seawater desalination solar-powered MD unit has also been performed [215]. The model has been trained and tested using experimental data collected for the purpose. Afterwards, the NN model has been used for the analysis of the process performance under various operating conditions similar to one conducted recently by Shirazian and Alibabaei [216].

Other researchers have applied the response surface methodology for modeling and optimization of MD desalination process [112]. Regression models have been developed to predict the performance index and the specific performance index which takes into consideration the energy consumption as function of different variables. They validated the model statistically by analysis of variance and good agreement was found with experimental data. AlcheikhHamdon et al. [217] analyzed a complete set of experimental data on AGMD using the methods of FD. They investigated a two-level and three-level FD to examine the influence of the main operating parameters on permeation flux of water. In another work, heuristic approaches have been used to optimize AGMD system based on the analysis of heat and mass transfers within the system [218]. An algorithm was developed and employed to find the optimal set of variables for the maximum permeate flux of distilled water. The variables considered include feed water temperature, coolant water temperature, air gap width, feed flow rate, and coolant flow rate.

One research work focused only on a separate module section of the AGMD module. Warsinger et al. [84,211] carried out a modeling study of the feed channel, the air gap, and the coolant channel separately. The model involved mass and energy conservation equations applied to each of the module sections. Each section was coupled with suitable transport equations. They considered mass transport through the membrane to be governed by binary diffusion as described by Lienhard [219]. The coupled equations were solved using Engineering Equation Solver. They have generated a grid independent solution.

The above studies modeled the module sections as a 0D, 1D, or 2D case and used simplified heat and mass transfer correlations. Detailed modeling in 2D or 3D using computational fluid dynamics (CFD) techniques has also carried out [220,221]. The goal was to understand the effect of, for example, using spacers in the module channels to reduce the effect of temperature polarization and to enhance the mass transfer rate [222]. To enhance production of AGMD systems, a channeled coolant plate was used and about 50% increase in mass transfer was reported [81]. In that study, 1D heat transfer model was developed and validated using the experimental data. Karbasi et al. [223] simulated the hydrodynamics in the feed channel of the MD modules. They investigated the effect of using turbulent promoters such as baffles, number of baffles, and change in the geometry of the module on the trans-membrane mass flux. They used the commercial package Ansys Fluent. In a modified AGMD module in which a temperature difference across the air gap is introduced, Chouikh et al. [132] numerically studied the air gap space using a 2D model. They solved the model using finite volume method.

Other group of researchers focused on the transport properties of the membrane. Guijt et al. [101] described water vapor transport across the membrane by the dusty-gas model that uses constant membrane mass transport parameters to describe simultaneous Knudsen diffusion, molecular diffusion, and viscous flow. The membrane mass transport properties were determined experimentally in separate experiments to obtain a predictive model. The Knudsen diffusion and viscous flow membrane parameters were determined with single-gas permeation experiments. The molecular diffusion membrane parameter was determined with binary gas diffusion experiments. Martinez et al. [224] determined the vapor transfer coefficient of hydrophobic membranes which is required for predicting and simulating MD. Mandiang et al. [225] and Rochd et al. [226] presented three theoretical models of flow and heat and mass transfers in MD unit of AGMD. The results on the effect of membrane pore size have been analyzed for the different mechanisms of mass transfer involved by estimating the flow of generated steam.

8.3. Analytical model for heat and mass transfer inside the AGMD module

The system which is considered in this part is shown in Fig. 19. The modeling part is taken from Khalifa et al. [210] which is considered to be a good representation of the available AGMD models. Mass and energy balances across the AGMD units are carried out in order to determine the water permeate mass flux. A similar model was recently studied using similar techniques [227]. The process of heat and mass transfer through AGMD include the following steps [123]:

- Convective heat transfer from hot feed solution to the membrane surface.
- Evaporation at the membrane pores entrance (feed membrane interface).
- Diffusion of water vapor across the membrane pores.
- Water vapor diffusion across the stagnant air gap.
- Vapor condensation onto the cooling plate.
- Heat transfer across the cooling plate.
- Convective heat transfer between cold solution and the cooling surface.

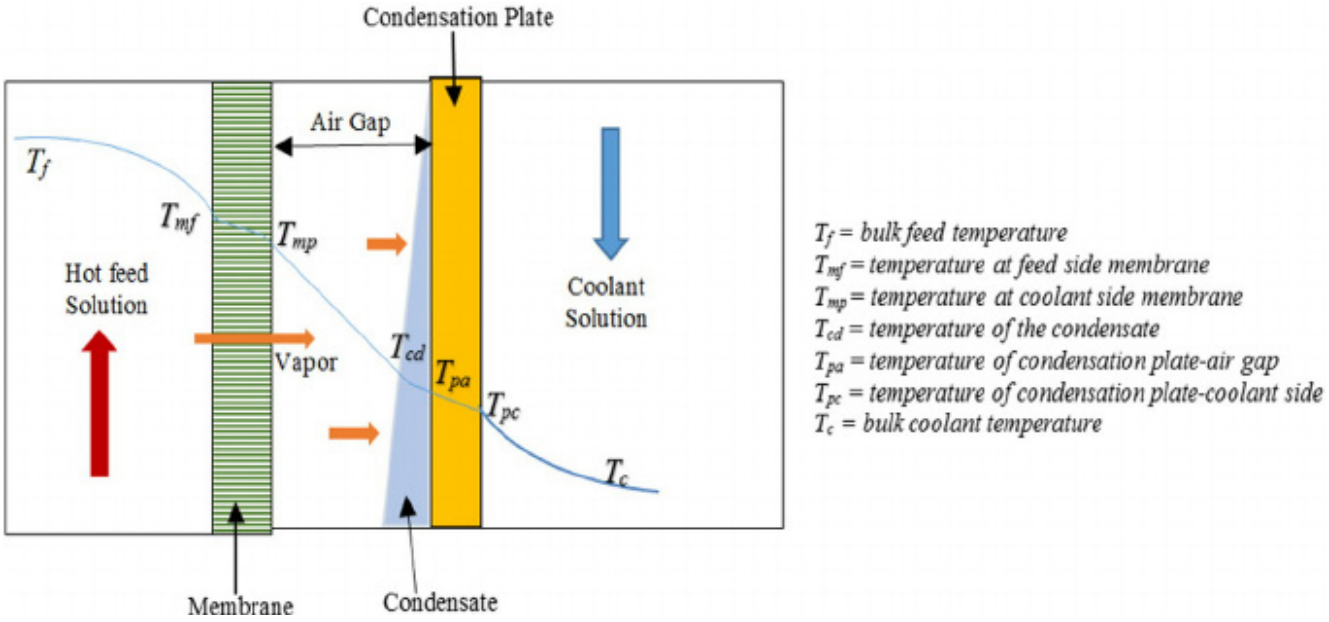

Fig. 19. Model of heat and mass transfer in the AGMD [93].

Both heat and mass transfer are discussed in detail in the following sections.

8.3.1. Heat transfer

Heat transfer takes place from the hot feed to evaporate water and to heat the membrane surface. This can be described at steady state as [131]:

$$Q = J_w C_{\mathrm{pf}} \left(T_f - T_{\mathrm{mf}}\right) + h_f \left(T_f - T_{\mathrm{mf}}\right) \tag{1}$$

where C_f, h_f, T_f, and T_{mf} are heat capacity, the convective heat transfer coefficient, the feed temperature, and the temperature at feed-side membrane, respectively. J_w is the water vapor mass transfer rate.

The heat transferred across the membrane consists of the conduction heat transfer of the membrane material and the gas filled pores which act as a stagnant film, and the heat from evaporation [123]. This heat flux is described by:

$$Q = \frac{k_m}{\delta_m}\left(T_{\mathrm{mf}} - T_{\mathrm{mp}}\right) + J_w H_{\mathrm{vl}} \tag{2}$$

where k_m is the thermal conductivity of membrane, δ_m is the membrane thickness, and H_{vl} is the evaporation enthalpy in kJ/kg which may be calculated using the following equation [74]:

$$H_{\mathrm{vl}} = 1.753T + 2024.3 \tag{3}$$

The heat transfer from the permeate side to the condensation side can be described by:

$$Q = Q_s + J_w H_{\mathrm{vl}} \tag{4}$$

where Q_s is the sensible heat transfer defined as $Q_s = h^*(T_{\mathrm{mp}} - T_{\mathrm{cd}})$. Here h^* is given in the literature [131,228] as $h^* = h_y(\mathrm{pe}/1 - e^{-\mathrm{pe}})$, where $\left(\mathrm{pe} = J_w C_{\mathrm{pg}} / h_y\right)$ and $h_y = k/b$.

Here k is the thermal conductivity of the gas phase, h_y is the convective heat transfer coefficient in the gaseous phase, pe is Peclet number, C_{pg} is the heat capacity of the gas phase. On the other hand, heat transfer from the condensation layer to bulk cold liquid is calculated using the following equations:

$$\begin{aligned} Q &= h_d\left(T_{\mathrm{cd}} - T_{\mathrm{pa}}\right) = \frac{k_c}{l}\left(T_{\mathrm{pa}} - T_{\mathrm{pc}}\right) \\ Q &= h_c\left(T_{\mathrm{pc}} - T_c\right) = h_p\left(T_{\mathrm{cd}} - T_c\right) \end{aligned} \tag{5}$$

where k_c is the thermal conductivity of the condensation plate, h_d is the condensate heat transfer coefficient, l is the plate thickness, and h_c is the coolant film heat transfer coefficient. The overall heat transfer coefficient from vapor/condensate liquid interface to the cooling water h_p is given by:

$$h_p = \left(\frac{1}{h_d} + \frac{1}{k_c} + \frac{1}{h_c}\right)^{-1} \tag{6}$$

The condensate heat transfer coefficient h_d can be obtained from the following equation [74,122,228]:

$$h_d = \left(\frac{g\rho^2 H_w k_p^3}{L\mu_d\left(T_{cd} - T_{pa}\right)}\right)^{\frac{1}{4}} \tag{7}$$

where ρ, k_p, and μ_d are the fluid density, thermal conductivity, and dynamic viscosity at the condensate film temperature, respectively. L is the height of air gap (height of the cooling plate) and g is the acceleration due to gravity.

The above equations can be combined together and rearranged to get:

$$\begin{aligned} T_{\mathrm{mf}} &= T_f - \frac{H}{h_{\mathrm{hf}}}\left(\left(T_f - T_c\right) + \frac{J_w H_v}{h^*}\right) \\ T_{\mathrm{cd}} &= T_c + \frac{H}{h_{\mathrm{hf}}}\left(\left(T_f - T_c\right) + \frac{J_w H_v}{h^*}\right) \end{aligned} \tag{8}$$

where $H = \left(\frac{1}{h_f} + \frac{1}{h^*} + \frac{1}{h_p}\right)^{-1}$

The convective heat transfer coefficient is obtained from empirical correlations of the dimensionless Nusselt number (Nu) depending on the Reynolds number in the flow region [74,122,228]. Eqs. (9) and (10) are used to determine Nu for laminar and turbulent flow, respectively:

$$\mathrm{Nu} = 1.86\left(\mathrm{Re}\,\mathrm{Pr}\frac{d}{L}\right)^{0.33} \tag{9}$$

$$\mathrm{Nu} = 0.023 \times \mathrm{Re}^{0.8}\,\mathrm{Pr}^{1/3}\left(\frac{\mu}{\mu_s}\right)^{0.33} \tag{10}$$

Here μ_s is the fluid viscosity at the heat-transfer boundary surface temperature, Nu is given by $\mathrm{Nu} = hd/k$, Pr is the Prandtl number expressed as $\mathrm{Pr} = \mu C_p / k$, and Re is the Reynolds number given by $\mathrm{Re} = \rho u d / \mu$. Other correlations of Nu are found in the literature and listed in Table 4.

8.3.2. Mass transport

Vapor permeation through in AGMD process depends on the vapor pressure difference between both sides of the membrane. The mass transfer rate can be described by [55]:

$$J_w = B_w \Delta P_w \tag{11}$$

where B_w is the overall mass transfer coefficient and ΔP_w is the vapor pressure difference between the two sides of the membrane, which is estimated by $\Delta P_w = P_{\mathrm{mf}} - P_{\mathrm{cd}}$.

Where P_{mf} is the vapor pressure at the feed side of the membrane while P_{cd} is the vapor pressure at the condensation surface. The vapor pressure can be obtained from Antoine equation as:

$$P_{\mathrm{mf}} = e^{\left(22.328-\frac{3841}{T_{\mathrm{mf}}-41}\right)}$$
$$P_{\mathrm{cd}} = e^{\left(22.328-\frac{3841}{T_{\mathrm{cd}}-41}\right)} \quad (12)$$

The mass transfer in AGMD is conducted in two steps: (1) mass transfer across the membrane and (2) mass transfer across the air gap. The mass transfer resistance within the membrane is governed by three mechanisms: molecular diffusion, Knudsen diffusion and Poiseuille flow. In the AGMD process, the Poiseuille flow can be neglected with a low operational temperature less than 100°C [88]. The Knudsen diffusion and molecular diffusion exist simultaneously, and thus the overall resistance can be written as [123]:

$$R = R_k + R_m \quad (13)$$

where R_k is mass transfer due to Knudsen diffusion and R_m is mass transfer due to molecular diffusion. Therefore, the water vapor flux can be calculated from the following equation:

Table 4
Nu correlations in the literature used to estimate heat transfer coefficient

Equation	Types of flow	Reference
$\mathrm{Nu} = 0.027\,\mathrm{Re}^{\frac{4}{5}}\,\mathrm{Pr}^{n}\left(\frac{\mu}{\mu_s}\right)^{0.14}$ n = 0.4 for heating and n = 0.3 for cooling	Turbulent flow	[229]
$\mathrm{Nu} = 0.023\,\mathrm{Re}^{0.8}\,\mathrm{Pr}^{n}$ n = 0.4 for heating and n = 0.3 for cooling	Turbulent flow	[230]
$\mathrm{Nu} = 0.023\,\mathrm{Re}^{0.8}\,\mathrm{Pr}^{0.33}\left(\frac{\mu}{\mu_s}\right)^{0.14}$	Turbulent flow	[11]
$\mathrm{Nu} = 0.023\left(1+\frac{6d}{L}\right)\mathrm{Re}^{0.8}\,\mathrm{Pr}^{\frac{1}{3}}$	Turbulant flow	[231]
$\mathrm{Nu} = 1.86\left(\mathrm{Re}\,\mathrm{Pr}\frac{d}{L}\right)^{0.33}\left(\frac{\mu}{\mu_s}\right)^{\frac{1}{7}}$	Laminar flow	[232]
$\mathrm{Nu} = 1.62\left(\mathrm{Re}\,\mathrm{Pr}\frac{d}{L}\right)^{0.33}$	Laminar flow	[11]
$\mathrm{Nu} = 0.298\mathrm{Re}^{0.646}\mathrm{Pr}^{0.316}$	Laminar flow	[233]
$\mathrm{Nu} = 0.74\mathrm{Re}^{0.2}(\mathrm{GrPr})^{0.1}\mathrm{Pr}^{0.2}$	Laminar flow	[234]
$\mathrm{Nu} = 0.036\,\mathrm{Re}^{0.8}\,\mathrm{Pr}^{0.33}\left(\frac{d}{L}\right)^{0.055}$	Turbulent flow	[235]
$\mathrm{Nu} = 0.036\,\mathrm{Re}^{0.96}\,\mathrm{Pr}^{0.33}\left(\frac{d}{L}\right)^{0.055}$	Turbulent flow	[236]

$$J_w = J_{\mathrm{wm}} + J_{\mathrm{wk}} = C_m(P_{\mathrm{mf}} - P_{\mathrm{mp}}) \quad (14)$$

where J_{wm} and J_{wk} are the mass flux due to molecular and Knudsen diffusion, respectively. C_m is the mass transfer coefficient of the membrane or membrane permeability and is dependent on the physical properties of the membrane, such as porosity, tortuosity, and diffusivity of water vapor. Alsaadi et al. [94] proposed an empirical equation to calculate the value of C_m. The water vapor flux in the air gap is only controlled by molecular diffusion mechanism [50], which is determined by:

$$J_w = C_a(P_{\mathrm{mp}} - P_{\mathrm{cd}}) \quad (15)$$

where C_a is the mass transfer coefficient in the air gap and is given by Geng et al. [88].

On the other hand, the overall mass transfer coefficient for porous membrane and the air gap was calculated based on free diffusion [74,131] and given by the following equation:

$$B_w = \frac{\varepsilon P D_{\mathrm{ia}}}{RT_m \acute{b} P_{a_{\mathrm{ln}}}} \quad (16)$$

where $P_{a_{\mathrm{ln}}} = \frac{P_{\mathrm{amf}} - P_{\mathrm{acd}}}{\ln\left(\frac{P_{\mathrm{amf}}}{P_{\mathrm{acd}}}\right)}$ and $\acute{b} = b + \delta\tau$. Here b is the air gap thickness, δ is the membrane thickness, and τ is the membrane tortuosity. $D_{\mathrm{ia}} = 1.895x10^{-5}T^{2.072}/P$ and $\tau = \varepsilon/\delta\varepsilon_e$, where ε_e is the effective membrane porosity and it is the ratio of the membrane porosity ε to the pore length. T_m is the mean temperature in Kelvin (K) and given by $T_m = T_{\mathrm{mf}} + T_{\mathrm{gp}}/2$. Therefore, the permeate flux of the water vapor across the membrane and the air gap is given by:

$$J_w = \frac{\varepsilon P D_{\mathrm{ia}}}{RT\acute{b}P_{a_{\mathrm{ln}}}}\left(P_{\mathrm{mf}} - P_{\mathrm{cd}}\right) \quad (17)$$

8.3.3. Flux prediction

The permeate flux is calculated using an iterative method. Guessed values are assumed for membrane surface temperatures (T_{mf}, T_{cd}), then using Eqs. (12) and (17), the permeate flux is calculated. Heat transfer coefficient is estimated based on Nusselt number equations. Eq. (8) is then used to estimate the values of T_{mf} and T_{cd}. The obtained temperature results are compared with the initial assumed values of temperatures. This procedure is repeated until the difference between assumed temperatures and calculated temperatures is small enough (0.1%). Similar algorithm was used by Attia et al. [104].

8.4. Thermal efficiency

The thermal efficiency of MD system can be expressed as [74]:

$$\eta(100\%) = \frac{Q_v}{Q_v + Q_c} x(100\%) \tag{18}$$

where Q_v is the latent heat of the vaporized liquid which is expressed as $Q_v = J_w H_{vl}$, and Q_c is the heat transfer by conduction via the membrane and the air gap. The total heat supply to MD process is distributed as heat of vaporization for feed and a waste heat in the form of conduction heat transfer through the membrane. Hence, the conduction heat lost from the feed to the permeate in AGMD may be expressed as:

$$Q_c = \frac{(T_{mf} - T_{cd})}{\frac{\delta}{K_m} + \frac{b}{K_g}} \tag{19}$$

where δ is the membrane thickness, K_m is the effective thermal conductivity of the membrane material and the gas filling it. K_m can be estimated from the following expression [74]:

$$K_m = \varepsilon K_g + (1 - \varepsilon) K_p \tag{20}$$

where K_g and K_p are the thermal conductivity of the gas filling the membrane pores and membrane material, respectively.

Temperature polarization (θ) is the ratio of differences in temperature between the liquid–vapor interface and the bulk temperature. It can be expressed as [74]:

$$\theta = \frac{T_{mf} - T_{cd}}{T_f - T_c} \tag{21}$$

The value of θ is expected to be one in ideal case. However, θ is always lower than one because the bulk temperatures are always greater than the difference in temperature between the interfaces of liquid–vapor. The value of θ is used to determine whether the MD module is suitable or not. The MD module is of an unsuitable design if θ is less than 0.2. The MD module is considered to be suitably designed if θ is greater than 0.6 [74]. On the other hand, θ can be determined as:

$$\theta = \frac{1}{1 + \frac{H}{h}} \tag{22}$$

where H is the overall heat transfer coefficient, and h is the heat transfer coefficient of both the feed and permeate boundary layers [74]. Another method called the velocity extrapolation method was used to calculate θ [69]. This method is based on the fact that the thickness of the boundary layer decreases with the feed and permeate flow rates. By performing MD tests at different circulation velocities and extrapolating the data to an infinite velocity, the temperature polarization effect can be estimated if distilled water is used as feed. Therefore, θ can be calculated as [69]:

$$\theta = \frac{J_w}{J_{w,\infty}} \tag{23}$$

where $J_{w,\infty}$ is the flux that corresponds to an infinite velocity in absence of the polarization effect.

8.5. Gain output ratio

GOR represents the ratio between the energy used for evaporation to the energy consumed by the system. It is considered as another possible measure of the performance of MD system. GOR is defined as:

$$\text{GOR} = \frac{J_w H_w A}{Q_{in}} \tag{24}$$

where A is the effective membrane area and Q_{in} is the total heat supply to the system and it can be expressed as:

$$Q_{in} = mC_p(T_{f,in} - T_{f,out}) \tag{25}$$

Here m is the mass flow rate of the feed solution, C_p is the specific heat capacity of the feed solution, while $T_{f,in}$ and $T_{f,out}$ are the bulk feed inlet and outlet temperature, respectively. On the other hand, Q_{in} consists of the heat given to the AGMD (Q) and heat loss (Q_l) to the surrounding according to this equation:

$$Q_{in} = Q + Q_l \tag{26}$$

9. Economic aspects of AGMD

MD was considered to be a low-cost desalination technology due to its energy versatility potential by using both heat (fuel, solar, and waste) and electricity. MD does not operate under high pressure as RO, therefore allowing for thinner piping made from cheaper materials (i.e., plastics vs. stainless steel or expensive alloys) and reduced leaks and pump failure [237]. Banat and Jwaied [238] showed that the cost of desalination plants is usually a function of plant capacity, feed water salinity, pretreatment, process technology, energy cost, plant life, and investments amortization. The major cost elements for desalination plants are capital cost and annual operating costs. Capital cost covers purchasing cost of equipment, auxiliary equipment, land, installation charges, and pretreatment of water. Annual operating costs are the TACs of operating a desalting plant. These include amortization or fixed charges, operating and maintenance (O&M) costs, and membrane replacement costs. Based on this definition, the potable water production cost was calculated to be \$15/m^3 and \$18/m^3 for the compact and large systems, respectively. The authors showed that membrane lifetime and plant lifetime were the key parameters in determining the water production cost. The cost decreases with increasing membrane and/or plant lifetime. Arroyo and Shirazi [239] calculated the total RO unit cost of desalinated water as follows:

$$\text{Total unit cost of water} = \frac{\text{Annual debt service}}{365 \text{ X design capacity}} + \frac{\text{Operation and maintenance}}{\text{Production volume}} \quad (27)$$

In this equation, the debt service cost includes the total capital cost, the interest on the capital, and the loan payback period. The operation and maintenance cost cover the cost of chemicals, power, equipment and membrane replacement, and labor. Table 5 shows estimated cost for some desalination plants in USA in 2011 [239].

Saffarini et al. [240] estimated a cost model called solar-powered MD system for DCMD, AGMD, and VMD configurations. It is based on economic formulas utilizing capital cost data and variable and fixed operation costs of the unit as shown in Fig. 20. For the AGMD, the authors showed that the operation parameters were membrane length, feed mass flow rate, air gap width, feed channel depth, and solar collector efficiency. Moreover, they found that only the air gap width and solar collector efficiency have a linear effect on the cost model. Later Camacho et al. [31] summarized their results which is presented in Table 6. As each parameter was varied as shown in this table, all other parameters were held fixed to their value shown in Table 7. Based on the cost model, a comparison between MD configuration was carried out and shown in Fig. 21. It is clear that AGMD is the most expensive system. As mentioned earlier, Ali et al. [133] performed numerical modeling and factorial analysis using Saffarini et al. [240] model to determine the water production cost for small-scale, single-stage AGMD and DCMD processes driven by waste heat. They also studied the effect of membrane properties on the cost. In this model, the capital costs consist of membrane modules, pumps, piping, tanks, heat exchangers, and control systems. Membrane modules were taken at a cost of \$350/m^2 of membrane area. Pumps were assumed to cost \$700 each and all piping, control system, heat exchanger, and installation costs totaled \$5,500 for a small-scale MD system. Since these systems have small footprint, the cost of land was neglected.

Moreover, small-scale MD systems were assumed to be operated by their owner, so operator and administrator salaries are neglected. Maintenance costs were taken at 0.5% of the total capital cost per year. An average membrane replacement rate of 12% per year was assumed. Electricity needed to run the electric components was assumed to come from the grid at \$0.1/kW h. The results showed that, if the cost of waste heat input is neglected, the water production cost could be less than 1 USD/m^3. However, the authors mentioned that these values are only single-point estimates and that relative costs will change when the system geometry or operating conditions are optimized. Moreover, these costs are expected to decrease when the cost of solar collectors needed for heating the water in MD decreases especially when the renewable energies are used.

In this regards, Bouguecha et al. [241] investigated AGMD using sensible heat of geothermal water (AGMD-GW) at a small scale and compared it with other desalination processes such as RO-PV, and multiple-effect solar still (MESS). Table 8 shows the cost results for the three processes. The authors recommended the MESS based on his study for the sunny climates, while RO-PV has shown that the storage dissipation system removes the perturbation due to the fluctuation of solar radiation and is caused by short cloud passages. AGMD was preferable in this case as it had an ability to desalt very saline water with very low specific energy consumption.

Therefore, AGMD coupled with renewable energy such as geothermal resource presented a suitable design for small-scale desalination. Camacho et al. [31] compared cost of AGMD and others desalination process which is summarized in Table 9 as function of plant production.

Chang et al. [194] conducted a mathematical cost model of SMDDS by a systematic method which involves a pseudo-steady-state approach for equipment sizing and dynamic optimization taking into account the dynamic nature of the system. Two SMDDS employing an AGMD module with membrane areas of 11.5 m^2 operated at 500 kg/d and 23 m^2 operated at 1,000 kg/d were analyzed. The lowest water production costs were \$5.92/m^3 and \$5.16/m^3 for water production rates of 500 and 1,000 kg/d, respectively. The authors also claimed that the enhancement of the membrane mass transfer coefficient up to two times can result in the reduction of the unit production cost of the system. Moreover, they also recommended their model to be implemented for different MD configurations, such as LGMD, DCMD, and VMD, as well as different membrane modules, such as spiral-wound and hollow fiber. Another study by Saffarini et al. [240] showed that increasing the feed inlet temperature for the AGMD had a significant effect in lowering the cost while high feed flow rate resulted in increasing water production cost. In solar panel (SP)-MD systems, the MD will enhance the final cost of the water. In the same direction, a numerical modeling and factorial analysis including the effect of membrane properties was proposed to predict the cost of AGMD process [133]. The model was written for a small-scale, single-stage AGMD process driven by waste heat. The results showed that the

Table 5
Estimated water production cost of brackish groundwater desalination units in USA [239]

Brackish groundwater desalination plant (water salinity in TDS)	Desalination capacity × 10^6 gallons/d	Water treatment plant's capital cost (\$)	Unit capital cost (\$)	Power cost (¢/kW h)	O&M cost/10^3 gallons	Debt cost/10^3 gallons	Total production cost/10^3 gallons
Fort Hancock WCID (1,600–2,400 mg/L)	0.4	3,375,000	8.44	8.2	1.36	1.91	3.27
City of Roscoe (3,800 mg/L)	0.5	974,000	2.25	7	0.42	0.44	0.86
North Alamo WSC Donna (3,800 mg/L)	2.5	6,700,000	2.68	7	0.8	0.61	1.41

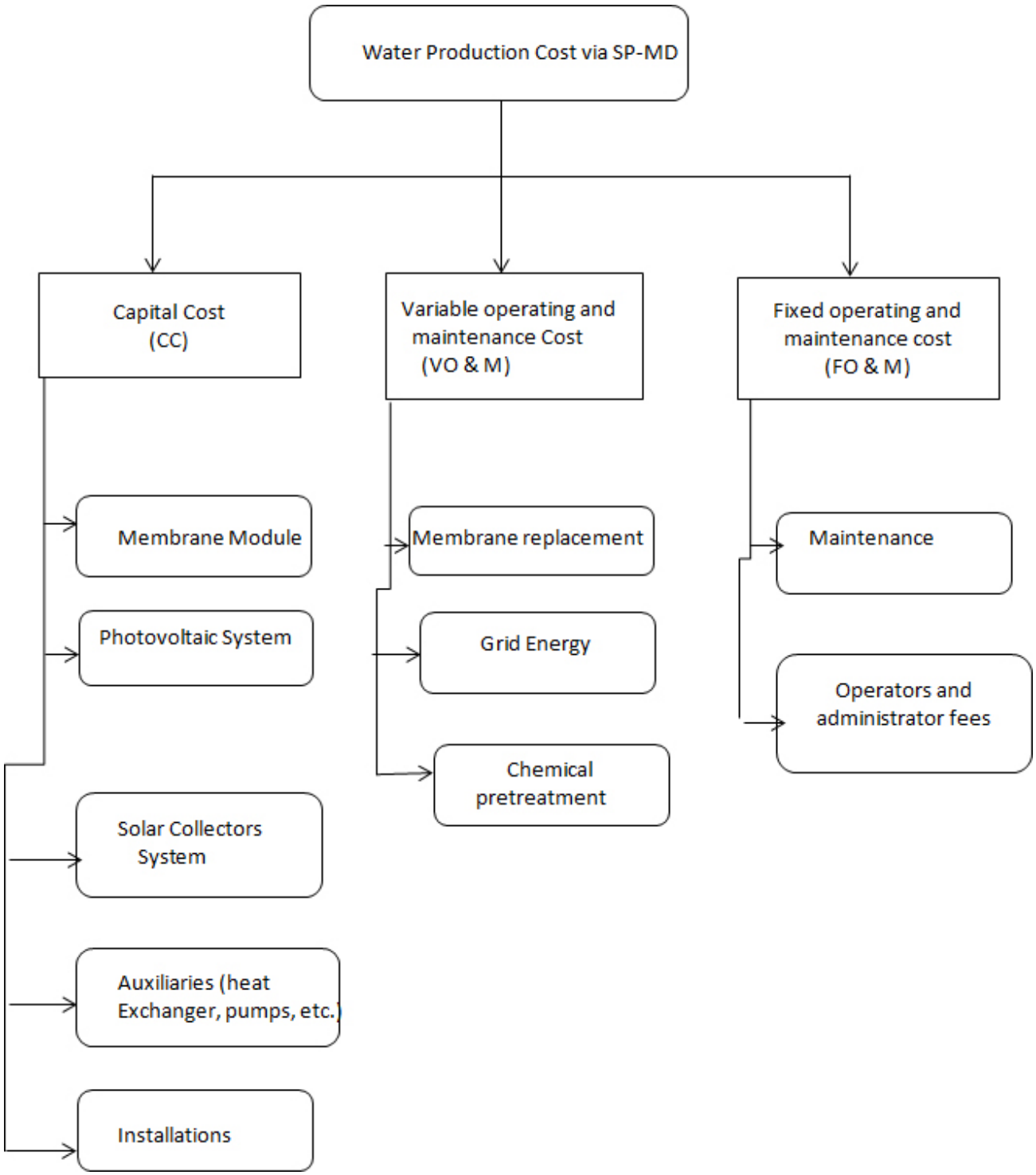

Fig. 20. Cost model breakdown [240].

water production cost could reach around \$1/m^3 if the cost of waste heat input to the system is neglected.

10. AGMD in seawater desalination process at large scale

AGMD has been investigated as a single or integrated with other process in desalination of seawater [95,242–244]. Guillen-Burrieza et al. [245] reported the thermal efficiency and the quality of the distillates produced by the two pre-commercials MD desalination pilot plants as a function of the operating parameters. The performance of two different solar-powered AGMD modules was analyzed and evaluated under real conditions for 2,400 h over a 2-year period. The two modules each with a total membrane surface area of 9 m^2

developed by the Singaporean enterprise Keppel Seghers were coupled with the static solar collector's field. The first module was a single compact unit while the second module consisted of three stages connected in series. Performance characteristics such as distillate amount and quality, thermal efficiency, and recovery ratio were evaluated. The aqueous NaCl with two different concentrations (1 and 35 g/L) was used as a feed. The minimum solar thermal energy consumption was found to be 1,805 and 294 kW h/m^3 for a single compact and multi-stage units, respectively. A maximum flux of 6 kg/m^2 h was obtained. Another similar module with similar feed concentration was developed and manufactured by the Swedish company Scarab AB (Sweden) [35,75] as shown in Fig. 22. This research was conducted at the Solar Platform of Almería (PSA) research centre in Spain. They investigated AGMD module coupled with static solar collector for a total membrane surface area per module of 2.8 m^2. The experiments which were conducted for long time gave a maximum flux value of 7 kg/m^2 h. The authors concluded that this hybrid process required more improvements in thermal energy, permeate flux, and rejection to be more competitive with other conventional desalination processes. The same AGMD module with membrane area of 2.94 m^2 with a solar pond was investigated by University of Texas at El Paso [237,246]. Low grade thermal energy (between 13°C and 75°C) was extracted from the pond and supplied via a heat exchanger to the membrane module. The hot brine was pumped from the bottom

Table 6
Effect of operation parameters on solar-powered AGMD water cost [240]

Operating parameter	Operating range	Water cost ($/m^3)
Effective membrane length (m)	10–140	13–20
Feed mass flow rate (kg/s)	0.2–1.2 (laminar–turbulent)	20–23
Air gap width (m)	0.001–0.005	15–46
Feed channel depth (m)	0.001–0.005	20–24
Solar collector efficiency (%)	35–60	19–30

Table 7
Typical parameters used in solar-powered MD system [240]

Membrane module	
Feed mass flow rate, $m_{f,in}$	1 kg/s
Membrane material	Teflon (PTFE)
Length, L	10 m
Width, w	0.7 m
Flow channel depth, d_{ch}	4 mm
Porosity, ξ	0.8
Thickness, δ_m	200 μm
Membrane distillation coefficient, B	16 × 10^{-7} kg/m^2 Pa s
Thermal conductivity, k	1.2 W/m K
Solar heater array efficiency	50%
Daily average irradiation	850 W/m^2

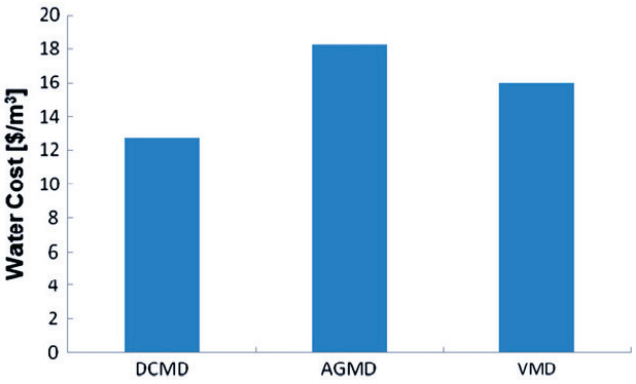

Fig. 21. Cost for a solar panel MD configurations at a recovery ratio of 4.4% with solar heaters [240].

Table 8
Basic design and cost data used for the studied cases [241]

Item	Life time	MESS		RO-PV		AGMD-GW	
		Basis cost	Annual cost	Basis cost	Annual cost	Basis cost	Annual cost
Modules of RO/MD	5	–		700	164.22	2,100	492.66
Stainless steel	10	504	59.12				
Wood	5	350	82.11				
FBC	15	–		–		700	57.74
PV panels	20	–		1,500	97.98	–	
Pumps	7	300	50.28	500	83.79	300	50.28
Control devices	7	500	83.79	500	83.79	500	83.79
Piping + tanks	10	100	11.73	50	5.89	50	5.89
Mirror + glass	5	280		–		–	
Carbon/cartridge filters	10			75	8.8	25	2.93
Sum		2,034	286.6	3,325	444.47	37,250	693.29
Capital investment cost ($/L)			0.04		0.07		0.11
O&M cost ($/L)			0.01		0.01		0.02
Total ($/L)			0.05		0.08		0.13

of the solar pond and circulated through a heat exchanger to supply heat to the saline solution. Cold water from the solar pond surface was passed through another heat exchanger to provide cooling. High and low temperatures for system operation were obtained by changing the flow rates for solar pond hot and cold water. The permeate flux was reached a maximum of 6 kg/m^2 h. Later, five Scarab AB modules were implemented in Sweden to produce water of 1–2 m^3/d [247]. These modules involved a plate and frame design with each featuring a 1 mm air gap, 2.3 m^2 membrane area, nine feeds and nine cooling channels (total stack thickness 17.5 cm). In another work, Aquastill spiral wound system based AGMD configuration was tested coupled to a solar thermal filed composed of stationary flat plate at PSA centre [248,249]. The performance plant was evaluated by measuring the flux and the heat efficiency. It was concluded that the differences in the channel length in plant have a stronger effect in their performance for seawater desalination than the configuration of the gap.

On the other hand, the Memstill® module was developed by TNO, a scientific institution in the Netherlands, for desalination of seawater by AGMD carried out in a counter current flow configuration as shown in Fig. 23 [18,250,251]. In this system, cold seawater flows through a tubular condenser with non-permeable well-wettable walls via a heat exchanger into the membrane evaporator which consists of a microporous hydrophobic membrane through which water vapor can diffuse. The condenser and evaporator tubes are separated by an air gap. This system gave a pure water price lower than that water produced by RO. This process has been installed and tried in different places as a pilot plant [252,253]. These plants were designed to produce a flow rate of 100 m^3/d,

Table 9
Comparison cost for MD hybrid processes [31]

Process	Capacity (m^3/d)	Cost ($/m^3)
Solar MED	72–85	2–10
Solar MSF	1	2.84
Solar PV-RO	1	12.05
Solar AGMD	66	8.9

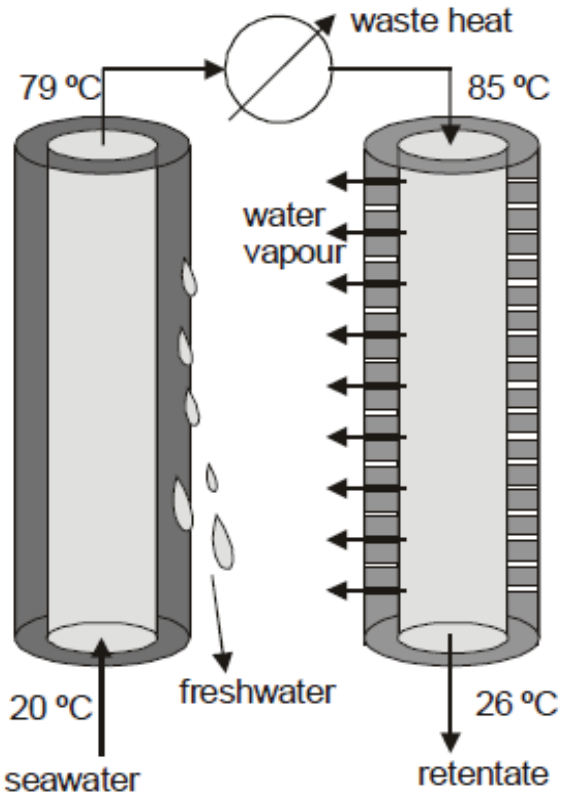

Fig. 23. Principle of Memstill® process [18].

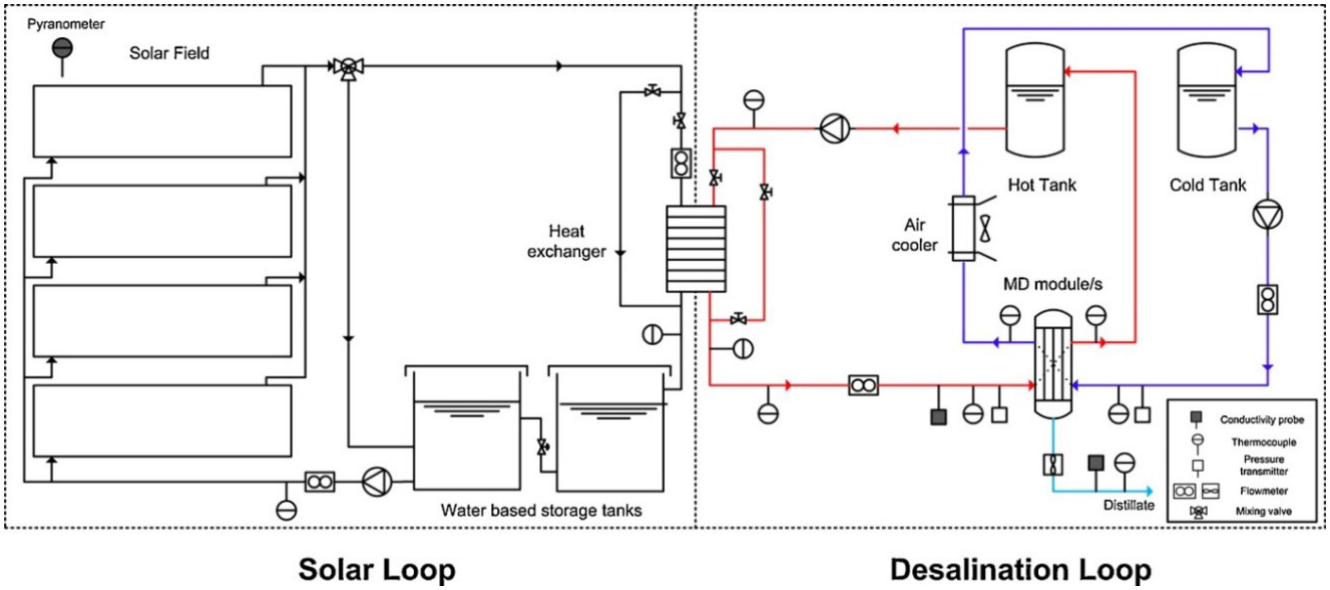

Fig. 22. Schematic diagram of the solar MD desalination experimental prototype erected within the MEDESOL project at PSA, Spain [75].

required a thermal energy of 56–100 kW h/m^3, and the feed water heated to 80°C–90°C to produce water with GOR up to 11.2. Moreover, Fraunhofer Institute for Solar Energy System (ISE) in Germany designed spiral-wound AGMD systems as pilot plants [33,47,254]. The thermal energy consumptions were found to be of 140–200 kW h/m^3 in their design with production flow of 100 L/d to 10 m^3/d. Eight pilot plants were installed in five different countries, that is, Gran Canaria, Egypt, Jordan, Germany, and Italy.

The memsys system used a vacuum multi-effect membrane distillation [142,185] is a relatively new MD technology that features a novel internal heat recycling concept that allows for reduced thermal consumption. It utilizes a multi-stage setup integrated into a compact plate and frame module. The system has been installed around the world, including Singapore, Australia, and India. Memsys requires 175–350 kW h/m^3 (GOR up to 3.6) of thermal energy, 0.75–1.75 kW h/m^3 of electrical energy, feed temperatures from 60°C to 100°C, and cooling lower than 40°C. The resulting fluxes are in the range of 6.8–9.5 kg/m^2 h. Another similar module named a continuous-effect membrane distillation was developed by Yao et al. [98] for desalination applications process. The process included an AGMD module consisting of strictly parallel evaporator and condenser fibers with internal heat-exchanging functions and an external heat exchanger. Two sets of different hollow fiber sand porous fibers are mixed well and closely packed parallel together inside a cylindrical shell. The space between adjacent fibers is filled with air. The authors claimed that this module has the advantages of both MD and MSF with an external heat exchanger. The vacuum is not required in this case because the porous hydrophobic membrane is used as the evaporator. Later, the authors implemented successfully this module for deep concentration of brine at high temperature [255]. Another work used multi-stage flat sheet AGMD modules coupled with an evaporative crystallizer was developed for design and optimization of the zero-liquid discharge water desalination [95].

In another work, a hybrid fluidized bed crystallizer (FBC) with AGMD was conducted for desalination of geothermal water [256] at a pilot plant level. A maximum flux value of 7.5 kg/m^2 h was obtained which is lower than the flux obtained from RO process (75 kg/m^2 h). To improve the efficiency of the process, the authors suggested other combining these processes with their model such as coupling solar plant collectors with geothermal energy and integrating RO with MD, where RO uses softening and warm brine of MD. The solar loop supplies the thermal energy to the system and operates with RO treated water, and the desalination loop which is in turn divided into two circuits. The solar loop is composed of 252 stationary solar collectors, with a total area of 500 m^2 arranged in four rows (with 35° tilt) and has a 24 m^2 thermal storage system based on water [257]. The desalination loop consists of two 2 m^3 PP tanks (PP-H), which are used as hot and cold water reservoirs. Feed solution, prepared with DI water and marine salt is heated up through the heat exchanger and pumped into AGMD modules. Both cold and hot water are returned to their corresponding tanks thus closing both circuits while distillate is discarded. Khan and Martin [258], and Mohan et al. [259] integrated a polygeneration pilot plant which consisted of biogas digester, SP, storage battery, inverter, charge controller, biogas generator, and AGMD for clean energy provision and pure water production as depicted in Fig. 24. The plant, located in Pani Para village in Faridpur, provided electricity via a PV array and animal and agriculture waste-fed digester, which in turn is coupled to a gas engine. Excess digester gas is employed for cooking and lighting, while waste heat from the process drives the AGMD unit for water treatment. The system required 12 kW solar PV panels together with a 10 kW biogas engine and 10 converter/batteries each with nominal voltage of 2 V and capacity of 800 Ah for 52 rural off-grid families.

In the same direction, a tri-generation plant based on the integration of power, cooling using absorption chiller and AGMD desalination thermal cycles was installed in Al Hamra area, Ras Al Khaimah, UAE [260]. This system was optimized for the utilization of waste heat by driving four thermal cycles based on quality and temperature of thermal energy. The results showed that efficiency of this system reached up to 85% in summer due to lower fuel consumption and full-scale operation of absorption chiller. Moreover, it was found that this system gave district cooling for 124 duplex houses with a production capacity of 4,600 kW along with water production in the range of 33–37 m^3/h. Later, this system was successfully implemented experimentally in weather condition of UAE [261].

In another work, a solar thermal cogeneration system was investigated by integrating AGMD module with solar thermal collectors with DHW supply [262]. The system involved evacuated tube collectors, thermal storage, MD unit, and heat exchangers. System performance was determined for three integration strategies: (1) thermal store integration (TSI), which resembles a conventional indirect SDHW system; (2) direct solar integration connecting collectors directly to the MD unit without thermal storage; and (3) direct solar with thermal store integration (DSTSI), a combination of these two approaches. The DSTSI strategy offered the best performance given its operational flexibility. Here the maximum distillate productivity was 43 L/d for a total gross solar collector area of 96 m^2. An economic analysis shows that the DSTSI strategy has a payback period of 3.9 years with net cumulative savings of $325,000 during the 20-year system lifetime.

In a very recent integrated work of solar and AGMD, Kumar and Martin [263] studied a pilot plant consisting of SDHW, single cassette SMD systems and their integrated operation in two different configurations; solar thermal store integrated MD (STSMD) and direct solar combined MD (SCMD) for co-production of pure water and heat as depicted in Figs. 25 and 26. This new pilot plant was designed to obtain a relatively hot and pure water. The experimental rig consisted of eight flat plate solar thermal collectors and three evacuated tubular collectors. Different arrays were designed and connected in series/parallel combinations in order to operate with varying collector areas. Solar thermal energy is charged either to a stratified storage tank of 520 L capacity or to a 300 L normal mixing storage tank. The AGMD configuration consisted of an air gap of 2.4 cm using aluminum condensing plates with 0.2 m^2 PTFE membrane.

The STSMD mode involved integration of AGMD to thermal storage tank that desalinate the salty water filled in the tank. In comparison with the other solar plants, this mode reduced overall system cost by eliminating heat exchanger

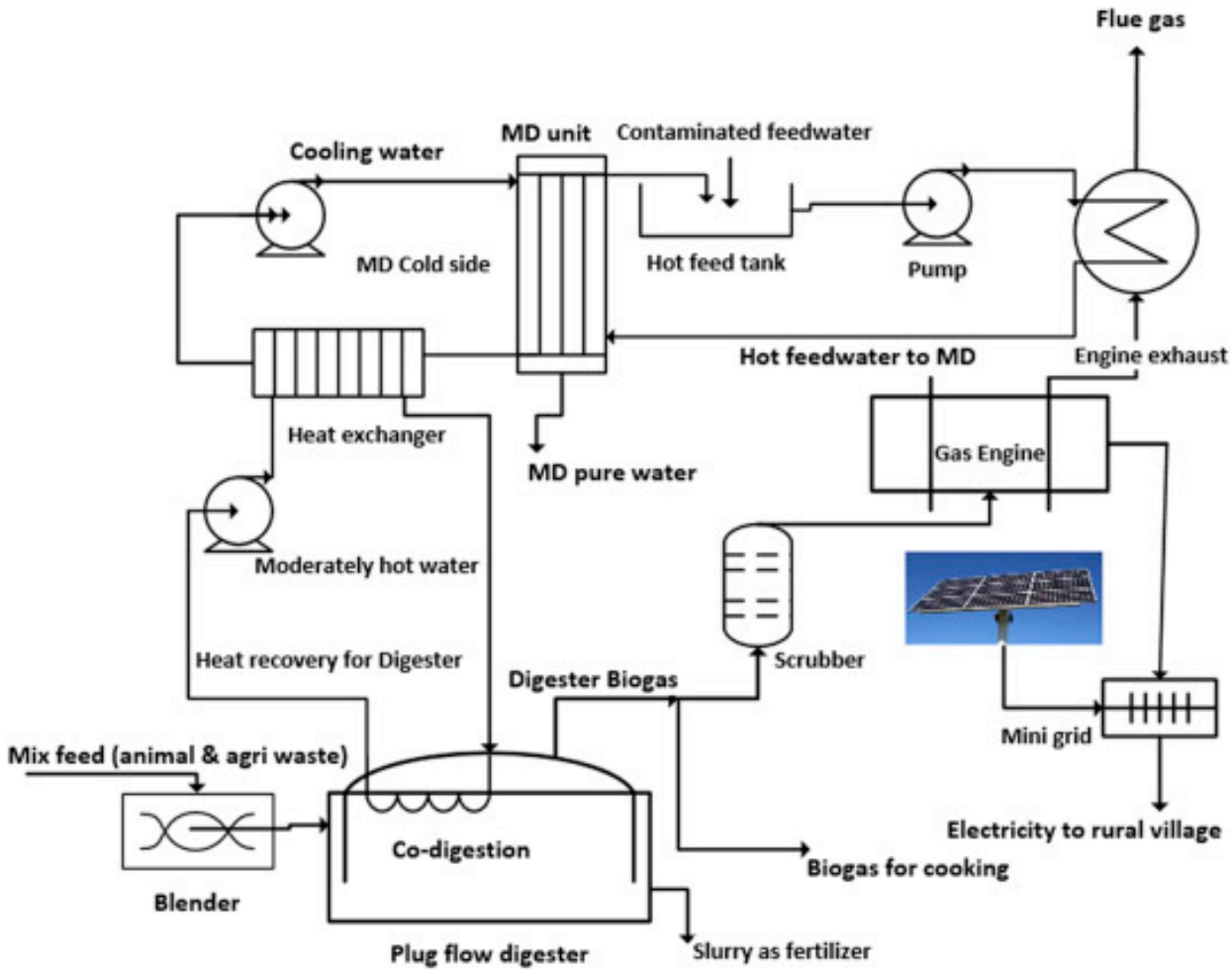

Fig. 24. Integrated hybrid polygeneration system with AGMD [258].

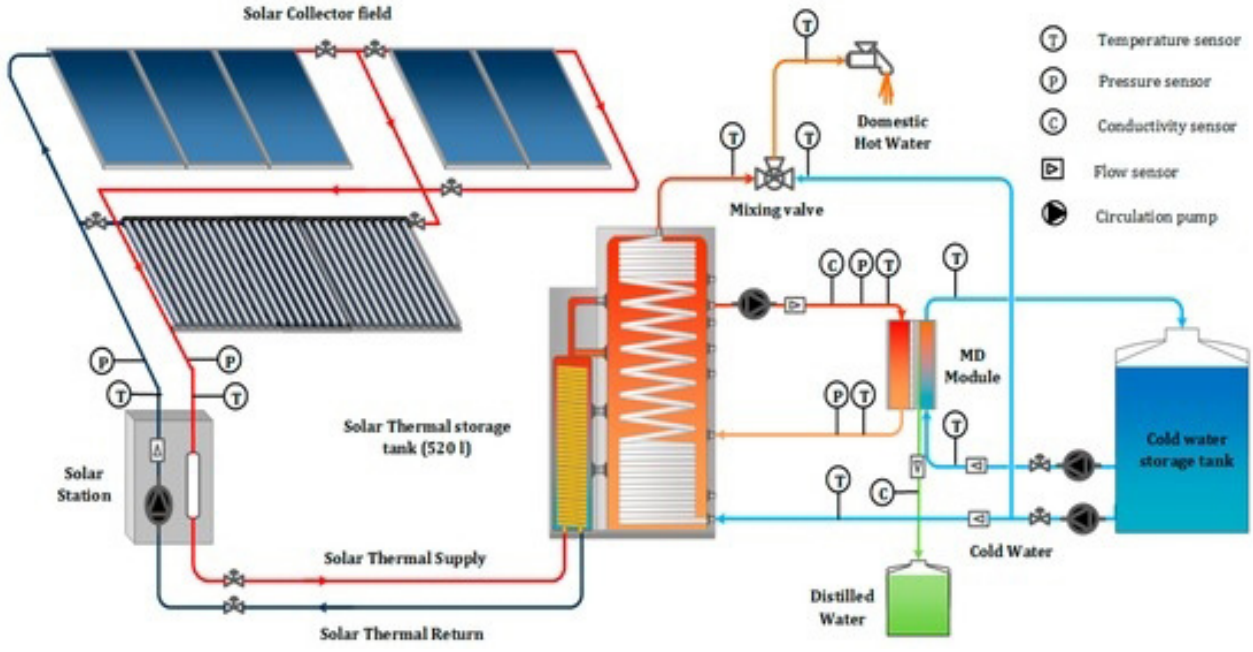

Fig. 25. Schematic representation of solar thermal store integrated MD (STSMD) [263].

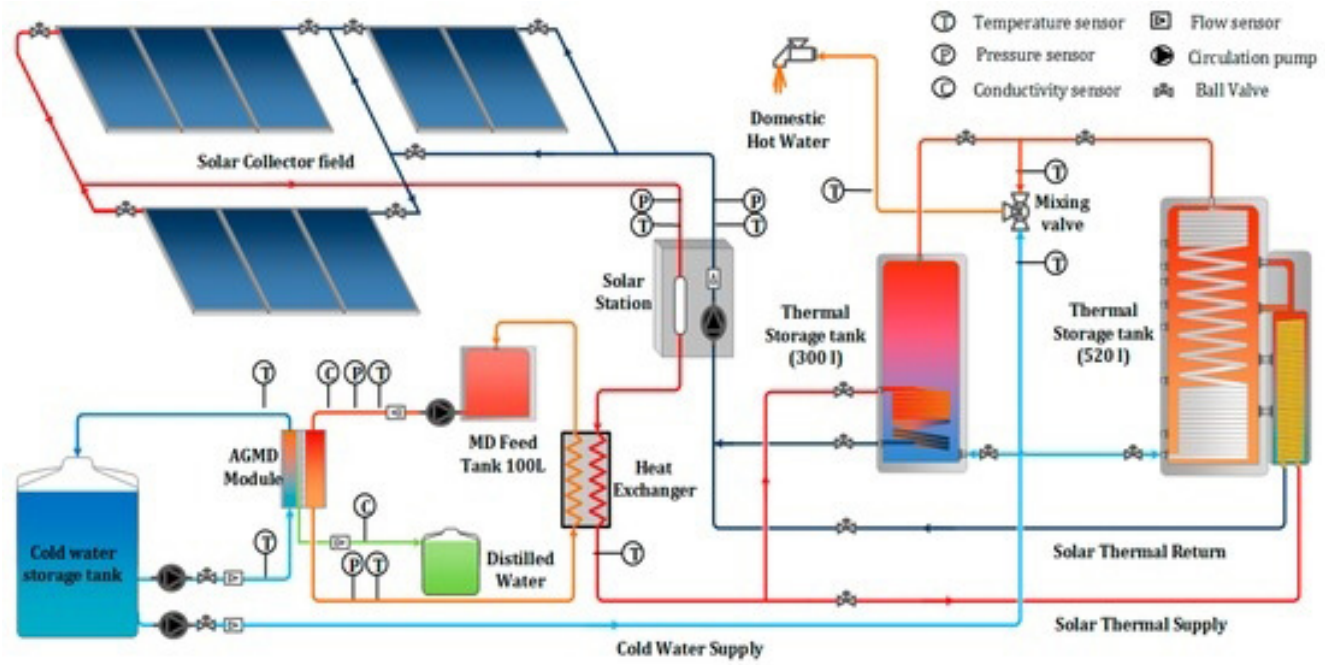

Fig. 26. Schematic representation of direct solar combined MD system (SCMD) [263].

and separate buffer storage for MD feed. In SCMD mode, AGMD has been separated from thermal energy storage and installed in solar thermal collector for direct energy gain for solar collectors and a heat exchanger was installed in solar circuit to heat up MD feed stream circulated via a small buffer storage tank of 100 L capacity. This new design overcomes the pressure fluctuations on feed inlet appeared in STSMD mode. The results showed that energy usage in SCMD mode was higher by 6%–7% than that STSMD mode. Further, the distillate flux decreased by only 6% in SCMD in comparison with DHW mode. The experimental data of SCMD system were successfully validated using TRNSYS simulation model.

Recently, Woldemariam et al. [264] introduced the exergy efficiency analyses for the AGMD configuration on a pilot scale. The AGMD showed different exergy efficiencies mainly due to the differences in module size and the type of condensation plates used. They were also affected to different degrees by the feed–coolant temperature differences in both types of modules. The exergy efficiency results showed that the materials selection of the condensation plate plays a role in optimizing the performance of MD systems. As an example, materials such as stainless steel and high-density polyethylene, which have better thermal conductivities than PP, could be considered for optimum heat transfer across modules and hence less exergy destruction from MD modules.

11. Conclusions and future trends of research

MD has been introduced since the early 1960s. The interest in MD has substantially grown over the last two decades due to advances in membrane technology and the ability to use renewable energy. Therefore, it has a potential to compete with well-established technologies such as RO, MED, and MSF in water purification and desalination processes as it has low sensitivity to feed concentration and operates at low temperatures. In this work, a comprehensive review of AGMD process was conducted to highlight its applications and its main drawbacks and future trends of research. Therefore, the paper has reviewed all aspects related to AGMD including properties, updated configurations, optimum operating conditions, fouling, modified membranes, modeling, integration with solar energy, economic aspects, its hybrid with other process for desalination processes at large scale.

The main advantage of the air gap in AGMD is to solve the problem of high heat loss by conduction through the membrane (as compared with DCMD), which leads to relatively low efficiency of the MD process. AGMD has high thermal efficiency due to air insulation between the heated feed stream and the coolant stream. Moreover, AGMD configuration provides the freedom of using any coolant fluid since the coolant does not mix with the condensate as is the case in DCMD. On the other hand, AGMD can deal easily with membrane leakage and damage, in which the MD process can be stopped for a while and the distillate does not have the chance to get contaminated as that in DCMD. However, AGMD configuration suffers from producing low flux compared with other MD configurations. Therefore, many studies were conducted to overcome this problem by modifying AGMD configuration, modifying and casting new membranes, and decreasing the required energy by using a renewable energy and energy recovery systems. Further research is needed to improve the permeate flux in AGMD by using highly permeable membranes and suitable modules with improved hydrodynamics. It was shown in the literature that flux using different modified material in casting membranes was reached up to 23.4 kg/m^2 h as shown in Table 2 which still its value is relatively lower than that DCMD. Some researcher used modified MD configurations in order to improve the flux such as using material in the gap instead

of air which improved the flux around 200% [43], and integrated the AGMD with four multi-effect evaporator which again gave a high flux (166.4 kg/m^2 h) [89]. However, this point represents a challenging situation to the researchers to study different scenarios and techniques to enhance the permeate flux at low energy cost.

There was no much research in literature covering the modification of members with nanotubes for AGMD applications, which it makes the floor open for the future research. On the other hand, modified ceramic membranes have been implemented in MD membrane instead of polymeric membranes. They have some potential properties such as higher thermal resistance, mechanical strength, chemical stability, and oxidant tolerance. The obtained fluxes and salt rejection were relatively higher in comparison with using polymeric membranes. However, additional researches are required to modify the ceramic membranes which change its hydrophilic nature into hydrophobic membranes.

Mathematical modeling of AGMD process is very important as it allows to design and scale-up the process at optimum conditions leading to a breakthrough of the technology. Several models have been proposed in the literature for the heat and mass transport in the water channels of the AGMD module as well as inside the porous membranes. The models were developed using either 0D, 1D, 2D, or 3D cases for different AGMD modules such as flat sheet type and spiral-wound modules. Different techniques have been investigated to stimulate the AGMD models such as Aspen Plus platform, CFD, and the commercial package of Ansys Fluent. Some researchers used different methods for modeling such as ANN, FD, and regression technique. Some points are important to be investigated in modeling AGMD system such as changing of membrane pore length and surface diffusion transport mechanism inside the membrane.

Recently, more attention is given to the integration of AGMD with solar energy and poly-generation systems to provide electricity, potable water, and DHW from salty water in remote areas at small and large scales. Different parameters have been investigated in this field such as thermal efficiency, specific energy consumption, recovery ratio, feed concentrations, cost of energy, economic analysis, and geometry of SP. Considering the advantages of this integrations, it is expected that this integration will dominate the conventional desalination process in future. Further research is required in modification of this solar AGMD hybrid process to reduce the water production cost and the energy consumption by studying suitable modules, renewable energy systems, waste energy, hybrid systems and membrane types.

Symbols

AGMD	—	Air gap membrane distillation
ACM	—	Aspen custom modeler
b	—	Air gap thickness, mm
B	—	Membrane distillation coefficient, kg/m^2 Pa s
B_w	—	Overall mass transfer coefficient
C_a	—	Mass transfer coefficient in the air gap (m/s)
C_m	—	Mass transfer coefficient of the membrane, m/s
C_{pf}	—	Heat capacity, kJ/kg K
C_{pg}	—	Heat capacity of the gas phase, kJ/kg K
CPV/T	—	Concentrated photovoltaic/thermal
CSG	—	Coal seam gas
DCMD	—	Direct contact membrane distillation
DP-AGMD-M	—	Double-pipe air gap membrane distillation module
d_{ch}	—	Flow channel depth, mm
FBC	—	Fluidized bed crystallizer
G/PVDF	—	Graphene polyvinylidene fluoride
GOR	—	Gained output ratio
g	—	Acceleration due to gravity, m/s^2
h_f	—	Convective heat transfer coefficient, kW/m^2
H_{vl}	—	Evaporation enthalpy, kJ/kg
h_y	—	Convective heat transfer coefficient in the gaseous phase, kW/m^2
h_c	—	Coolant film heat transfer coefficient
h_p	—	Overall heat transfer coefficient from vapor/condensate liquid interface to the cooling water, kW/m^2
h_d	—	Condensate heat transfer coefficient, kW/m^2
iPP	—	Isotactic polypropylene
J_w	—	Water vapor mass transfer rate, kg/m^2 s
k	—	Thermal conductivity of the gas phase, W/m K
k_c	—	Thermal conductivity of the condensation plate, W/m K
k_m	—	Thermal conductivity of membrane, W/m K
l	—	Plate thickness, mm
L	—	Length, m
LEP_w	—	Liquid water entry pressure, Pa
MD	—	Membrane distillation
MSF	—	Multi-stage flash distillation
MED	—	Multiple-effect distillation
$m_{f,in}$	—	Feed mass flow rate, kg/s
NF	—	Nanofiltration
Nu	—	Nusselt numbers
PGMD	—	Permeate gap membrane distillation
ppm	—	Parts per million
P_{mf}	—	Vapor pressure at the feed side of the membrane, Pa
P_{cd}	—	Vapor pressure at the condensation surface, Pa
PTFE	—	Polytetrafluoroethylene
PP	—	Polypropylene
PVDF	—	Polyvinylidene fluoride
PVDF-HFP	—	Polyvinylidene fluoride-*co*-hexafluoropropylene
PVA	—	Polyvinyl alcohol
PES	—	Polyethersulfone
P	—	Working gas pressure
PH	—	Polyvinylidene fluoride-*co*-hexafluoropropylene
ΔP_w	—	Vapor pressure difference, Pa
P_r	—	Prandtl number
Q_s	—	Sensible heat transfer, J

Q_v	—	Latent heat of the vaporized liquid, J
Q_c	—	Heat transfer by conduction via the membrane and the air gap, J
Q_l	—	Heat lost to the surrounding, J
R	—	Overall resistance
R_k	—	Mass transfer due to Knudsen diffusion, m²/s
R_m	—	Mass transfer due to molecular diffusion, m²/s
RO	—	Reverse osmosis
SGMD	—	Sweeping gas membrane distillation
SEM	—	Scanning electron microscopy
SMM	—	Surface-modifying macromolecules
S_a	—	Distance between the target and the substrate
SMDDS	—	Solar membrane distillation desalination system
SDHW	—	Solar domestic hot water
TDS	—	Total dissolved solids, ppm
T_p	—	Temperature polarization coefficient
T_f	—	Feed temperature, K
TAC	—	Total annual cost, $
T_{bf}	—	Bulk feed temperature, K
Ti	—	Titania
V-AGMD	—	Vacuum air gap membrane distillation
VMD	—	Vacuum membrane distillation
Zr	—	Zirconia

Greek letters

ξ	–	Porosity
θ	–	Temperature polarization
τ	–	Membrane tortuosity
ε_e	–	Effective membrane porosity
δ_m	–	Membrane thickness, mm
μ_d	–	Dynamic viscosity
$	–	US dollar

Acknowledgment

The authors would like to thank Imam Abdulrahman Bin Faisal University for funding our project titled "modelling and experimental testing of membrane distillation process for water desalination" with project number of 2016-241-ENG.

References

[1] N.M. Wade, Distillation plant development and cost update, Desalination, 136 (2001) 3–12.
[2] N. Hilal, H. Al-Zoubi, N.A. Darwish, A.W. Mohammad, M. Abu Arabi, A comprehensive review of nanofiltration membranes: treatment, pretreatment, modelling, and atomic force microscopy, Desalination, 170 (2004) 281–308.
[3] E. Drioli, A. Ali, F. Macedonio, Membrane distillation: recent developments and perspectives, Desalination, 356 (2015) 56–84.
[4] M.E. Findley, Vaporization through porous membranes, Ind. Eng. Chem. Process Des. Dev., 6 (1967) 226–230.
[5] E. Drioli, Y.L. Wu, Membrane distillation—an experimental-study, Desalination, 53 (1985) 339–346.
[6] S.I. Andersson, N. Kjellander, B. Rodesjo, Design and field-tests of a new membrane distillation desalination process, Desalination, 56 (1985) 345–354.
[7] H. Maab, L. Francis, A. Al-Saadi, C. Aubry, N. Ghaffour, G. Amy, S.P. Nunes, Synthesis and fabrication of nanostructured hydrophobic polyazole membranes for low-energy water recovery, J. Membr. Sci., 423 (2012) 11–19.
[8] C. Gostoli, G.C. Sarti, S. Matulli, Low-temperature distillation through hydrophobic membranes, Sep. Sci. Technol., 22 (1987) 855–872.
[9] C. Gostoli, G.C. Sarti, Separation of liquid-mixtures by membrane distillation, J. Membr. Sci., 41 (1989) 211–224.
[10] W.T. Hanbury, T. Hodgkiess, Membrane distillation—an assessment, Desalination, 56 (1985) 287–297.
[11] K.W. Lawson, D.R. Lloyd, Membrane distillation, J. Membr. Sci., 124 (1997) 1–25.
[12] H. Susanto, Towards practical implementations of membrane distillation, Chem. Eng. Process., 50 (2011) 139–150.
[13] C. Cabassud, D. Wirth, Membrane distillation for water desalination: how to chose an appropriate membrane?, Desalination, 157 (2003) 307–314.
[14] L. Carlsson, The new generation in sea-water desalination SU membrane distillation system, Desalination, 45 (1983) 221–222.
[15] S. Kubota, K. Ohta, I. Hayano, M. Hirai, K. Kikuchi, Y. Murayama, Experiments on seawater desalination by membrane distillation, Desalination, 69 (1988) 19–26.
[16] A.A. Alshahrani, H. Al-Zoubi, L.D. Nghiem, M.I.H. Panhuis, Synthesis and characterisation of MWNT/chitosan and MWNT/chitosan-crosslinked buckypaper membranes for desalination, Desalination, 418 (2017) 60–70.
[17] S. Adham, A. Hussain, J.M. Matar, R. Dores, A. Janson, Application of membrane distillation for desalting brines from thermal desalination plants, Desalination, 314 (2013) 101–108.
[18] G.W. Meindersma, C.M. Guijt, A.B. de Haan, Desalination and water recycling by air gap membrane distillation, Desalination, 187 (2006) 291–301.
[19] D. Singh, P. Prakash, K.K. Sirkar, Deoiled produced water treatment using direct-contact membrane distillation, Ind. Eng. Chem. Res., 52 (2013) 13439–13448.
[20] A. Alkhudhiri, N. Darwish, N. Hilal, Produced water treatment: application of air gap membrane distillation, Desalination, 309 (2013) 46–51.
[21] M. Gryta, Application of membrane distillation process for tap water purification, Membr. Water Treat., 1 (2010) 1–12.
[22] R.Z. Asadi, F. Suja, F. Tarkian, F. Mashhoon, S. Rahimi, A.A. Jameh, Solar desalination of gas refinery wastewater using membrane distillation process, Desalination, 291 (2012) 56–64.
[23] M.A. Izquierdo-Gil, M.C. Garcia-Payo, C. Fernandez-Pineda, Air gap membrane distillation of sucrose aqueous solutions, J. Membr. Sci., 155 (1999) 291–307.
[24] M.A. Izquierdo-Gil, M.C. Garcia-Payo, C. Fernandez-Pineda, Direct contact membrane distillation of sugar aqueous solutions, Sep. Sci. Technol., 34 (1999) 1773–1801.
[25] M. Khayet, J.I. Mengual, T. Matsuura, Porous hydrophobic/hydrophilic composite membranes—application in desalination using direct contact membrane distillation, J. Membr. Sci., 252 (2005) 101–113.
[26] D.M. Woldemariam, A. Kullab, A.R. Martin, District heat-driven water purification via membrane distillation: new possibilities for applications in pharmaceutical industries, Ind. Eng. Chem. Res., 56 (2017) 2540–2548.
[27] J. Szczerbinska, W. Kujawski, J.M. Arszynska, J. Kujawa, Assessment of air-gap membrane distillation with hydrophobic porous membranes utilized for damaged paintings humidification, J. Membr. Sci., 538 (2017) 1–8.
[28] M. Matheswaran, T.O. Kwon, J.W. Kim, I.S. Moon, Factors affecting flux and water separation performance in air gap membrane distillation, J. Ind. Eng. Chem., 13 (2007) 965–970.
[29] H. Kurokawa, K. Ebara, O. Kuroda, S. Takahashi, Vapor permeate characteristics of membrane distillation, Sep. Sci. Technol., 25 (1990) 1349–1359.
[30] L. Francis, N. Ghaffour, A.S. Alsaadi, S.P. Nunes, G.L. Amy, Performance evaluation of the DCMD desalination process under bench scale and large scale module operating conditions, J. Membr. Sci., 455 (2014) 103–112.
[31] L.M. Camacho, L. Dumee, J.H. Zhang, J.D. Li, M. Duke, J. Gomez, S. Gray, Advances in membrane distillation for water

desalination and purification applications, Water, 5 (2013) 94–196.
[32] Program on Technology Innovation: Electric Efficiency through Water Supply Technologies—A Roadmap, Electric Power Research Institute, Palo Alto, California, USA 1019360, June 2009.
[33] J. Koschikowski, M. Wieghaus, M. Rommel, V.S. Ortin, B.P. Suarez, J.R.B. Rodriguez, Experimental investigations on solar driven stand-alone membrane distillation systems for remote areas, Desalination, 248 (2009) 125–131.
[34] N. Dow, S. Gray, J.D. Li, J.H. Zhang, E. Ostarcevic, A. Liubinas, P. Atherton, G. Roeszler, A. Gibbs, M. Duke, Pilot trial of membrane distillation driven by low grade waste heat: membrane fouling and energy assessment, Desalination, 391 (2016) 30–42.
[35] E. Guillen, J. Blanco, D. Alarcon, G. Zaragoza, P. Palenzuela, M. Ibarra, Comparative evaluation of two membrane distillation modules, Desal. Wat. Treat., 31 (2011) 226–234.
[36] R.W. Schofield, A.G. Fane, C.J.D. Fell, Gas and vapor transport through microporous membranes. 1. Knudsen-Poiseuille transition, J. Membr. Sci., 53 (1990) 159–171.
[37] M.S. El-Bourawi, Z. Ding, R. Ma, M. Khayet, A framework for better understanding membrane distillation separation process, J. Membr. Sci., 285 (2006) 4–29.
[38] D.Y. Hou, J. Wang, X.C. Sun, Z.G. Ji, Z.K. Luan, Preparation and properties of PVDF composite hollow fiber membranes for desalination through direct contact membrane distillation, J. Membr. Sci., 405 (2012) 185–200.
[39] C. Feng, K.C. Khulbe, I. Matsuura, R. Gopal, S. Kaur, S. Rarnakrishna, M. Khayet, Production of drinking water from saline water by air-gap membrane distillation using polyvinylidene fluoride nanofiber membrane, J. Membr. Sci., 311 (2008) 1–6.
[40] C.H. Lee, W.H. Hong, Effect of operating variables on the flux and selectivity in sweep gas membrane distillation for dilute aqueous isopropanol, J. Membr. Sci., 188 (2001) 79–86.
[41] M. Khayet, M.P. Godino, J.I. Mengual, Theoretical and experimental studies on desalination using the sweeping gas membrane distillation method, Desalination, 157 (2003) 297–305.
[42] J.I. Mengual, M. Khayet, M.P. Godino, Heat and mass transfer in vacuum membrane distillation, Int. J. Heat Mass Transfer, 47 (2004) 865–875.
[43] L. Francis, N. Ghaffour, A.A. Alsaadi, G.L. Amy, Material gap membrane distillation: a new design for water vapor flux enhancement, J. Membr. Sci., 448 (2013) 240–247.
[44] R. Aryapratama, H. Koo, S. Jeong, S. Lee, Performance evaluation of hollow fiber air gap membrane distillation module with multiple cooling channels, Desalination, 385 (2016) 58–68.
[45] J. Swaminathan, H.W. Chung, D.M. Warsinger, F.A. AlMarzooqi, H.A. Arafat, J.H. Lienhard, Energy efficiency of permeate gap and novel conductive gap membrane distillation, J. Membr. Sci., 502 (2016) 171–178.
[46] D. Winter, J. Koschikowski, S. Ripperger, Desalination using membrane distillation: flux enhancement by feed water deaeration on spiral-wound modules, J. Membr. Sci., 423 (2012) 215–224.
[47] D. Winter, J. Koschikowski, M. Wieghaus, Desalination using membrane distillation: experimental studies on full scale spiral wound modules, J. Membr. Sci., 375 (2011) 104–112.
[48] A. Ruiz-Aguirre, M.I. Polo-Lopez, P. Fernandez-Ibanez, G. Zaragoza, Integration of membrane distillation with solar photo-Fenton for purification of water contaminated with Bacillus sp. and Clostridium sp. spores, Sci. Total Environ., 595 (2017) 110–118.
[49] A.E. Khalifa, Water and air gap membrane distillation for water desalination—an experimental comparative study, Sep. Purif. Technol., 141 (2015) 276–284.
[50] A.S. Alsaadi, L. Francis, H. Maab, G.L. Amy, N. Ghaffour, Evaluation of air gap membrane distillation process running under sub-atmospheric conditions: experimental and simulation studies, J. Membr. Sci., 489 (2015) 73–80.
[51] M.A. Abu-Zeid, L. Zhang, W.Y. Jin, T. Feng, Y.E. Wu, H.L. Chen, L. Hou, Improving the performance of the air gap membrane distillation process by using a supplementary vacuum pump, Desalination, 384 (2016) 31–42.
[52] Z.Y. Liu, Q.J. Gao, X.L. Lu, Z. Ma, H. Zhang, C.R. Wu, Experimental study of the optimal vacuum pressure in vacuum assisted air gap membrane distillation process, Desalination, 414 (2017) 63–72.
[53] E. Curcio, E. Drioli, Membrane distillation and related operations—a review, Sep. Purif. Rev., 34 (2005) 35–86.
[54] A.M. Alklaibi, N. Lior, Membrane-distillation desalination: status and potential, Desalination, 171 (2005) 111–131.
[55] A. Alkhudhiri, N. Darwish, N. Hilal, Membrane distillation: a comprehensive review, Desalination, 287 (2012) 2–18.
[56] A.S. Hassan, H.E.S. Fath, Review and assessment of the newly developed MD for desalination processes, Desal. Wat. Treat., 51 (2013) 574–585.
[57] M.M.A. Shirazi, A. Kargari, A review on applications of membrane distillation (MD) process for wastewater treatment, J. Membr. Sci. Res., 1 (2015) 101–112.
[58] B.L. Pangarkar, M.G. Sane, S.B. Parjane, M. Guddad, Status of membrane distillation for water and wastewater treatment–a review, Desal. Wat. Treat., 52 (2014) 5199–5218.
[59] M. Qtaishat, M. Khayet, T. Matsuura, Guidelines for preparation of higher flux hydrophobic/hydrophilic composite membranes for membrane distillation, J. Membr. Sci., 329 (2009) 193–200.
[60] P. Wang, T.S. Chung, Recent advances in membrane distillation processes: membrane development, configuration design and application exploring, J. Membr. Sci., 474 (2015) 39–56.
[61] L. Eykens, K. De Sitter, C. Dotremont, L. Pinoy, B. Van der Bruggen, Membrane synthesis for membrane distillation: a review, Sep. Purif. Technol., 182 (2017) 36–51.
[62] D.M. Warsinger, J. Swarninathan, E. Guillen-Burrieza, H.A. Arafat, J.H. Lienhard, Scaling and fouling in membrane distillation for desalination applications: a review, Desalination, 356 (2015) 294–313.
[63] G. Naidu, S. Jeong, S. Vigneswaran, T.M. Hwang, Y.J. Choi, S.H. Kim, A review on fouling of membrane distillation, Desal. Wat. Treat., 57 (2016) 10052–10076.
[64] M. Laqbaqbi, J. Sanmartino, M. Khayet, M.C. García-Payo, M. Chaouch, Fouling in membrane distillation, osmotic distillation and osmotic membrane distillation, Appl. Sci., 7 (2017) 334.
[65] M. Khayet, Solar desalination by membrane distillation: dispersion in energy consumption analysis and water production costs (a review), Desalination, 308 (2013) 89–101.
[66] Y.G. Zhang, Y.L. Peng, S.L. Ji, Z.H. Li, P. Chen, Review of thermal efficiency and heat recycling in membrane distillation processes, Desalination, 367 (2015) 223–239.
[67] E. Mathioulakis, V. Belessiotis, E. Delyannis, Desalination by using alternative energy: review and state-of-the-art, Desalination, 203 (2007) 346–365.
[68] A. Cipollina, G. Micale, Coupling Sustainable Energy with Membrane Distillation Processes for Seawater Desalination, 2010 1st International Nuclear and Renewable Energy Conference (INREC), Jordan, pp. 1–6.
[69] M. Khayet, Membranes and theoretical modeling of membrane distillation: a review, Adv. Colloid Interface Sci., 164 (2011) 56–88.
[70] I. Hitsov, T. Maere, K. De Sitter, C. Dotremont, I. Nopens, Modelling approaches in membrane distillation: a critical review, Sep. Purif. Technol., 142 (2015) 48–64.
[71] L. Eykens, K. De Sitter, C. Dotremont, L. Pinoy, B. Van der Bruggen, How to optimize the membrane properties for membrane distillation: a review, Ind. Eng. Chem. Res., 55 (2016) 9333–9343.
[72] M.A. Abu-Zeid, Y.Q. Zhang, H. Dong, L. Zhang, H.L. Chen, L. Hou, A comprehensive review of vacuum membrane distillation technique, Desalination, 356 (2015) 1–14.
[73] B.B. Ashoor, S. Mansour, A. Giwa, V. Dufour, S.W. Hasan, Principles and applications of direct contact membrane distillation (DCMD): a comprehensive review, Desalination, 398 (2016) 222–246.

[74] M. Khayet, T. Matsuura, Membrane Distillation: Principles and Applications, Elsevier, Oxford, 2011.
[75] E. Guillen-Burrieza, J. Blanco, G. Zaragoza, D.C. Alarcon, P. Palenzuela, M. Ibarra, W. Gernjak, Experimental analysis of an air gap membrane distillation solar desalination pilot system, J. Membr. Sci., 379 (2011) 386–396.
[76] A.M. Alklaibi, N. Lior, Comparative study of direct-contact and air-gap membrane distillation processes, Ind. Eng. Chem. Res., 46 (2007) 584–590.
[77] N. Loussif, J. Orfi, Comparative study of air gap, direct contact and sweeping gas membrane distillation configurations, Membr. Water Treat., 7 (2016) 71–86.
[78] L. Eykens, T. Reyns, K. De Sitter, C. Dotremont, L. Pinoy, B. Van der Bruggen, How to select a membrane distillation configuration? Process conditions and membrane influence unraveled, Desalination, 399 (2016) 105–115.
[79] R. Tian, H. Gao, X.H. Yang, S.Y. Yan, S. Li, A new enhancement technique on air gap membrane distillation, Desalination, 332 (2014) 52–59.
[80] M.N. Chernyshov, G.W. Meindersma, A.B. de Haan, Comparison of spacers for temperature polarization reduction in air gap membrane distillation, Desalination, 183 (2005) 363–374.
[81] R. Bahar, M.N.A. Hawlader, T.F. Ariff, Channeled coolant plate: a new method to enhance freshwater production from an air gap membrane distillation (AGMD) desalination unit, Desalination, 359 (2015) 71–81.
[82] V.V. Ugrozov, I.B. Elkina, V.N. Nikulin, L.I. Kataeva, Theoretical and experimental research of liquid-gap membrane distillation process in membrane module, Desalination, 157 (2003) 325–331.
[83] D. Singh, K.K. Sirkar, Desalination by air gap membrane distillation using a two hollow-fiber-set membrane module, J. Membr. Sci., 421 (2012) 172–179.
[84] D.E.M. Warsinger, J. Swaminathan, L.A. Maswadeh, J.H. Lienhard, Superhydrophobic condenser surfaces for air gap membrane distillation, J. Membr. Sci., 492 (2015) 578–587.
[85] A. Criscuoli, Improvement of the membrane distillation performance through the integration of different configurations, Chem. Eng. Res. Des., 111 (2016) 316–322.
[86] D.U. Lawal, A.E. Khalifa, Experimental investigation of an air gap membrane distillation unit with double-sided cooling channel, Desal. Wat. Treat., 57 (2016) 11066–11080.
[87] Z.Y. Liu, Q.J. Gao, X.L. Lu, L.H. Zhao, S. Wu, Z. Ma, H. Zhang, Study on the performance of double-pipe air gap membrane distillation module, Desalination, 396 (2016) 48–56.
[88] H.X. Geng, J. Wang, C.Y. Zhang, P.L. Li, H.Y. Chang, High water recovery of RU brine using multi-stage air gap membrane distillation, Desalination, 355 (2015) 178–185.
[89] B.L. Pangarkar, S.K. Deshmukh, Theoretical and experimental analysis of multi-effect air gap membrane distillation process (ME-AGMD), J. Environ. Chem. Eng., 3 (2015) 2127–2135.
[90] A.E. Khalifa, S.M. Alawad, M.A. Antar, Parallel and series multistage air gap membrane distillation, Desalination, 417 (2017) 69–76.
[91] H.C. Duong, P. Cooper, B. Nelemans, T.Y. Cath, L.D. Nghiem, Evaluating energy consumption of air gap membrane distillation for seawater desalination at pilot scale level, Sep. Purif. Technol., 166 (2016) 55–62.
[92] A.E. Khalifa, D.U. Lawal, Application of response surface and Taguchi optimization techniques to air gap membrane distillation for water desalination—a comparative study, Desal. Wat. Treat., 57 (2016) 28513–28530.
[93] A.E. Khalifa, D.U. Lawal, Performance and optimization of air gap membrane distillation system for water desalination, Arabian J. Sci. Eng., 40 (2015) 3627–3639.
[94] A.S. Alsaadi, N. Ghaffour, J.D. Li, S. Gray, L. Francis, H. Maab, G.L. Amy, Modeling of air-gap membrane distillation process: a theoretical and experimental study, J. Membr. Sci., 445 (2013) 53–65.
[95] H.F. Guo, H.M. Ali, A. Hassanzadeh, Simulation study of flat-sheet air gap membrane distillation modules coupled with an evaporative crystallizer for zero liquid discharge water desalination, Appl. Therm. Eng., 108 (2016) 486–501.
[96] M.N. Chernyshov, G.W. Meindersma, A.B. de Haan, Modelling temperature and salt concentration distribution in membrane distillation feed channel, Desalination, 157 (2003) 315–324.
[97] L.H. Cheng, P.C. Wu, J.H. Chen, Numerical simulation and optimal design of AGMD-based hollow fiber modules for desalination, Ind. Eng. Chem. Res., 48 (2009) 4948–4959.
[98] K. Yao, Y.J. Qin, Y.J. Yuan, L.Q. Liu, F. He, Y. Wu, A continuous-effect membrane distillation process based on hollow fiber AGMD module with internal latent-heat recovery, AIChE J., 59 (2013) 1278–1297.
[99] H.X. Geng, H.Y. Wu, P.L. Li, Q.F. He, Study on a new air-gap membrane distillation module for desalination, Desalination, 334 (2014) 29–38.
[100] H.X. Geng, Q.F. He, H.Y. Wu, P.L. Li, C.Y. Zhang, H.Y. Chang, Experimental study of hollow fiber AGMD modules with energy recovery for high saline water desalination, Desalination, 344 (2014) 55–63.
[101] C.M. Guijt, G.W. Meindersma, T. Reith, A.B. de Haan, Air gap membrane distillation—1. Modelling and mass transport properties for hollow fibre membranes, Sep. Purif. Technol., 43 (2005) 233–244.
[102] H.X. Geng, L. Lin, P.L. Li, C.Y. Zhang, H.Y. Chang, Study on the heat and mass transfer in AGMD module with latent heat recovery, Desal. Wat. Treat., 57 (2016) 15276–15284.
[103] A.S. Jonsson, R. Wimmerstedt, A.C. Harrysson, Membrane distillation—a theoretical-study of evaporation through microporous membranes, Desalination, 56 (1985) 237–249.
[104] H. Attia, M.S. Osman, D.J. Johnson, C. Wright, N. Hilal, Modelling of air gap membrane distillation and its application in heavy metals removal, Desalination, 424 (2017) 27–36.
[105] L. Cheng, Y.J. Zhao, P.L. Li, W.L. Li, F. Wang, Comparative study of air gap and permeate gap membrane distillation using internal heat recovery hollow fiber membrane module, Desalination, 426 (2018) 42–49.
[106] D.E. Moudjeber, A. Ruiz-Aguirre, D. Ugarte-Judge, H. Mahmoudi, G. Zaragoza, Solar desalination by air-gap membrane distillation: a case study from Algeria, Desal. Wat. Treat., 57 (2016) 22718–22725.
[107] C.M. Guijt, G.W. Meindersma, T. Reith, A.B. de Haan, Air gap membrane distillation—2. Model validation and hollow fibre module performance analysis, Sep. Purif. Technol., 43 (2005) 245–255.
[108] L. Eykens, I. Hitsov, K. De Sitter, C. Dotremont, L. Pinoy, B. Van der Bruggen, Direct contact and air gap membrane distillation: differences and similarities between lab and pilot scale, Desalination, 422 (2017) 91–100.
[109] J. Swaminathan, H.W. Chung, D.M. Warsinger, J.H. Lienhard V, Energy efficiency of membrane distillation up to high salinity: evaluating critical system size and optimal membrane thickness, Appl. Energy, 211 (2018) 715–734.
[110] F.A. Banat, J. Simandl, Theoretical and experimental-study in membrane distillation, Desalination, 95 (1994) 39–52.
[111] B.L. Pangarkar, M.G. Sane, Performance of air gap membrane distillation for desalination of ground water and seawater, World Academy of Science, Engineering, and Technology, Int. J. Geol. Environ. Eng., 5 (2011) 177–181.
[112] M. Khayet, C. Cojocaru, Air gap membrane distillation: desalination, modeling and optimization, Desalination, 287 (2012) 138–145.
[113] A. Khalifa, D. Lawal, M. Antar, M. Khayet, Experimental and theoretical investigation on water desalination using air gap membrane distillation, Desalination, 376 (2015) 94–108.
[114] A.M. Alklaibi, N. Lior, Transport analysis of air-gap membrane distillation, J. Membr. Sci., 255 (2005) 239–253.
[115] M. Asghari, A. Harandizadeh, M. Dehghani, H.R. Harami, Persian Gulf desalination using air gap membrane distillation: numerical simulation and theoretical study, Desalination, 374 (2015) 92–100.
[116] S. Kimura, S.I. Nakao, S.I. Shimatani, Transport phenomena in membrane distillation, J. Membr. Sci., 33 (1987) 285–298.
[117] M.C. Garcia-Payo, M.A. Izquierdo-Gil, C. Fernandez-Pineda, Air gap membrane distillation of aqueous alcohol solutions, J. Membr. Sci., 169 (2000) 61–80.

[118] S. Bouguecha, R. Chouikh, M. Dhahbi, Numerical study of the coupled heat and mass transfer in membrane distillation, Desalination, 152 (2003) 245–252.
[119] Z. Ding, W. Liu, G. Zhang, R. Ma, Comparative study on direct contact and air gap membrane distillation, Mod. Chem. Ind., 22 (2002) 26–29.
[120] M.N.A. Hawlader, R. Bahar, K.C. Ng, L.J.W. Stanley, Transport analysis of an air gap membrane distillation (AGMD) process, Desal. Wat. Treat., 42 (2012) 333–346.
[121] I. Janajreh, K. El Kadi, R. Hashaikeh, R. Ahmed, Numerical investigation of air gap membrane distillation (AGMD): seeking optimal performance, Desalination, 424 (2017) 122–130.
[122] G.L. Liu, C. Zhu, C.S. Cheung, C.W. Leung, Theoretical and experimental studies on air gap membrane distillation, Heat Mass Transfer, 34 (1998) 329–335.
[123] Q.F. Alsalhy, S.S. Ibrahim, F.A. Hashim, Experimental and theoretical investigation of air gap membrane distillation process for water desalination, Chem. Eng. Res. Des., 130 (2018) 95–108.
[124] K. He, H.J. Hwang, I.S. Moon, Air gap membrane distillation on the different types of membrane, Korean J. Chem. Eng., 28 (2011) 770–777.
[125] A. Alkhudhiri, N. Darwish, N. Hilal, Treatment of saline solutions using air gap membrane distillation: experimental study, Desalination, 323 (2013) 2–7.
[126] L. Martinez, Comparison of membrane distillation performance using different feeds, Desalination, 168 (2004) 359–365.
[127] Y.B. Yun, R.Y. Ma, W.Z. Zhang, A.G. Fane, J.D. Li, Direct contact membrane distillation mechanism for high concentration NaCl solutions, Desalination, 188 (2006) 251–262.
[128] A. Alkhudhiri, N. Darwish, N. Hilal, Treatment of high salinity solutions: application of air gap membrane distillation, Desalination, 287 (2012) 55–60.
[129] A. Alkhudhiri, N. Hilal, Air gap membrane distillation: a detailed study of high saline solution, Desalination, 403 (2017) 179–186.
[130] U. Dehesa-Carrasco, C.A. Perez-Rabago, C.A. Arancibia-Bulnes, Experimental evaluation and modeling of internal temperatures in an air gap membrane distillation unit, Desalination, 326 (2013) 47–54.
[131] F.A. Banat, J. Simandl, Desalination by membrane distillation: a parametric study, Sep. Sci. Technol., 33 (1998) 201–226.
[132] R. Chouikh, S. Bouguecha, M. Dhahbi, Modelling of a modified air gap distillation membrane for the desalination of seawater, Desalination, 181 (2005) 257–265.
[133] M.I. Ali, E.K. Summers, H.A. Arafat, J.H. Lienhard, Effects of membrane properties on water production cost in small scale membrane distillation systems, Desalination, 306 (2012) 60–71.
[134] J. Woods, J. Pellegrino, J. Burch, Generalized guidance for considering pore-size distribution in membrane distillation, J. Membr. Sci., 368 (2011) 124–133.
[135] J. Kim, S.E. Park, T.S. Kim, D.Y. Jeong, K.H. Ko, Isotopic water separation using AGMD and VEMD, Nukleonika, 49 (2004) 137–142.
[136] H. Cho, Y.J. Choi, S. Lee, J. Koo, T. Huang, Comparison of hollow fiber membranes in direct contact and air gap membrane distillation (MD), Desal. Wat. Treat., 57 (2016) 10012–10019.
[137] A.M. Alklaibi, N. Lior, Heat mass transfer resistance analysis of membrane distillation, J. Membr. Sci., 282 (2006) 362–369.
[138] J.L. Xu, Y.B. Singh, G.L. Amy, N. Ghaffour, Effect of operating parameters and membrane characteristics on air gap membrane distillation performance for the treatment of highly saline water, J. Membr. Sci., 512 (2016) 73–82.
[139] J.A. Sanmartino, M. Khayet, M.C. Garcia-Payo, Reuse of discarded membrane distillation membranes in microfiltration technology, J. Membr. Sci., 539 (2017) 273–283.
[140] Y.C. Woo, Y. Kim, W.G. Shim, L.D. Tijing, M.W. Yao, L.D. Nghiem, J. Choi, S. Kim, H.K. Shon, Graphene/PVDF flat-sheet membrane for the treatment of RO brine from coal seam gas produced water by air gap membrane distillation, J. Membr. Sci., 513 (2016) 74–84.
[141] Y.C. Woo, L.D. Tijing, W.G. Shim, J.S. Choi, S.H. Kim, T. He, E. Drioli, H.K. Shon, Water desalination using graphene-enhanced electrospun nanofiber membrane via air gap membrane distillation, J. Membr. Sci., 520 (2016) 99–110.
[142] W. Heinzl, S. Buttner, G. Lange, Industrialized modules for MED desalination with polymer surfaces, Desal. Wat. Treat., 42 (2012) 177–180.
[143] R.B. Saffarini, E.K. Summers, H.A. Arafat, J.H. Lienhard, Technical evaluation of stand-alone solar powered membrane distillation systems, Desalination, 286 (2012) 332–341.
[144] R. Moradi, J. Karimi-Sabet, M. Shariaty-Niassar, Y. Amini, Experimental investigation of nanofibrous poly(vinylidene fluoride) membranes for desalination through air gap membrane distillation process, Korean J. Chem. Eng., 33 (2016) 2953–2960.
[145] R. Moradi, J. Karimi-Sabet, M. Shariaty-Niassara, Y. Amini, Air gap membrane distillation for enrichment of ($H_2{}^{18}O$) isotopomers in natural water using poly(vinylidene fluoride) nanofibrous membrane, Chem. Eng. Process. Process Intensif., 100 (2016) 26–36.
[146] M. Essalhi, M. Khayet, Application of a porous composite hydrophobic/hydrophilic membrane in desalination by air gap and liquid gap membrane distillation: a comparative study, Sep. Purif. Technol., 133 (2014) 176–186.
[147] M. Essalhi, M. Khayet, Surface segregation of fluorinated modifying macromolecule for hydrophobic/hydrophilic membrane preparation and application in air gap and direct contact membrane distillation, J. Membr. Sci., 417 (2012) 163–173.
[148] Y.C. Woo, Y. Chen, L.D. Tijing, S. Phuntsho, T. He, J.S. Choi, S.H. Kim, H.K. Shon, CF_4 plasma-modified omniphobic electrospun nanofiber membrane for produced water brine treatment by membrane distillation, J. Membr. Sci., 529 (2017) 234–242.
[149] S. Pedram, H.R. Mortaheb, H. Fakhouri, F. Arefi-Khonsari, Polytetrafluoroethylene sputtered PES membranes for membrane distillation: influence of RF magnetron sputtering conditions, Plasma Chem. Plasma Process., 37 (2017) 223–241.
[150] I. Gancarz, M. Bryjak, J. Kujawski, J. Wolska, J. Kujawa, W. Kujawski, Plasma deposited fluorinated films on porous membranes, Mater. Chem. Phys., 151 (2015) 233–242.
[151] S. Al-Obaidani, E. Curcio, F. Macedonio, G. Di Profio, H. Ai-Hinai, E. Drioli, Potential of membrane distillation in seawater desalination: thermal efficiency, sensitivity study and cost estimation, J. Membr. Sci., 323 (2008) 85–98.
[152] J.A. Prince, V. Anbharasi, T.S. Shanmugasundaram, G. Singh, Preparation and characterization of novel triple layer hydrophilic-hydrophobic composite membrane for desalination using air gap membrane distillation, Sep. Purif. Technol., 118 (2013) 598–603.
[153] C. Zhu, G.L. Liu, C.S. Cheung, C.W. Leung, Z.C. Zhu, Ultrasonic stimulation on enhancement of air gap membrane distillation, J. Membr. Sci., 161 (1999) 85–93.
[154] M. Tomaszewska, Preparation and properties of flat-sheet membranes from poly(vinylidene fluoride) for membrane distillation, Desalination, 104 (1996) 1–11.
[155] J. Wang, Q.F. He, Y.J. Zhao, P.L. Li, H.Y. Chang, Preparation and properties of iPP hollow fiber membranes for air gap membrane distillation, Desal. Wat. Treat., 57 (2016) 23546–23555.
[156] Y.C. Woo, L.D. Tijing, M.J. Park, M. Yao, J.S. Choi, S. Lee, S.H. Kim, K.J. An, H.K. Shon, Electrospun dual-layer nonwoven membrane for desalination by air gap membrane distillation, Desalination, 403 (2017) 187–198.
[157] R. Das, K. Sondhi, S. Majumdar, S. Sarkar, Development of hydrophobic clay-alumina based capillary membrane for desalination of brine by membrane distillation, J. Asian Ceram. Soc., 4 (2016) 243–251.
[158] S.R. Krajewski, W. Kujawski, M. Bukowska, C. Picard, A. Larbot, Application of fluoroalkylsilanes (FAS) grafted ceramic membranes in membrane distillation process of NaCl solutions, J. Membr. Sci., 281 (2006) 253–259.
[159] A. Larbot, L. Gazagnes, S. Krajewski, M. Bukowska, W. Kujawski, Water desalination using ceramic membrane distillation, Desalination, 168 (2004) 367–372.
[160] L. Garcia-Fernandez, B. Wang, M.C. Garcia-Payo, K. Li, M. Khayet, Morphological design of alumina hollow fiber membranes for desalination by air gap membrane distillation, Desalination, 420 (2017) 226–240.

[161] S. Khemakhem, R.B. Amar, Modification of Tunisian clay membrane surface by silane grafting: application for desalination with air gap membrane distillation process, Colloids Surf., A, 387 (2011) 79–85.
[162] I. Derbel, M. Khemakhem, S. Cerneaux, M. Cretin, R. Ben Amar, Grafting of low cost ultrafiltration ceramic membrane by Tunisian olive oil molecules and application to air gap membrane distillation, Desal. Wat. Treat., 82 (2017) 20–25.
[163] L. Gazagnes, S. Cerneaux, M. Persin, E. Prouzet, A. Larbot, Desalination of sodium chloride solutions and seawater with hydrophobic ceramic membranes, Desalination, 217 (2007) 260–266.
[164] S. Cerneaux, I. Struzynska, W.M. Kujawski, M. Persin, A. Larbot, Comparison of various membrane distillation methods for desalination using hydrophobic ceramic membranes, J. Membr. Sci., 337 (2009) 55–60.
[165] J. Kujawa, S. Cerneaux, W. Kujawski, Investigation of the stability of metal oxide powders and ceramic membranes grafted by perfluoroalkylsilanes, Colloids Surf., A, 443 (2014) 109–117.
[166] Z.Y. Ma, Y. Hong, L.Y. Ma, M. Su, Superhydrophobic membranes with ordered arrays of nanospiked microchannels for water desalination, Langmuir, 25 (2009) 5446–5450.
[167] J.G. Lee, E.J. Lee, S. Jeong, J.X. Guo, A.K. An, H. Guo, J. Kim, T. Leiknes, N. Ghaffour, Theoretical modeling and experimental validation of transport and separation properties of carbon nanotube electrospun membrane distillation, J. Membr. Sci., 526 (2017) 395–408.
[168] S.R. Krajewski, W. Kujawski, F. Dijoux, C. Picard, A. Larbot, Grafting of ZrO_2 powder and ZrO_2 membrane by fluoroalkylsilanes, Colloids Surf., A, 243 (2004) 43–47.
[169] G. Amy, Fundamental understanding of organic matter fouling of membranes, Desalination, 231 (2008) 44–51.
[170] S. Shirazi, C.J. Lin, D. Chen, Inorganic fouling of pressure-driven membrane processes—a critical review, Desalination, 250 (2010) 236–248.
[171] M. Gryta, The assessment of microorganism growth in the membrane distillation system, Desalination, 142 (2002) 79–88.
[172] M. Krivorot, A. Kushmaro, Y. Oren, J. Gilron, Factors affecting biofilm formation and biofouling in membrane distillation of seawater, J. Membr. Sci., 376 (2011) 15–24.
[173] M. Gryta, Concentration of NaCl solution by membrane distillation integrated with crystallization, Sep. Sci. Technol., 37 (2002) 3535–3558.
[174] M. Gryta, Long-term performance of membrane distillation process, J. Membr. Sci., 265 (2005) 153–159.
[175] H.C. Duong, A.R. Chivas, B. Nelemans, M. Duke, S. Gray, T.Y. Cath, L.D. Nghiem, Treatment of RO brine from CSG produced water by spiral-wound air gap membrane distillation—a pilot study, Desalination, 366 (2015) 121–129.
[176] E. Guillen-Burrieza, A. Ruiz-Aguirre, G. Zaragoza, H.A. Arafat, Membrane fouling and cleaning in long term plant-scale membrane distillation operations, J. Membr. Sci., 468 (2014) 360–372.
[177] X.H. Yang, R. Tian, S.J. Ma, H.L. Lv, Study on membrane fouling experiment of stacked AGMD module in low temperature, Adv. Mater. Res., 396–398 (2011) 458–462.
[178] M. Gryta, M. Tomaszewska, A.W. Morawski, Water purification by membrane distillation, Inz. Chem. Procesowa, 22 (2001) 311–322.
[179] H.C. Duong, M. Duke, S. Gray, P. Cooper, L.D. Nghiem, Membrane scaling and prevention techniques during seawater desalination by air gap membrane distillation, Desalination, 397 (2016) 92–100.
[180] K. Karakulski, M. Gryta, Water demineralisation by NF/MD integrated processes, Desalination, 177 (2005) 109–119.
[181] J.A. Sanmartino, M. Khayet, M.C. Garcia-Payo, H. El Bakouri, A. Riaza, Desalination and concentration of saline aqueous solutions up to supersaturation by air gap membrane distillation and crystallization fouling, Desalination, 393 (2016) 39–51.
[182] J. Koschikowski, M. Wieghaus, M. Rommel, Solar thermal driven desalination plants based on membrane distillation, Desalination, 156 (2003) 295–304.
[183] H.E.S. Fath, S.M. Elsherbiny, A.A. Hassan, M. Rommel, M. Wieghaus, J. Koschikowski, M. Vatansever, PV and thermally driven small-scale, stand-alone solar desalination systems with very low maintenance needs, Desalination, 225 (2008) 58–69.
[184] A.T. Diaby, P. Byrne, P. Loulergue, B. Balannec, A. Szymczyk, T. Mare, O. Sow, Design study of the coupling of an air gap membrane distillation unit to an air conditioner, Desalination, 420 (2017) 308–317.
[185] A. Cipollina, M.G. Di Sparti, A. Tamburini, G. Micale, Development of a membrane distillation module for solar energy seawater desalination, Chem. Eng. Res. Des., 90 (2012) 2101–2121.
[186] W.G. Shim, K. He, S. Gray, I.S. Moon, Solar energy assisted direct contact membrane distillation (DCMD) process for seawater desalination, Sep. Purif. Technol., 143 (2015) 94–104.
[187] J.P. Mericq, S. Laborie, C. Cabassud, Evaluation of systems coupling vacuum membrane distillation and solar energy for seawater desalination, Chem. Eng. J., 166 (2011) 596–606.
[188] S. Ben Abdallah, N. Frikha, S. Gabsi, Design of an autonomous solar desalination plant using vacuum membrane distillation, the MEDINA project, Chem. Eng. Res. Des., 91 (2013) 2782–2788.
[189] F. Banat, N. Jwaied, M. Rommel, J. Koschikowski, M. Wieghaus, Desalination by a "compact SMADES" autonomous solar-powered membrane distillation unit, Desalination, 217 (2007) 29–37.
[190] F. Banat, N. Jwaied, M. Rommel, J. Koschikowski, M. Wieghaus, Performance evaluation of the "large SMADES" autonomous desalination solar-driven membrane distillation plant in Aqaba, Jordan, Desalination, 217 (2007) 17–28.
[191] H. Chang, C.L. Chang, C.D. Ho, C.C. Li, P.H. Wang, Experimental and simulation study of an air gap membrane distillation module with solar absorption function for desalination, Desal. Wat. Treat., 25 (2011) 251–258.
[192] H. Chang, S.G. Lyu, C.M. Tsai, Y.H. Chen, T.W. Cheng, Y.H. Chou, Experimental and simulation study of a solar thermal driven membrane distillation desalination process, Desalination, 286 (2012) 400–411.
[193] H.A. Chang, G.B. Wang, Y.H. Chen, C.C. Li, C.L. Chang, Modeling and optimization of a solar driven membrane distillation desalination system, Renew. Energy, 35 (2010) 2714–2722.
[194] H. Chang, C.L. Chang, C.Y. Hung, T.W. Cheng, C.D. Ho, Optimization study of small-scale solar membrane distillation desalination systems (s-SMDDS), Int. J. Environ. Res. Public Health, 11 (2014) 12064–12087.
[195] Y.H. Chen, Y.W. Li, H. Chang, Optimal design and control of solar driven air gap membrane distillation desalination systems, Appl. Energy, 100 (2012) 193–204.
[196] J.B. Galvez, L. Garcia-Rodriguez, I. Martin-Mateos, Seawater desalination by an innovative solar-powered membrane distillation system: the MEDESOL project, Desalination, 246 (2009) 567–576.
[197] E.K. Summers, H.A. Arafat, J.H. Lienhard, Energy efficiency comparison of single-stage membrane distillation (MD) desalination cycles in different configurations, Desalination, 290 (2012) 54–66.
[198] E.K. Summers, J.H. Lienhard, Experimental study of thermal performance in air gap membrane distillation systems, including the direct solar heating of membranes, Desalination, 330 (2013) 100–111.
[199] E.K. Summers, J.H. Lienhard, A novel solar-driven air gap membrane distillation system, Desal. Wat. Treat., 51 (2013) 1344–1351.
[200] A.J. Hughes, T.S. O'Donovan, T.K. Mallick, Experimental Evaluation of a Membrane Distillation System for Integration with Concentrated Photovoltaic/Thermal (CPV/T) Energy, P.C. Ghosh, Ed., 4th International Conference on Advances in Energy Research, Vol. 54, Elsevier Science B.V., Amsterdam, 2014, pp. 725–733.
[201] A. Kullab, C. Liu, A.R. Martin, Solar Desalination Using Membrane Distillation: Technical Evaluation Case Study, Proc. Solar World Congress 2005: Bringing Water to the World, Proc. 34th ASES Annual Conference and Proc. 30th National Passive Solar Conference, 2005, pp. 2732–2737.

[202] E.U. Khan, B. Mainali, A. Martin, S. Silveira, Techno-economic analysis of small scale biogas based polygeneration systems: Bangladesh case study, Sustain. Energy Technol. Assess., 7 (2014) 68–78.
[203] E.U. Khan, A.R. Martin, Hybrid Renewable Energy with Membrane Distillation Polygeneration for Rural Households in Bangladesh: Pani Para Village Case Study, 2014 International Conference on Renewable Energy Research and Application, New York, 2014, pp. 359–362.
[204] G. Mohan, U. Kumar N.T, M. Kumar P, A. Martin, Solar Thermal Polygeneration System for Cooling, Fresh Water, and Domestic Hot Water Supply: Experimental Analysis, A. Sayigh, Ed., Renewable Energy in the Service of Mankind Vol II: Selected Topics from the World Renewable Energy Congress WREC 2014, Springer International Publishing, Cham, 2016, pp. 781–791.
[205] P. Pal, A.K. Manna, Removal of arsenic from contaminated groundwater by solar-driven membrane distillation using three different commercial membranes, Water Res., 44 (2010) 5750–5760.
[206] M. Asim, N.T.U. Kumar, A.R. Martin, Feasibility analysis of solar combi-system for simultaneous production of pure drinking water via membrane distillation and domestic hot water for single-family villa: pilot plant setup in Dubai, Desal. Wat. Treat., 57 (2016) 21674–21684.
[207] N.T.U. Kumar, A. Martin, Co-generation of Drinking Water and Domestic Hot Water Using Solar Thermal Integrated Membrane Distillation System, J. Yan, D.J. Lee, S.K. Chou, U. Desideri, H. Li, Eds., International Conference on Applied Energy, ICAE2014, Vol. 61, Elsevier Science B.V., Amsterdam, 2014, pp. 2666–2669.
[208] J.D. Gil, L. Roca, A. Ruiz-Aguirre, G. Zaragoza, M. Berenguel, Optimal operation of a solar membrane distillation pilot plant via nonlinear model predictive control, Comput. Chem. Eng., 109 (2018) 151–165.
[209] A.A. Tashvigh, B. Nasernejad, Soft computing method for modeling and optimization of air and water gap membrane distillation—a genetic programming approach, Desal. Wat. Treat., 76 (2017) 30–39.
[210] A.E. Khalifa, D.U. Lawal, M.A. Antar, Performance of Air Gap Membrane Distillation Unit for Water Desalination, American Society of Mechanical Engineers, New York, 2015.
[211] D.E.M. Warsinger, J. Swaminathan, J.H. Lienhard V. Effect of Module Inclination Angle on Air Gap Membrane Distillation, Proc. 15th International Heat Transfer Conference, IHTC-15, 10–15 August, Kyoto, Japan, 2014.
[212] H. Chang, J.S. Liau, C.D. Ho, W.H. Wang, Simulation of membrane distillation modules for desalination by developing user's model on Aspen Plus platform, Desalination, 249 (2009) 380–387.
[213] D.J. Cheng, W. Gong, N. Li, Response surface modeling and optimization of direct contact membrane distillation for water desalination, Desalination, 394 (2016) 108–122.
[214] M. Khayet, C. Cojocaru, Artificial neural network modeling and optimization of desalination by air gap membrane distillation, Sep. Purif. Technol., 86 (2012) 171–182.
[215] R. Porrazzo, A. Cipollina, M. Galluzzo, G. Micale, A neural network-based optimizing control system for a seawater-desalination solar-powered membrane distillation unit, Comput. Chem. Eng., 54 (2013) 79–96.
[216] S. Shirazian, M. Alibabaei, Using neural networks coupled with particle swarm optimization technique for mathematical modeling of air gap membrane distillation (AGMD) systems for desalination process, Neural Comput. Appl., 28 (2017) 2099–2104.
[217] A.A. AlcheikhHamdon, N.A. Darwish, N. Hilal, The use of factorial design in the analysis of air-gap membrane distillation data, Desalination, 367 (2015) 90–102.
[218] A.E. Khalifa, B.A. Imteyaz, D.U. Lawal, M.A. Abido, Heuristic optimization techniques for air gap membrane distillation system, Arabian J. Sci. Eng., 42 (2017) 1951–1965.
[219] J.H. Lienhard, A Heat Transfer Textbook, 4th ed., Dover Publications, Mineola, NY, 2011.
[220] E. Karbasi, J. Karimi-Sabet, J. Mohammadi-Rovshandeh, M.A. Moosavian, H. Ahadi, Y. Amini, Experimental and numerical study of air-gap membrane distillation (AGMD): novel AGMD module for Oxygen-18 stable isotope enrichment, Chem. Eng. J., 322 (2017) 667–678.
[221] M. Shakaib, S.M.F. Hasani, M. Ehtesham-ul Haque, I. Ahmed, R.M. Yunus, A CFD study of heat transfer through spacer channels of membrane distillation modules, Desal. Wat. Treat., 51 (2013) 3662–3674.
[222] S. Al-Sharif, M. Albeirutty, A. Cipollina, G. Micale, Modelling flow and heat transfer in spacer-filled membrane distillation channels using open source CFD code, Desalination, 311 (2013) 103–112.
[223] E. Karbasi, J. Karimi-Sabet, J.M. Roshandeh, M.A. Moosavian, H. Ahadi, Experimental study and numerical simulation of the air gap membrane distillation (AGMD) Process, Chem. Prod. Process Model., 11 (2016) 41–45.
[224] L. Martinez, F.J. Florido-Diaz, A. Hernandez, P. Pradanos, Estimation of vapor transfer coefficient of hydrophobic porous membranes for applications in membrane distillation, Sep. Purif. Technol., 33 (2003) 45–55.
[225] Y. Mandiang, M. Sene, A. Thiam, Mathematical modeling and simulation of coupling parameters transfers of steam in a membrane-type solar still AGMD, J. Mater. Sci. Eng., 4 (2015) doi: 10.4172/2169-0022.1000157.
[226] S. Rochd, H. Zerradi, S. Mizani, A. Dezairi, S. Ouaskit, Modelisation of membrane distillation: mass and heat transfer in air gap membrane distillation, J. Membr. Sci. Technol., 6 (2016) 1–9.
[227] I. Hitsov, K. De Sitter, C. Dotremont, P. Cauwenberg, I. Nopens, Full-scale validated air gap membrane distillation (AGMD) model without calibration parameters, J. Membr. Sci., 533 (2017) 309–320.
[228] R.B. Bird, W.E. Stewart, E.N. Lightfoot, Transport Phenomena, Revised 2nd ed., John Wiley & Sons, New York, 2007.
[229] M. Khayet, A. Velazquez, J.I. Mengual, Modelling mass transport through a porous partition: effect of pore size distribution, J. Non-Equilib. Thermodyn., 29 (2004) 279–299.
[230] S. Srisurichan, R. Jiraratananon, A.G. Fane, Mass transfer mechanisms and transport resistances in direct contact membrane distillation process, J. Membr. Sci., 277 (2006) 186–194.
[231] J. Phattaranawik, R. Jiraratananon, A.G. Fane, Heat transport and membrane distillation coefficients in direct contact membrane distillation, J. Membr. Sci., 212 (2003) 177–193.
[232] C.M. Tun, A.G. Fane, J.T. Matheickal, R. Sheikholeslami, Membrane distillation crystallization of concentrated salts—flux and crystal formation, J. Membr. Sci., 257 (2005) 144–155.
[233] M. Gryta, M. Tomaszewska, A.W. Morawski, Membrane distillation with laminar flow, Sep. Purif. Technol., 11 (1997) 93–101.
[234] L. Martinez-Diez, M.I. Vazquez-Gonzalez, Temperature and concentration polarization in membrane distillation of aqueous salt solutions, J. Membr. Sci., 156 (1999) 265–273.
[235] M.A. Izquierdo-Gil, C. Fernandez-Pineda, M.G. Lorenz, Flow rate influence on direct contact membrane distillation experiments: different empirical correlations for Nusselt number, J. Membr. Sci., 321 (2008) 356–363.
[236] G.C. Sarti, C. Gostoli, S. Matulli, Low-energy cost desalination processes using hydrophobic membranes, Desalination, 56 (1985) 277–286.
[237] J. Walton, H. Lu, C. Turner, S. Solis, H. Hein, Solar and Waste Heat Desalination by Membrane Distillation, Desalination and Water Purification Research and Development Program Report No. 81, 2004, p. 20.
[238] F. Banat, N. Jwaied, Economic evaluation of desalination by small-scale autonomous solar-powered membrane distillation units, Desalination, 220 (2008) 566–573.
[239] J. Arroyo, S. Shirazi, Cost of Brackish Groundwater Desalination in Texas, Texas Water Development Board—Innovative Water Technologies, Texas, 2012.
[240] R.B. Saffarini, E.K. Summers, H.A. Arafat, J.H. Lienhard, Economic evaluation of stand-alone solar powered membrane distillation systems, Desalination, 299 (2012) 55–62.

[241] S. Bouguecha, B. Hamrouni, M. Dhahbi, Small scale desalination pilots powered by renewable energy sources: case studies, Desalination, 183 (2005) 151–165.
[242] A. El Amali, S. Bouguecha, M. Maalej, Experimental study of air gap and direct contact membrane distillation configurations: application to geothermal and seawater desalination, Desalination, 168 (2004) 357–357.
[243] F. Macedonio, E. Curcio, E. Drioli, Integrated membrane systems for seawater desalination: energetic and exergetic analysis, economic evaluation, experimental study, Desalination, 203 (2007) 260–276.
[244] R. Schwantes, A. Cipollina, F. Gross, J. Koschikowski, D. Pfeifle, M. Rolletschek, V. Subiela, Membrane distillation: solar and waste heat driven demonstration plants for desalination, Desalination, 323 (2013) 93–106.
[245] E. Guillen-Burrieza, G. Zaragoza, S. Miralles-Cuevas, J. Blanco, Experimental evaluation of two pilot-scale membrane distillation modules used for solar desalination, J. Membr. Sci., 409 (2012) 264–275.
[246] H.M. Lu, J.C. Walton, A.H.P. Swift, Desalination coupled with salinity-gradient solar ponds, Desalination, 136 (2001) 13–23.
[247] A. Kullab, A. Martin, Membrane distillation and applications for water purification in thermal cogeneration plants, Sep. Purif. Technol., 76 (2011) 231–237.
[248] A. Ruiz-Aguirre, D.C. Alarcon-Padilla, G. Zaragoza, Productivity analysis of two spiral-wound membrane distillation prototypes coupled with solar energy, Desal. Wat. Treat., 55 (2015) 2777–2785.
[249] A. Ruiz-Aguirre, J.A. Andres-Manas, J.M. Fernandez-Sevilla, G. Zaragoza, Comparative characterization of three commercial spiral-wound membrane distillation modules, Desal. Wat. Treat., 61 (2017) 152–159.
[250] C.M. Guijt, I.G. Racz, J.W. van Heuven, T. Reith, A.B. de Haan, Modelling of a transmembrane evaporation module for desalination of seawater, Desalination, 126 (1999) 119–125.
[251] G.W. Meindersma, C.M. Guijt, A.B. de Haan, Water recycling and desalination by air gap membrane distillation, Environ. Prog., 24 (2005) 434–441.
[252] J.H. Hanemaaijer, J. van Medevoort, A.E. Jansen, C. Dotremont, E. van Sonsbeek, T. Yuan, L.D. Ryck, Memstill membrane distillation—a future desalination technology, Desalination, 199 (2006) 175–176.
[253] K. Tarnacki, M. Meneses, T. Melin, J. van Medevoort, A. Jansen, Environmental assessment of desalination processes: reverse osmosis and memstill (R), Desalination, 296 (2012) 69–80.
[254] F. Banat, N. Jwaied, Autonomous membrane distillation pilot plant unit driven solar energy: experiences and lessons learned, Int. J. Sustain. Water Environ. Syst., 1 (2010) 21–24.
[255] J. Jin, Y. Qin, B. Wang, B. Wang, D. Cui, L. Liu, Deep concentration of brine by multiple-effect membrane distillation at high temperature, Chem. Ind. Eng. (Chin.), 40 (2014) 31–37.
[256] S. Bouguecha, M. Dhahbi, Fluidised bed crystalliser and air gap membrane distillation as a solution to geothermal water desalination, Desalination, 152 (2003) 237–244.
[257] D.C. Alarcon-Padilla, J. Blanco-Galvez, L. Garcia-Rodriguez, W. Gernjak, S. Malato-Rodriguez, First experimental results of a new hybrid solar/gas multi-effect distillation system: the AQUASOL project, Desalination, 220 (2008) 619–625.
[258] E.U. Khan, A.R. Martin, Optimization of hybrid renewable energy polygeneration system with membrane distillation for rural households in Bangladesh, Energy, 93 (2015) 1116–1127.
[259] G. Mohan, U. Kumar, M.K. Pokhrel, A. Martin, A novel solar thermal polygeneration system for sustainable production of cooling, clean water and domestic hot water in United Arab Emirates: dynamic simulation and economic evaluation, Appl. Energy, 167 (2016) 173–188.
[260] G. Mohan, S. Dahal, U. Kumar, A. Martin, H. Kayal, Development of natural gas fired combined cycle plant for tri-generation of power, cooling and clean water using waste heat recovery: techno-economic analysis, Energies, 7 (2014) 6358–6381.
[261] G. Mohan, N.T.U. Kumar, M.K. Pokhreland A. Martin, Experimental investigation of a novel solar thermal polygeneration plant in United Arab Emirates, Renewable Energy, 91 (2016) 361–373.
[262] N.T.U. Kumar, G. Mohan, A. Martin, Performance analysis of solar cogeneration system with different integration strategies for potable water and domestic hot water production, Appl. Energy, 170 (2016) 466–475.
[263] T.N. Kumar, R.A. Martin, Co-production performance evaluation of a novel solar combi system for simultaneous pure water and hot water supply in urban households of UAE, Energies, 10 (2017) 481.
[264] D. Woldemariam, A. Martin, M. Santarelli, Exergy analysis of air-gap membrane distillation systems for water purification applications, Appl. Sci., 7 (2017) 301.